USAID
FROM THE AMERICAN PEOPLE

MALI CLIMATE VULNERABILITY MAPPING

JANUARY 2014

This report is made possible by the support of the American people through the U.S. Agency for International Development (USAID). The contents are the sole responsibility of Tetra Tech ARD and do not necessarily reflect the views of USAID or the U.S. Government.

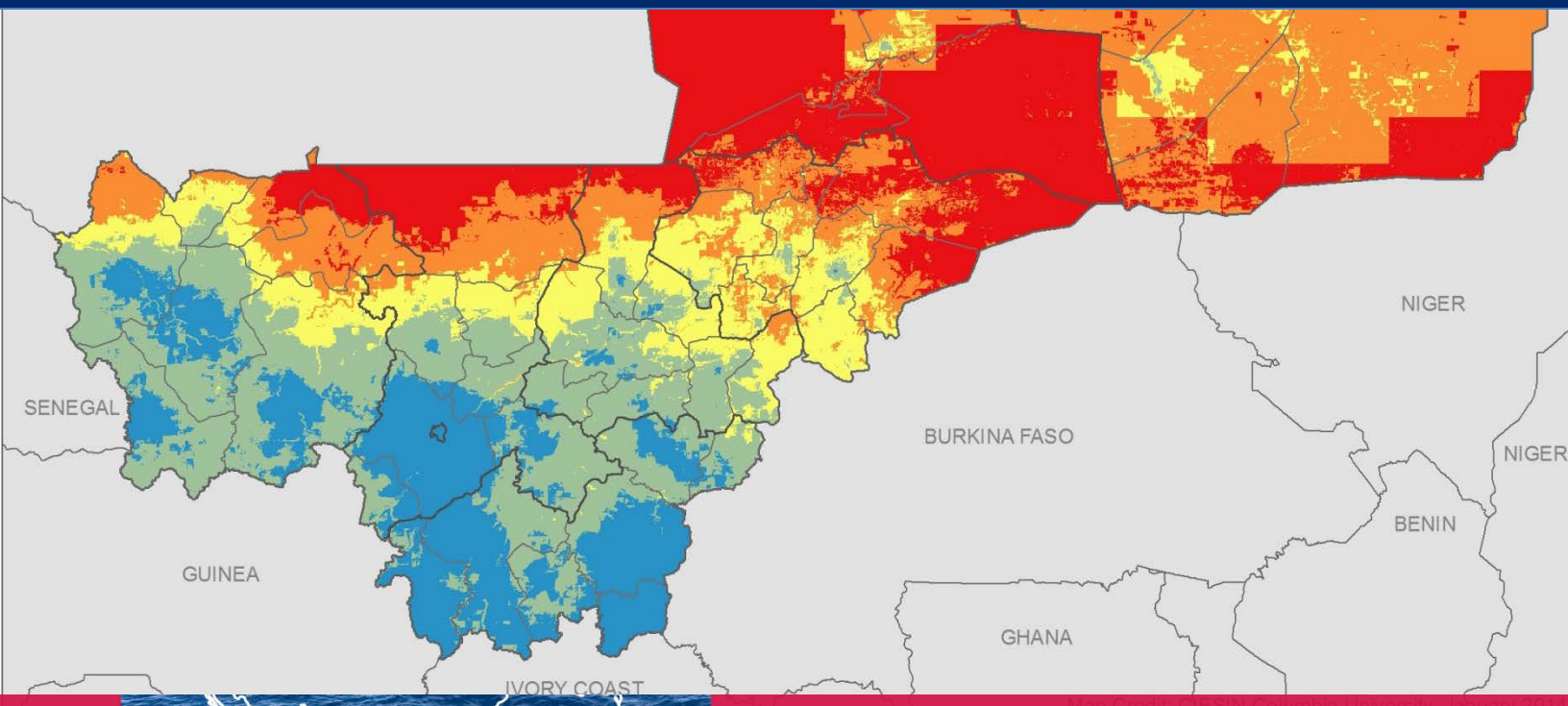

Map Credit: CIESIN Columbia University, January 2014

ARCC

African and Latin American Resilience to Climate Change Project

Contributors to this report include: Alex de Sherbinin[1], Tricia Chai-Onn[1], Alessandra Giannini[2], Malanding Jaiteh[1], Marc Levy[1], Valentina Mara[1], Linda Pistolesi[1], and Sylwia Trzaska[1] through subcontracts to Tetra Tech ARD.

[1] Center for International Earth Science Information Network (CIESIN), The Earth Institute at Columbia University

[2] International Research Institute for Climate and Society (IRI), The Earth Institute at Columbia University

Cover Photo: Overall vulnerability map of Mali (quintile map legend), CIESIN, 2013.

This publication was produced for the United States Agency for International Development by Tetra Tech ARD, through a Task Order under the Prosperity, Livelihoods, and Conserving Ecosystems (PLACE) Indefinite Quantity Contract Core Task Order (USAID Contract No. AID-EPP-I-00-06-00008, Order Number AID-OAA-TO-11-00064).

Tetra Tech ARD Contacts:

Patricia Caffrey
Chief of Party
African and Latin American Resilience to Climate Change (ARCC)
Burlington, Vermont
Tel.: 802.658.3890
Patricia.Caffrey@tetratech.com

Anna Farmer
Project Manager
Burlington, Vermont
Tel.: 802-658-3890
Anna.Farmer@tetratech.com

MALI CLIMATE VULNERABILITY MAPPING

AFRICAN AND LATIN AMERICAN RESILIENCE TO CLIMATE CHANGE (ARCC)

JANUARY 2014

TABLE OF CONTENTS

ACRONYMS AND ABBREVIATIONS

ACLED	Armed Conflict Location and Event Dataset
AIS	AIDS Indicator Survey
ARCC	African and Latin American Resilience to Climate Change
ASACOs	Community Health Associations
AVHRR	Advanced Very High Resolution Radiometer
CHV	community health volunteer
CIAT	Centro Internacional de Agricultura Tropical
CIESIN	Center for International Earth Science Information Network, Columbia University
CILSS	Permanent Interstate Committee for Drought Control in the Sahel
CSCOMs	Community Health Centers
CSREFs	Reference Health Centers
CSV	comma-separated values
CV	coefficient of variation
DEWA	Division of Early Warning and Assessment
DFO	Dartmouth Flood Observatory
DHS	Demographic and Health Survey
EROS	Earth Resources Observation and Science
FEWSNET	Famine Early Warning Systems Network
GAR	Global Assessment Report on Risk Reduction
GCM	general circulation model
GIMMS	Global Inventory Modeling and Mapping Studies
GPS	Global Positioning System
GRID	Global Resource Information Database
GRUMP	Global Rural-Urban Mapping Project
IER	Institut de l'Economie Rurale
IFPRI	International Food Policy Research Institute
IMR	infant mortality rate

IPCC	Intergovernmental Panel on Climate Change
ISRIC	International Soil Reference and Information Centre
NCHS	National Center for Health Statistics
NDVI	Normalized Difference Vegetation Index
NIMA	National Imagery and Mapping Agency
NOAA	National Oceanic and Atmospheric Administration
OCHA	Office for the Coordination of Humanitarian Affairs
ODHD	Observatoire du Developpement Durable Humain
PCA	principal components analysis
PCs	principal components
RCP	Representative Concentration Pathway
SEDAC	Socioeconomic Data and Applications Center
SoVI	Social Vulnerability Index
TTREND	temperature trend
UNICEF	United Nations Children's Fund
UNEP	United Nations Environment Program
USAID	United States Agency for International Development
USGS	United States Geological Survey
VMAP0	Vector Map Level 0
WHO	World Health Organization

EXECUTIVE SUMMARY

This report presents the results of a climate vulnerability mapping exercise that is intended to assist the United States Agency for International Development (USAID)/Mali with strategic planning. The approach utilizes a spatial vulnerability index comprising 18 indicators that are grouped into three vulnerability components: climate exposure, sensitivity, and adaptive capacity. Results are presented in map outputs, with the overall vulnerability map found in Figure 5.

Due to high levels of poverty, all of Mali's territory and population could be said to be highly vulnerable to future climate change. In spite of the fact that Mali, like its Sahelian neighbors, has a long history of coping with climate variability — and its livelihood systems are diversified in such a way as to reduce risk — the country has higher levels of overall vulnerability as compared to countries with higher levels of income and more stable/humid climates. The purpose of this mapping exercise is to highlight hotspots of particularly high *relative* vulnerability *within* Mali due to constellations of high climatic stress, high sensitivity (or susceptibility), and low adaptive capacity.

The results for current vulnerability show that relatively large swaths of northern Mali are hotspots, yet these areas are thinly settled with only 6 percent of Mali's population. Due to high capacity and relatively low sensitivity, Bamako is considered to have low vulnerability, as is the region immediately around Sikasso. The most densely settled agricultural region, in southeastern Mali, generally has medium to medium-high vulnerability. Approximately 75 percent of Mali's population resides in these vulnerability categories. Although the overall index may capture the greatest attention, much of the richness of this report lies in exploring the spatial patterns of vulnerability in the original 18 indicators and components.

We also considered two statistically downscaled future climate scenarios, representative concentration pathway (RCP) 4.5 and 8.5, representing low and high emissions scenarios, respectively, for time periods centered on 2030 and 2050. Results for the 2030 time period suggest relatively modest changes in overall vulnerability, but results for 2050 suggest that large areas in northern Mali will shift from medium-high to high vulnerability. The northern limit for rain-fed millet and sorghum has already shifted southward by approximately 50km in the past sixty years, and is likely to continue to do so as temperature increases affect the moisture availability for agriculture. In addition, our analysis could not adequately capture future changes in rainfall variability, which are likely to have as much of an impact on livelihoods as long-term trends.

While the vulnerability mapping can identify broad regions that are likely to be more vulnerable to climate stressors, any given community within that region could be more or less vulnerable than the average for the region for a host of context-specific reasons. Also, as with any spatial vulnerability index approach, the results depend on the robustness of the underlying data and are also sensitive to a range of methodological assumptions. There are multiple sources of uncertainty, ranging from the climate and socioeconomic data to the nature of the underlying causal mechanisms that produce vulnerability. A sensitivity analysis finds, however, that results for the vulnerability index are relatively robust, with the maximum potential decline or increase between each of five vulnerability classes limited to one step lower or higher on a five-step vulnerability scale for any given location on the map. We urge users to review the alternative approach to aggregation presented in Annex II (principal components analysis) and the sensitivity analysis presented in Annex III, as well as to understand the data limitations presented in the indicator metadata (Annex IV).

1.0 INTRODUCTION

As part of the African and Latin American Resilience to Climate Change (ARCC) program, the Center for International Earth Science Information Network, Columbia University (CIESIN) has developed climate vulnerability maps to be used by USAID/Mali to inform its climate adaptation and broader development programming. The approach uses a spatial vulnerability index comprising 18 indicators grouped into three vulnerability components: climate exposure, sensitivity, and adaptive capacity. The results are summarized in map outputs with accompanying text. This report is divided into the following sections: Section 2 summarizes our approach, including the framework, data, and methods; Section 3 presents results and maps; Section 4 provides conclusions; Annex I provides climate projection results; Annex II provides the results of a principal components analysis (PCA); Annex III provides a sensitivity analysis; and Annex IV provides indicator maps and data documentation (metadata).

In terms of high-level findings, the two approaches that were taken to develop an aggregate vulnerability map, the additive approach and a PCA (de Sherbinin, 2014), yielded broadly similar results. These include higher vulnerability in the northern areas, where rainfall is most limited and climate variability is highest; and lower vulnerability in the southern and southwestern portions of the country, with the lowest vulnerability around Bamako. Much of the richness, however, lies in examining the spatial patterns for the underlying components and examination of the maps of the individual indicators, found in Annex IV.

The results need to be qualified as being broadly indicative of patterns of vulnerability. In this regard, four points are worth highlighting:

- Vulnerability maps and resulting "hotspots" are built on assumptions regarding the mechanisms that produce vulnerability and data layers of varying accuracy. While we have provided a rationale section for each indicator layer in the metadata, in which we state our underlying assumptions, ideally we would be able to test these assumptions against outcome measures (e.g., morbidity, mortality, crop losses, or economic losses) related to specific climate events (e.g., floods or droughts).
- We collated the best available sub-national data for Mali, which proved to be a remarkably information rich environment for a least developed country. Nevertheless, limitations in global, regional, and national data mean that there is uncertainty associated with the results. This means that maps should be used in conjunction with ground validation when results are to be applied in specific localities. While we sought to keep our indicator layers to a reduced set, avoiding some data sets of questionable quality, some of the indicator data layers in this analysis have unknown levels of uncertainty. We were only able to characterize uncertainty in 7 out of 18 data layers. We have sought to address known data quality issues in the limitations section of the metadata.
- While maps can appear to provide unambiguous guidance on where to focus attention, map interpretation needs to be guided by accompanying text describing underlying uncertainties, because small changes in data and methods could produce different results. We provide a preliminary sensitivity analysis in Annex III to investigate the influence of our underlying assumptions regarding the construction of vulnerability on the overall vulnerability map.

- Map development would be improved by better data as well as a better understanding of the underlying functional form of the relationship among indicators (how a unit increase in one indicator relates to a unit increase in another indicator in terms of its impact on vulnerability); fungability (the degree to which a low score on one indicator compensates for high scores in another); and threshold effects for certain indicators. We further address these issues in the conclusion (Section 4.1).

Further discussion on the challenges of measuring vulnerability through aggregate indices are addressed by Baptista (2014) and Hinkel (2011).

2.0 FRAMEWORK, DATA, AND METHODS

For this mapping exercise, we utilize the Intergovernmental Panel on Climate Change (IPCC) conceptual framework, which separates vulnerability into three components: exposure, sensitivity, and adaptive capacity to climate stressors (Parry et al., 2007). This framework and variants thereof are commonly used in vulnerability mapping exercises in Africa and globally (e.g., Midgley et al., 2011; Yusuf and Francisco, 2009; Thow and De Blois, 2008). Our approach was to map the generic vulnerability of the population rather than to develop separate vulnerability layers for individual systems (e.g., ecosystems); sectors (e.g., water or agriculture); or population sub-groups (e.g., pastoralists). Following Fussel's (2009) recommendation that every quantitative vulnerability assessment clearly identify its focus, the attribute of value, the external hazards of concern, and its temporal reference, we define this vulnerability mapping as follows:

- Focus: vulnerability of populations to food and livelihood insecurity
- Valued attribute: food security, health, and wellbeing
- External hazard: changes in rainfall and increasing temperatures that threaten agricultural production systems
- Temporal reference: the years 2010, 2030, and 2050

The spatial indicators we utilized are found in Table 1. Full documentation for each indicator is included in Annex IV. Our guiding approach was to identify a limited number of high-quality spatial data sets that best represent the component of interest while avoiding the temptation to add low-quality data (data of high uncertainty or coarse spatial resolution), thereby "contaminating" the results.[1] We have reasonably high confidence in the validity and reliability of each of the data sets included, though limitations are further explored in the metadata.

Our processing involved the following steps. We converted all the original (raw) spatial data layers into grids at a common 30 arc-second (approximately 1 sq. km) resolution. We chose this grid cell size because it was the resolution of our highest-resolution data sets (flood frequency and soil organic carbon), and we felt that the interpolated surfaces for a number of our point-based data sets (e.g., the Demographic and Health Survey cluster-level data, conflict data, and health facilities data) could achieve a better representation of spatial variability at 1 sq. km. Yet it is worth noting that the climate and anthropogenic biomes data layers are at a spatial resolution of 5 to 6 arc-minutes (approximately 10-11 km on a side at the equator); and the poverty index and infant mortality are only available for administrative units (communes and cercles, respectively). Thus, while we strove to utilize the highest-

[1] For an example of a "big net" approach to indicator selection, see the indicator list for the Midgley et al. (2011) vulnerability mapping effort in Southern Africa. Their approach includes eight exposure indicators, 23 sensitivity indicators, and 12 adaptive capacity indicators. By contrast, we have chosen six exposure, seven sensitivity, and five adaptive capacity indicators.

resolution data sets available — with the climate data being a noteworthy example[2] — it is worth bearing in mind that the nominal 1 sq. km resolution of the outputs is based on inputs of varying resolutions.

TABLE 1. INDICATORS UTILIZED BY COMPONENT OF VULNERABILITY

Component	Indicator Code	Data Layer
Exposure	PRCP	Average annual precipitation (1950–2009)
	IACV	Inter-annual coefficient of variation in precipitation (1950–2009)
	DCVAR	Percent of precipitation variance explained by decadal component (1950–2009)
	NDVICV	Coefficient of variation of the Normalized Difference Vegetation Index (NDVI) (1981–2006)
	TTREND	Long-term trend in temperature in July-August-September (1950–2009)
	FLOOD	Flood frequency (1999–2007)
Sensitivity	HHWL	Household wealth (2006)
	STNT	Child stunting (2006)
	IMR	Infant mortality rate (IMR) (2006)
	POVI	Poverty index by commune (2008)
	CONF	Conflict events/political violence (1997–2012)
	CARB	Soil organic carbon/soil quality (1950–2005)
	MALA	Malaria stability index
Adaptive Capacity	EDMO	Education level of mother (2006)
	MARK	Market accessibility (travel time to major cities)
	HEALTH	Health infrastructure index (2012)
	ANTH	Anthropogenic biomes (2000)
	IRRI	Irrigated areas (area equipped for irrigation) (1990–2000)

The development of aggregate indices requires some sort of normalization (rescaling) of the raw data values (OECD, 2008). We chose to calculate indicator scores on a 0-100 scale, where 0 equates to lower vulnerability and 100 equates to high vulnerability (see the right-hand maps in the metadata,

[2] Historical climate data generally are only available in one-half to one degree resolution grid cells. We used climate data supplied by Famine Early Warning Systems Network (FEWSNET) at a much higher resolution thanks to a special data development effort that made use of a larger collection of ground stations blended with satellite data (Funk et al., 2012).

Annex IV).[3] We inverted indicators where high values in the raw data were associated with low vulnerability: average annual precipitation (exposure); soil organic carbon, child stunting, and household wealth (sensitivity); and mother's education, community health centers, and irrigation areas (adaptive capacity). Full details on the transformations that were applied to each indicator are provided in the "scoring system" section of the metadata. For most indicators, we simply created a percentile version of the raw data, maintaining the original data distribution. Several indicators had highly skewed distributions on the raw scale: average annual precipitation, the coefficient of variation of NDVI, flood frequency, soil organic carbon, and market accessibility. For these indicators, we trimmed the tails of the distribution, and the threshold (or winsorization) values are recorded in the metadata.

Expert judgment was required in processing a number of indicators, including development of continuous surfaces for two point data sets (conflict events and health infrastructure); and for the recoding of anthropogenic biome classes into vulnerability scores. In the normalization process we excluded from consideration all areas north of 17.2 degrees N latitude, a region that is very sparsely populated. We did this for two reasons. The first is because vulnerability results are less meaningful for a region that is so thinly populated and where climate variability and change may have less of an impact due to already harsh conditions. The second is methodological; inclusion of indicator data values for this region might skew results (due to extreme values) for the remainder of Mali, which is the primary region of interest.[4]

The indicators were then averaged to produce component maps for exposure, sensitivity, and adaptive capacity. We term this the "additive approach" to index construction (in contrast to the PCA in Annex II; for details on the additive approach, see de Sherbinin [2014]). Note that adaptive capacity was changed to "lack of adaptive capacity" for the mapping in order to retain the standard meaning across all components, in which high values equate to high vulnerability. All indicators were given equal weights except for the three indicators derived from Demographic and Health Survey (DHS) cluster-level data: household wealth, child stunting, and education level of the mother. The justification for this weighting was that these indicators were deemed to be closer to our interest in food and livelihood security, and because the data are at a higher spatial resolution than most of the other sensitivity and lack of adaptive capacity indicators. In the final step, since the ranges of scores in the resulting components significantly varied, we rescaled the resulting component scores so that they ranged from 0 to 100, and then averaged the three components together to create an overall vulnerability map.

The temporal reference for the baseline vulnerability mapping is the current period (circa 2010), though individual indicators are base-lined between the years 2000 and 2010. The climate indicators reference longer time periods. Section 3.5 and Annex I address future vulnerability based on projections of two indicators, precipitation and temperature trends, for future time periods centered on 2030 and 2050. Due to time and resource constraints we were unable to develop future scenarios for the sensitivity and adaptive capacity indicators.

---

[3] Prior to conversion, grids were converted to tabular comma-separated values (CSV)-format files using a common grid referencing system. All data transformations and aggregations were performed in the R statistical package, and the data were re-exported to ArcGIS for mapping.

[4] For further discussion of the influence of region of interest selection on vulnerability mapping results, see Abson et al. (2012), where results for separate ecoregions within Southern Africa were different than results for the entire region. Similarly, de Sherbinin (2014) includes a broader discussion on this topic.

3.0 RESULTS

We turn now to the results, first by component and then overall vulnerability based on past climate trends and variability. The maps are presented in vulnerability classes of 0-20 (low); 21-40 (medium-low); 41-60 (medium); 61-80 (medium-high); and 81-100 (high). The use of equal interval maps with set categories means that the areas (or number of grid cells) included in each class vary depending on the underlying statistical distribution of the components. The maps can be used to understand the components of vulnerability in a given location (how each component contributes to the overall score); and to identify areas of relatively higher exposure, sensitivity, lack of adaptive capacity, and overall vulnerability that may require programmatic interventions. Examples of these two applications follow:

1. An analyst would like a deeper understanding of the vulnerability profile of a given region. If he or she is interested in the vulnerability profile for the Kayes Region (the administrative unit in western-most Mali), he or she would find that exposure ranges from medium-low (in the south) to medium-high (in the north); its sensitivity ranges from medium (in the southwest) to medium-high (in the northeast and northwest), with pockets of high sensitivity in the extreme northeast; its lack of adaptive capacity is medium near the city of Kayes and west of Bamako, but otherwise medium-high; and its overall vulnerability is medium in the south and medium-high in the north, with a pocket of high vulnerability in the extreme northeast. An additional piece of information would be that the northernmost portion of Kayes has been affected during the past 60 years by declines in the reliability of rainfall meeting the threshold for rain-fed subsistence agriculture (e.g., millet or sorghum production), and a belt running through the center of the region has seen declines in the reliability of rainfall for cotton production (Figure 2). Finally, the principal components analysis (Annex II, Figure A2-5) finds that much of Kayes Region is in the lowest quintile of vulnerability, but that as with the overall vulnerability map, there is higher vulnerability in the north.
2. For targeting of resources, another analyst might focus activities on the Timbuktu region, where overall vulnerability is very high (due in particular to high sensitivity), and where there are obvious needs for post-conflict reconstruction and development. Or, taking the vulnerability information in conjunction with the population map in Figure 6, that analyst might identify the Ségou Region (the L-shaped region in central Mali that straddles the Niger River) as a higher priority, given its medium-high vulnerability in large portions; high sensitivity in the eastern portion (the Dogon Plateau); and its large population of almost 2.3m (or ~16 percent of Mali's total population).

These are the two primary approaches for using the maps, but other pieces of ancillary information could be useful for targeting resources (such as topographic maps, route networks, secondary population centers, or maps of existing donor programming [Figure 7]).

In a final section (3.5), future vulnerability is presented based on two climate scenarios projected to two time periods centered on 2030 and 2050.

3.1 EXPOSURE COMPONENT

The exposure component (Figure 1) is fairly straightforward to interpret; it reflects the south-to-north gradient of decreasing rainfall and increasing rainfall variability. Some of the more linear yellow, orange, and red features in areas with broad patterns of lower exposure reflect the influence of flood exposure along major river courses such as the Niger and its tributaries.

FIGURE 1. EXPOSURE

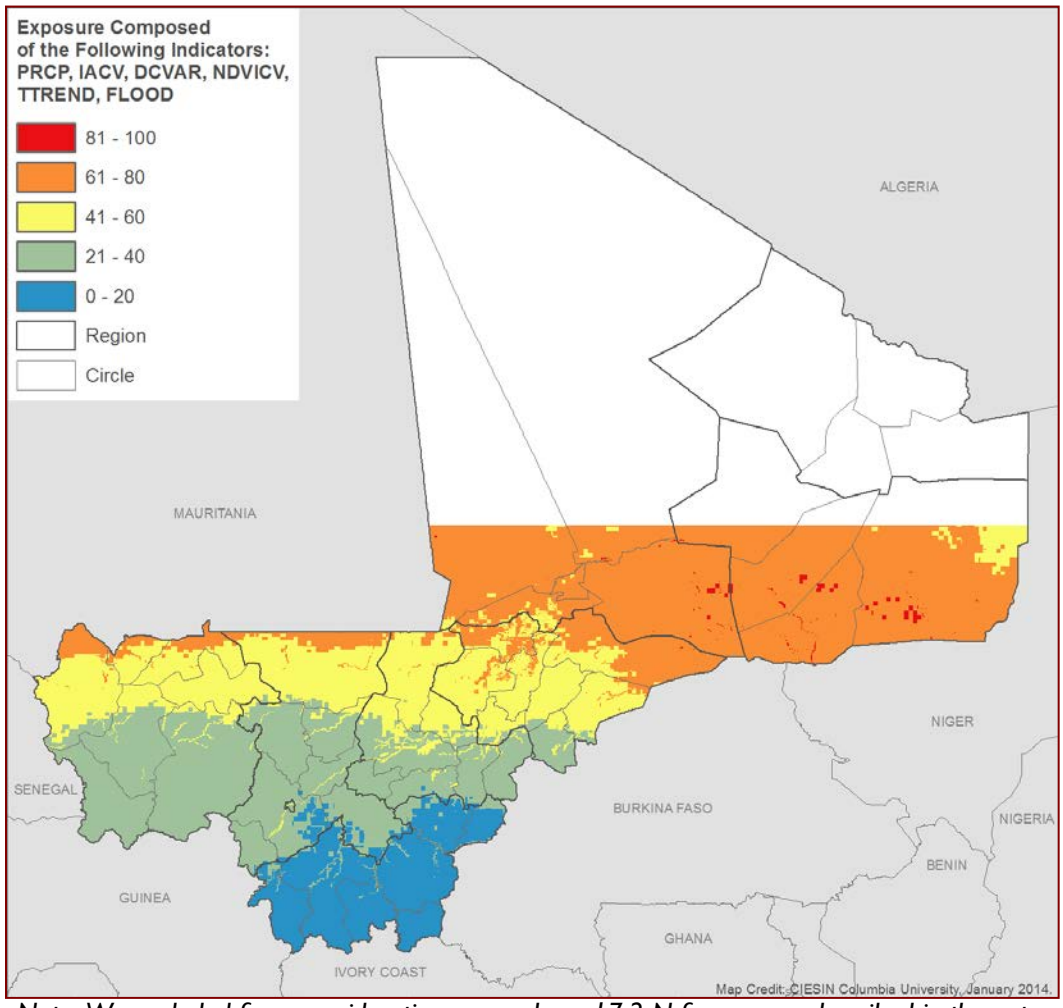

Note: We excluded from consideration areas above 17.2°N for reasons described in the note to Figure 5.

At an early stage, we explored an indicator that looks at changes in the number of years in two time periods (1990–2009 compared to 1950–1969), in which annual rainfall totals exceeded certain thresholds important to sorghum/millet (450mm) and cash crop/cotton (800mm) production. This approach created two bands — for 450mm in the north and 800mm in the south — with higher levels of exposure (Figure 2). What this points out is that changes in the reliability of rainfall along these two belts could be having important impacts on livelihoods in these regions. This idea would need to be validated by field data collection. In the end we decided not to include this information among the indicators in the exposure component or in the overall vulnerability map.

FIGURE 2. EXPOSURE COMPONENT INCLUDING THE PRECIPITATION THRESHOLD DATA

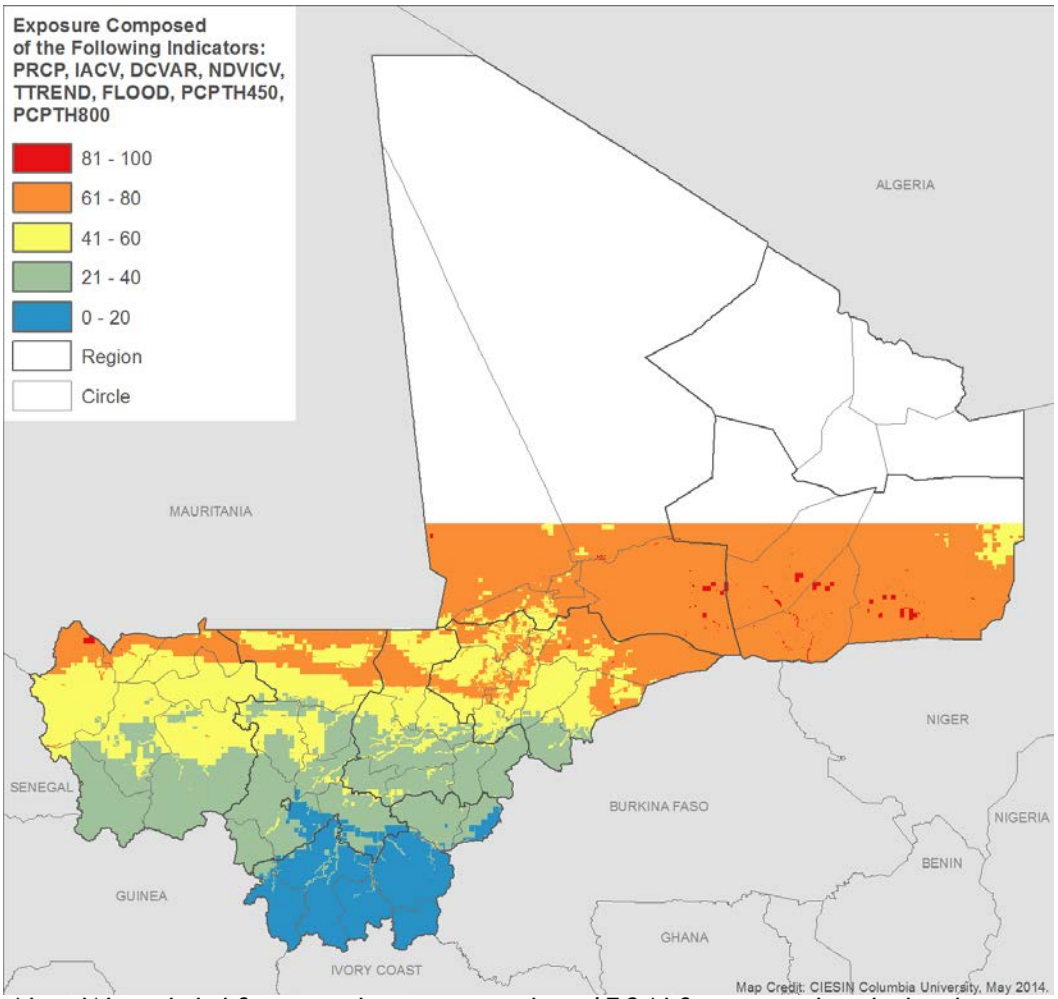

Note: We excluded from consideration areas above 17.2°N for reasons described in the note to Figure 5.

3.2 SENSITIVITY COMPONENT

The sensitivity component (Figure 3) reveals a pattern of generalized high to moderately high sensitivity across most of Mali, with pockets of lower vulnerability in the East and West as well as around Bamako. The high sensitivity in the southeastern portions of Mali reveals the influence of high infant mortality in this region. This region is also comparatively more densely settled (see Figure 7).

FIGURE 3. SENSITIVITY

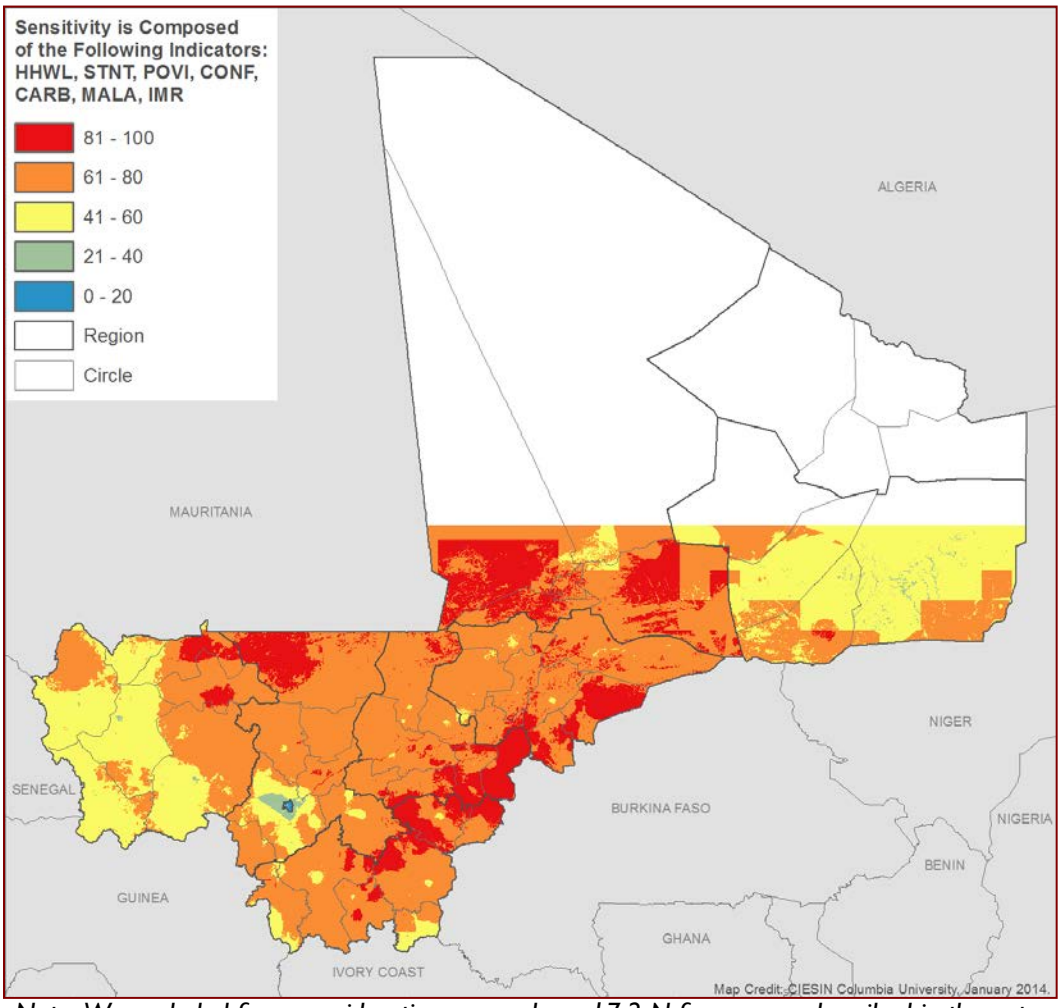

Note: We excluded from consideration areas above 17.2°N for reasons described in the note to Figure 5.

3.3 LACK OF ADAPTIVE CAPACITY COMPONENT

The lack of adaptive capacity component (Figure 4) has a fairly clear gradient, with adaptive capacity declining with distance from Bamako and from the Niger River. The results here are not overly surprising, reflecting the density of health posts and road infrastructure (and consequently market accessibility) in the areas around Bamako and southeastern Mali. Portions of the Niger River in northern Mali also have higher accessibility and a density of health infrastructure (e.g., around Timbuktu and Gao). In the West, the area around Kayes has higher adaptive capacity.

FIGURE 4. LACK OF ADAPTIVE CAPACITY

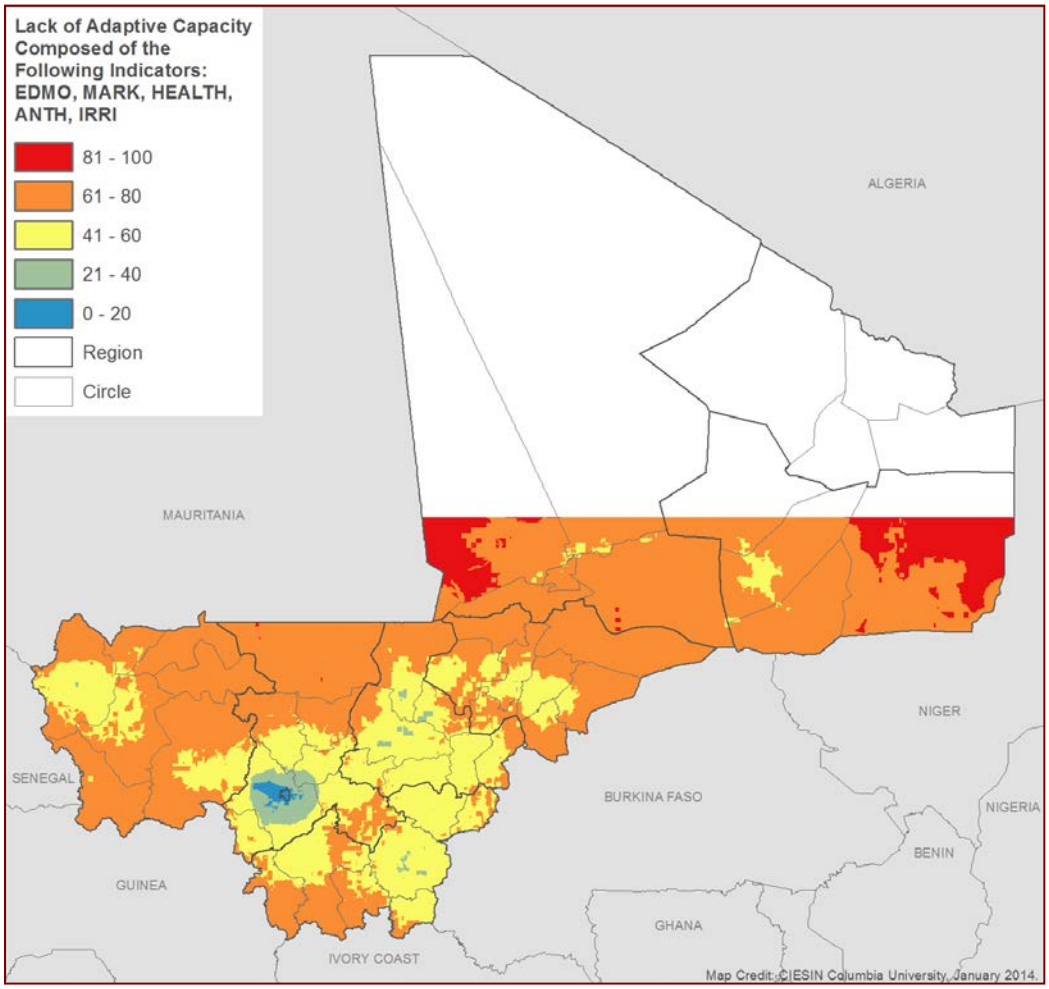

Note: We excluded from consideration areas above 17.2°N for reasons described in the note to Figure 5.

3.4 OVERALL VULNERABILITY

Figure 5 provides the overall vulnerability map, which averages the rescaled values from the exposure, sensitivity, and adaptive capacity components. (Annex II Figure A2-7 provides the same map, but with scores grouped in five quintiles, such that each quintile represents and equal area on the map, instead of five equal intervals.) Generally, vulnerability proceeds in a south-north gradient, with lowest vulnerability in the extreme south and around Bamako, and gradually increasing vulnerability northward with the exception of some areas of moderately low vulnerability in the Niger Delta and along the Niger River. In this map we have also included inset maps (Figure 5, bottom) that provide information on uncertainty levels in the DHS and climate data that provided the basis for seven out of 18 indicators. Although uncertainty levels cannot be assessed for all data sets, what these insets show is that error levels for the DHS and climate data are higher in regions to the west of Bamako and in the North owing to spatial gaps in measurements for both data sources (i.e., DHS sample clusters and meteorological stations). Results are more robust in areas that are white or lightly shaded in both inset maps; conversely, users should be more cautious about results in areas that are dark in both maps. Note that these maps reflect spatial gaps in measurement rather than measurement error *per se* (e.g., problems of survey design or instrumentation).

FIGURE 5. OVERALL VULNERABILITY INDEX

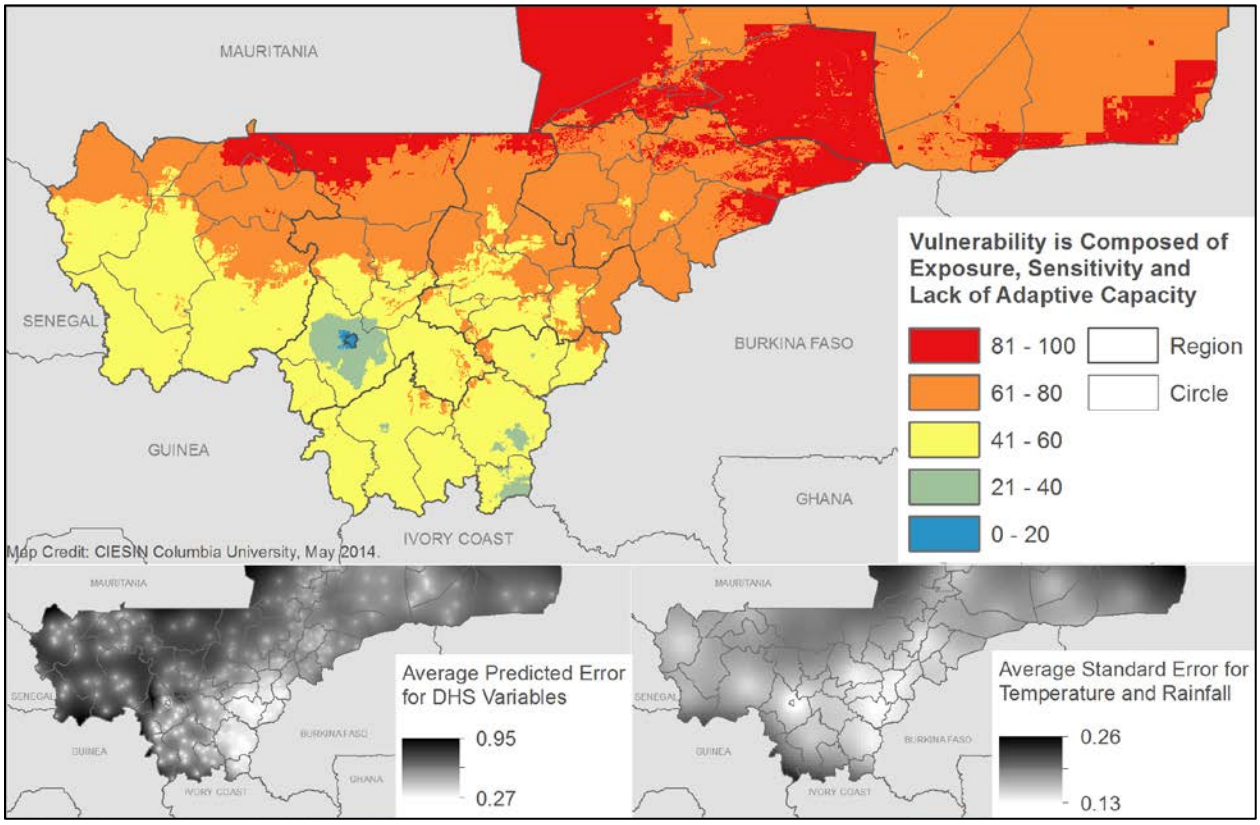

Note: In the normalization process we excluded from consideration all areas north of 17.2°N latitude, a region that is very sparsely populated. We did this for two reasons: (1) vulnerability results are less meaningful for a region that is so thinly populated and where climate variability and change may have less of an impact due to already harsh conditions, and (2) inclusion of indicator data values for this region might skew results (due to extreme values) for the remainder of Mali, which is the primary region of interest.

It is worth noting that the areas, population densities, and population counts vary substantially for each of the five vulnerability classes (Table 2). Approximately 40 percent of Mali's population resides in areas classified as medium vulnerability, and 32 percent reside in medium-high vulnerability. Only 6 percent reside in areas of highest vulnerability, and the population density in these mostly northern regions is only 7 persons per sq. km, compared with a density of more than 3,600 persons per sq. km for the low vulnerability category. The area of the lowest category is only 600 sq. km, and is confined to Bamako and its environs. The medium-high category comprises the largest area at almost 310,000 sq. km, or roughly one-quarter of Mali's total land area. Two of the adaptive capacity indicators, the health infrastructure index and market accessibility, are highly correlated with population density, and hence it should be noted that the vulnerability index is not completely independent of population distribution.

TABLE 2. AREA AND POPULATION STATISTICS FOR EACH VULNERABILITY CATEGORY

Vulnerability Index Categories	Area (sq. km)	Average Population Density (pop. / sq. km)	Population Count	% of Population
Low (0-20)	600	3,623	2,116,524	14.2
Medium-low (21-40)	11,034	104	1,107,342	7.4
Medium (41-60)	194,493	32	6,073,534	40.8
Medium-high (61-80)	307,357	16	4,727,328	31.8
High (81-100)	133,711	7	849,869	5.7

In Figures 6 and 7, we provide two reference maps that aid in analyzing results. Figure 6 provides a population density map for the year 2010. Figure 7 is the Sahel Regional "Supermap 2.0" of USAID Humanitarian and Development Programming and serves as a reference to visually compare how current USAID programming compares with climate vulnerability in mapping. In general, it is clear that development programing is concentrated in the more populated south, where climate vulnerability appears to be lowest. It is conceivable that USAID and other donor programming has contributed to lower vulnerability in this region than would otherwise have been the case.

FIGURE 6. POPULATION MAP OF MALI

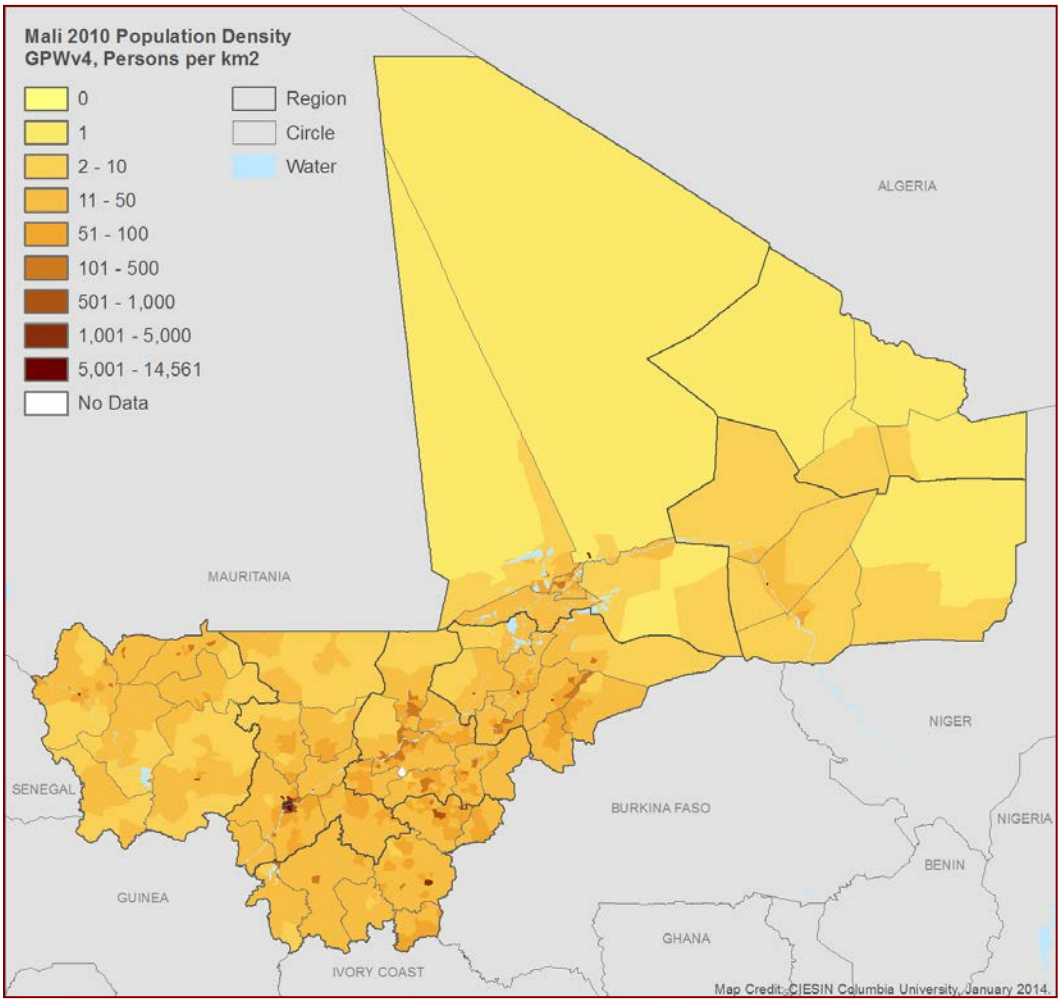

FIGURE 7. SAHEL "SUPERMAP" OF USAID PROGRAMMING

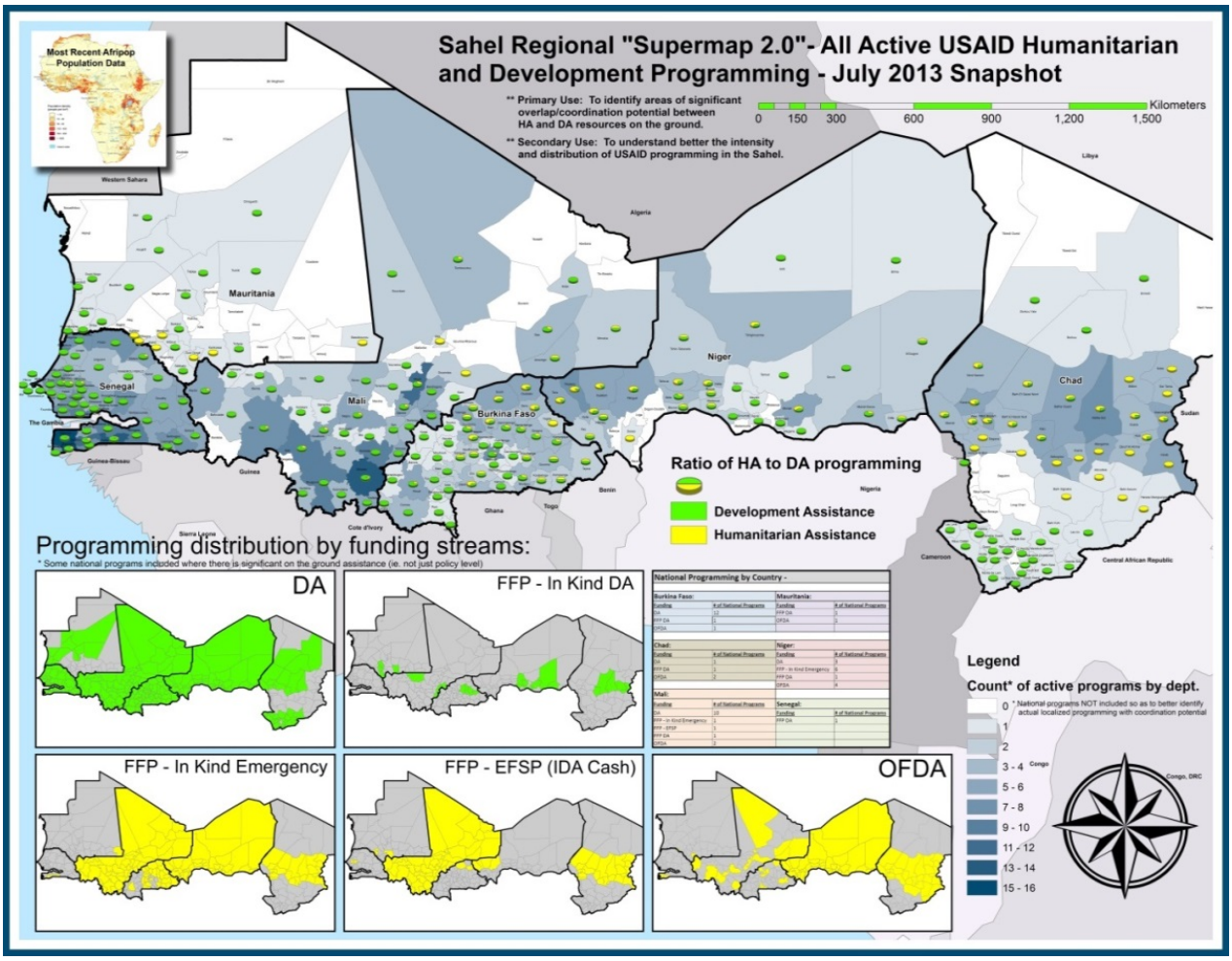

Source: Map courtesy of Jeremy Chevrier, USAID Dakar

3.5 FUTURE VULNERABILITY

Future scenarios were run for temperature trend (TTREND) and average annual precipitation (PRCP) based on RCP 4.5 and 8.5,[5] and for two 30-year time periods centered on 2030 and 2050. Details on the climate scenario data and methods, including the rationale and approaches to downscaling and bias-correction, are included in Annex I. It was not possible to project the other climate exposure indicators due to the fact that variability and extremes are difficult to capture with general circulation models (GCMs). Nor was it possible, given time and resource constraints, to develop future scenarios for the indicators included in the sensitivity and lack of adaptive capacity components.

The projected values for TTREND and PRCP were scaled in such a way that they could be lower or higher than the 0-100 historical time period scale, indicating reduced or increased exposure over the

[5] These RCP scenarios are named after a range of radiative forcing values in the year 2100 relative to pre-industrial values of +4.5 and +8.5 W/m^2, respectively. RCP 8.5 represents a warmer world than RCP 4.5 does.

baseline period (1950-2009). The approach for doing this was as follows. Because high values represent higher vulnerability for temperature trend (TTREND), in the historical period we calculated the transformed indicator value for a given pixel as follows:

Pixel Indicator Value = ((Pixel Raw Value - Y)/(X - Y))*100

Where X = Maximum Observed Value and Y = Minimum Observed Value in the raw data.

Because high values for precipitation (PRCP) represent lower vulnerability, we calculated the transformed indicator value for a pixel as follows (see also Table 3):

Pixel Indicator Value = 100-(((Pixel Raw Value - Y)/(X - Y))*100)

For the projected indicators, we wished to take into account the *incremental increase* or *decrease* in vulnerability as a result of climate change, so the transformed indicators were calculated using the historical minimum and maximum, and future indicator values were allowed to range from below 0 to above 100 (see lower half of Table 3), These future TTREND and PRCP indicator scores were then averaged with the other indicator scores that could not be projected.

TABLE 3. CALCULATION OF TRANSFORMED INDICATOR SCORES FOR HISTORICAL AND FUTURE VULNERABILITY (EXAMPLE OF PRCP)

Pixel Value (MM)	Historical Maximum (MM)	Historical Minimum (MM)	Transformed Indicator
Historical Values			
200	1200	200	100
400	1200	200	80
500	1200	200	70
800	1200	200	40
1200	1200	200	0
Future Projections			
100	1200	200	110
300	1200	200	90
400	1200	200	80
900	1200	200	30
1300	1200	200	-10

The projected normalized indicators for TTREND and PRCP were then aggregated per the methods described in Section 2.1, first into the exposure component, and then into an overall vulnerability index. To allow comparisons with current vulnerability and to highlight changes due to additional climate-related stress, the exposure component and vulnerability index were also normalized in a way that allowed them to exceed 100. While Annex 1 shows projected results for the multimodel average and "wet" and "dry" models, here we present only results for the multimodel average that is deemed to be the most probable projection. In total, there were four resulting exposure and vulnerability indices:

- Exposure and Vulnerability Index for Scenario RCP 4.5, year 2030
- Exposure and Vulnerability Index for Scenario RCP 4.5, year 2050
- Exposure and Vulnerability Index for Scenario RCP 8.5, year 2030
- Exposure and Vulnerability Index for Scenario RCP 8.5, year 2050

Figures 8 and 9 show the results. The overall patterns of exposure and vulnerability do not change, with highest exposure and vulnerability in the North, and lowest in the South and around Bamako. The levels of exposure and vulnerability estimated for the period centered on 2030 under both scenarios do not differ significantly from current levels, with the exception of increased exposure levels in the south. For the period centered on 2050, several areas will experience increased exposure with the extension of high levels further to the South and higher maximum levels in the North. This situation is particularly marked under RCP 8.5, where the lowest exposure category almost disappeared. It is further reflected in overall vulnerability for the 2030 timeframe, where changes are modest except in the southeastern portions of Mali. The increase in vulnerability is projected to be stronger in 2050, with larger areas of northern Mali being highly vulnerable, and the medium-high category covering almost the entire country for RCP 8.5 with the exception of the region surrounding Bamako.

Figure 10 provides a difference map for the RCP 8.5 scenario in 2050 compared to the baseline vulnerability map (Figure 5), which can be interpreted as the additional vulnerability that will result from the most extreme climate scenario.

FIGURE 8. EXPOSURE FOR SCENARIO RCP 4.5 (A) YEAR 2030 AND (B) YEAR 2050; AND RCP 8.5 (C) YEAR 2030 AND (D) YEAR 2050

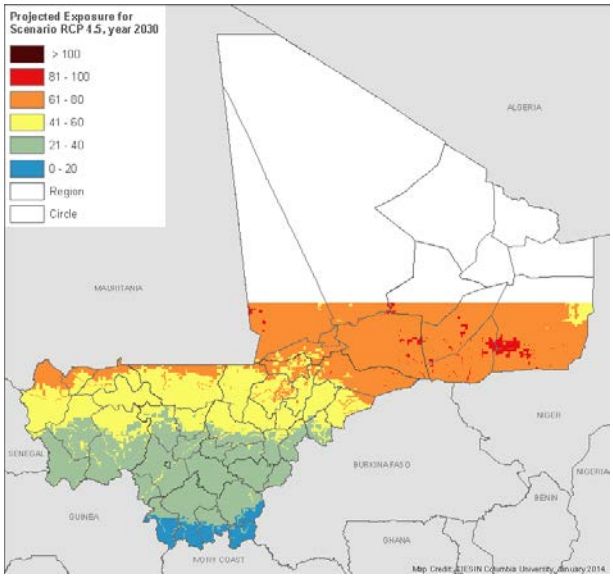

(a)

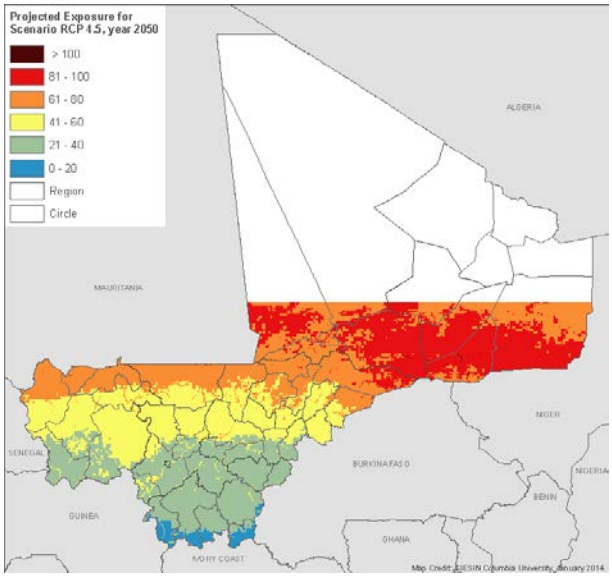

(b)

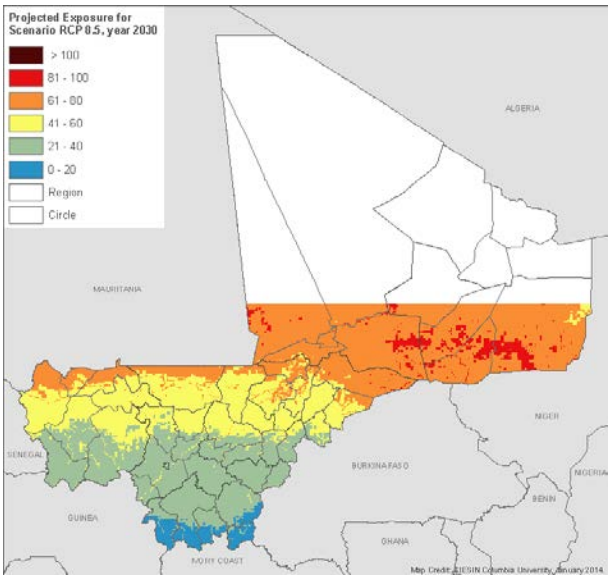

(c)

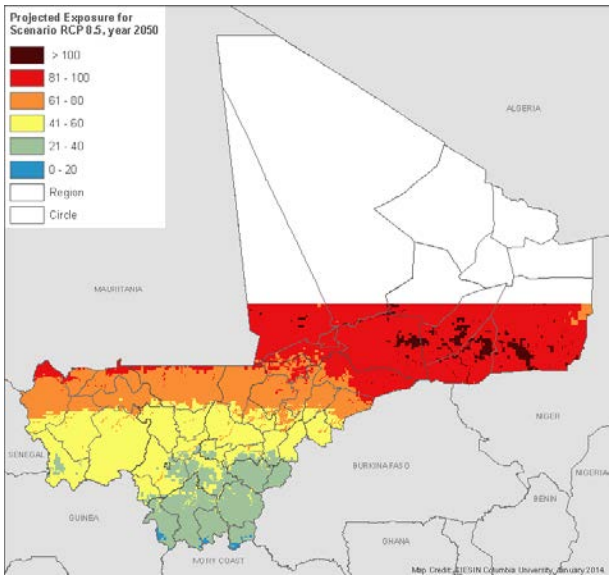

(d)

FIGURE 9. VULNERABILITY INDEX FOR SCENARIO RCP 8.5 (A) YEAR 2030 AND (B) YEAR 2050; AND RCP8.5 (C) YEAR 2030 AND (D) YEAR 2050

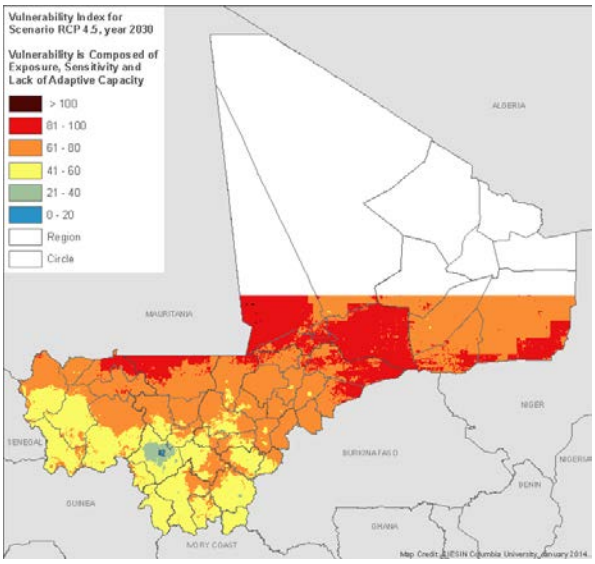

(a)

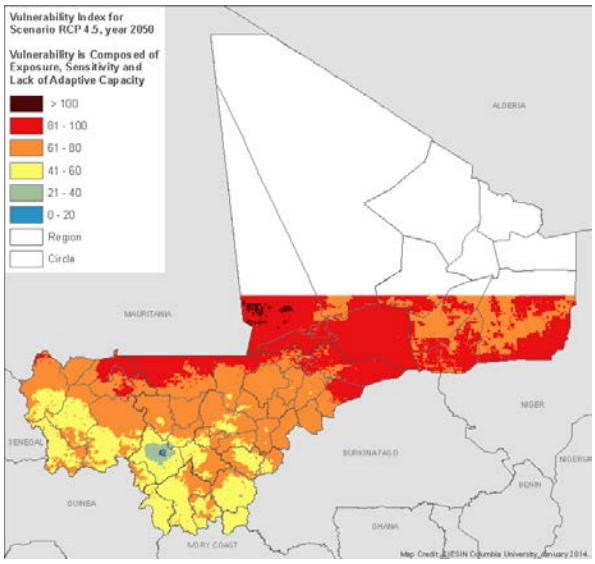

(b)

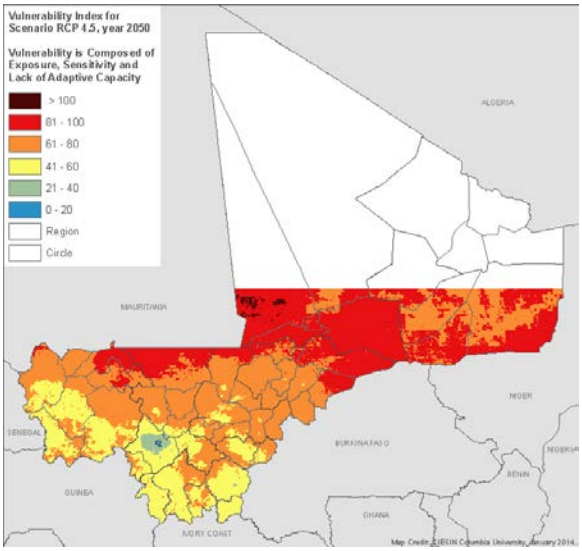

(c)

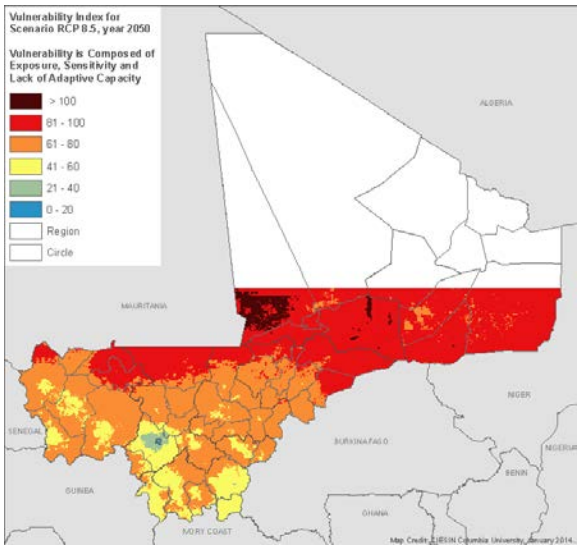

(d)

FIGURE 10. ADDITIONAL VULNERABILITY RESULTING FROM THE MOST EXTREME CLIMATE SCENARIO (RCP 8.5 2050 SCENARIO)

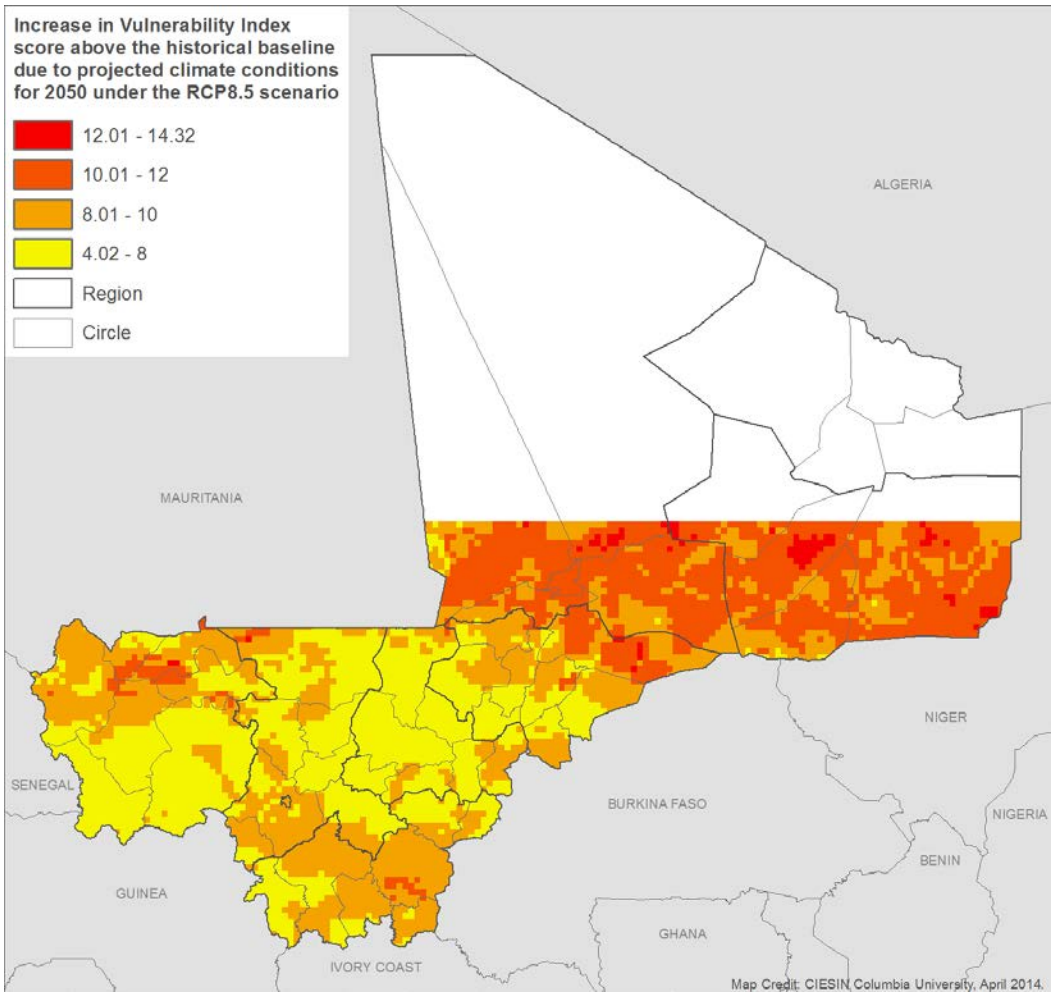

It should be emphasized that the projected changes in exposure indicators do not include changes in variability, and that the exposure indicator set did not include parameters most relevant to agriculture, such as temperature thresholds for crops, delays in rainy season onset, or projected gaps in rainfall during the rainy season. Thus, projected changes in exposure are most likely underestimated. Temperature increases are also likely to have significant impacts on potential evapotranspiration, rendering regions that are already marginal for rain-fed agriculture completely unproductive. In a changing climate, therefore, it is likely that future overall vulnerability will change more than is represented in these maps.

4.0 DISCUSSION AND CONCLUSIONS

4.1 ISSUES WITH THE SPATIAL INDEX APPROACH

There are a number of issues with vulnerability index construction more broadly that affect our results (for a more detailed discussion, see de Sherbinin [2014]). These issues are addressed here in the interest of transparency, and so that the results can be better interpreted.

The first issue is the relationships among the indicators. The reality is that the research community does not fully understand the functional form of the relationship among indicators or among the components that contribute to vulnerability (Hinkel, 2011). For example, in our current method, which follows standard practice, we assume that the observed minimum and maximum values (or their winsorized equivalents) have the same meaning across input layers. For example, the method implies that a travel time of 36 hours (2,160 minutes) to the nearest population center has the same impact on sensitivity and adaptive capacity as having an infant mortality rate (IMR) of 135 deaths per 1,000 live births, since both have a transformed score of 100. However, it is probable that an area with an IMR of 135 is significantly more vulnerable. Another simple factor that makes the extremes not comparable is that for some indicators, the values are based on an interpolated surface with high spatial precision, which generates more extreme values or "long tails" in the data distribution (e.g., market accessibility). Others (e.g., IMR and the poverty index by commune) are averaged within spatial units, which artificially reduces the extremes.[6] Although we have trimmed the tails of the continuous raster surfaces in such a way as to increase the vulnerability scores for lower values on the raw scale, we do not have empirical evidence that would allow us to benchmark any two indicators to any "absolute" vulnerability level. Vulnerability is a construct, the outcome of complex interactions in the coupled human-environment system; not an objective state.[7]

Following standard practice, another assumption we make is to assume a linear relationship between the input layers and the conceptual category being measured. But the functional relationship might be very different. It might be a step function, or sigmoid, or asymptotic if there are critical thresholds involved; or it might be exponential if high values trigger cascading problems that do not show up at lower levels. We considered taking the natural logarithm of the raw data as part of the transformation process for some indicators but did not have a strong theoretical justification for doing so.

The interaction among the components is another issue. Currently we use an additive approach, but the interaction might be multiplicative. For example, if capacity is high enough, it may not matter much if your sensitivity or exposure is very high. Another way to put this is that the assumption that the three components are fungible — that good levels in one component compensate for bad levels in another,

---

[6] Most of our indicators derived from DHS results were based on surfaces interpolated between survey cluster points, which avoided the problem of spatial averaging at the region level. As discussed in Section 2, we doubled the weights for these indicators.

[7] The literature speaks of vulnerability being an emergent phenomena (Birkmann and Fernando, 2008). It is revealed when the system is stressed by climatic, economic, or other shocks and perturbations.

across the whole range of values — might not be true. For example, it could be that, if over time a given area moved from the 60th to 80th percentile in the exposure indicator, it would have such dramatic impacts on overall vulnerability that it would not really make a difference if the same area moved from the 30th to the 10th percentile on the capacity indicator. Even if the core relationship is additive, we currently assume equal weights across components, but the relationship to overall vulnerability may be very different. For example, it could be that one unit of exposure has the same effect on vulnerability as 10 units in sensitivity.

The PCA overcomes some of the shortcomings of the additive approach by not assuming any prior relationships among the indicators, but allowing those relationships to emerge from the analysis. As Abson et al. (2012) state:

> [T]he generation of a single composite vulnerability index using a normalization/ summation approach, is problematic because potentially important information regarding the relations between the original variables are obscured in the resulting unitless, aggregated index (from many indicators to a single index). Moreover, when mapping socio-ecological vulnerability across large spatial extents (and therefore across diverse socio-ecological systems) it is likely that drivers of vulnerability will vary considerably across space. (p.516)

For this reason, we provide the PCA as an alternative aggregation method (Annex II). The overall results are fairly similar to the additive approach, though indicators reflecting proximity to major settlements, market accessibility, and health infrastructure appear to play a stronger role.

4.2 CONCLUSION

The maps in this report provide additional information for climate adaptation decision making in Mali. Although data-driven decision making using maps such as these is clearly preferable to decision-making based solely on intuition, convenience, or political considerations, it is important to remember the caveats listed above concerning the limitations of this kind of exercise. Although the overall vulnerability map (Figure 5) provides some useful information for programming, a great deal of additional information can be gleaned by reviewing the component maps, the PCA maps (Annex II), and the individual indicator maps in Annex IV.[8] Further analyses could also be constructed using a subset of data layers deemed to be most relevant for a particular development programming or resource allocation task.

Overall, the results are not overly surprising, since the northern regions are known to be climatically more marginal and also more remote and less economically developed. The influence of the recent conflict in northern Mali, which is only reflected in the conflict indicator (which extends through 2012), is likely to have only increased this region's overall climate vulnerability. The sensitivity map (Figure 3) shows relatively high sensitivity (or "social vulnerability") in southeastern Mali, a relatively densely settled region that also receives a higher proportion of USAID programming. The lower sensitivity in eastern Mali (around Gao) and western Mali (south of Kayes) is influenced by the relatively coarse resolution IMR data but is borne out by a number of other sensitivity metrics such as child stunting,

[8] A discussion of the statistical relationships among the indicators is found in Annex II. A number of the indicators are strongly spatially auto-correlated, including the exposure indicators and biophysical indicators such as soil carbon and malaria endemicity, which are strongly influenced by precipitation.

household wealth, and the poverty index. It would be interesting to see if DHS results for 2012 confirm the lower IMR and poverty metrics in these two regions.[9]

Particular attention may need to be paid to regions already at the margin of agriculture, as described in Figure 3 in Section 3.1 (see the accompanying text) and discussed at the end of Section 3.5. It is likely that the northern limit of rain-fed agriculture has shifted south due to temperature increase and that it will continue to do so as temperatures rise.

[9] The 2012 DHS survey results were not ready for public release at the time of this mapping exercise.

5.0 REFERENCES

Abson, D.J., A.J. Dougill, and L.C. Stringer. (2012). Using Principal Component Analysis for information-rich socio-ecological vulnerability mapping in Southern Africa. *Applied Geography*, 35:515-524.

Baptista, S. (2014). *Design and Use of Composite Indices in Assessments of Climate Change Vulnerability and Resilience*. Technical Paper for the USAID African and Latin American Resilience to Climate Change (ARCC) project. Washington, DC: USAID.

Baptista, S., L. Brottem, A. de Sherbinin, M. Edquist, A. Fischer, M. Levy, E. Schnarr, C. Simon, P.V. Sundreshwar, and S. Trzaska. (2013). *Background Paper for the ARCC West Africa Regional Climate Change Vulnerability Assessment*. Technical Paper for the USAID African and Latin American Resilience to Climate Change (ARCC) project. Washington, DC: USAID.

Birkmann, J., & N. Fernando. (2008). Measuring revealed and emergent vulnerabilities of coastal communities to tsunami in Sri Lanka. *Disasters*, 32(1):82-105. doi: 10.1111/j.1467-7717.2007.01028.x.

de Sherbinin, A. (2014). *Spatial Climate Change Vulnerability Assessments: A Review of Data, Methods and Issues*. Technical Paper for the USAID African and Latin American Resilience to Climate Change (ARCC) project. Washington, DC: USAID.

de Sherbinin, A. (2009). The Biophysical and Geographical Correlates of Child Malnutrition in Africa. *Population, Space and Place,* 15. Available at: http://dx.doi.org/10.1002/psp.599.

Funk, C., Michaelsen, J., and Marshall, M. (2012). Mapping recent decadal climate variations in precipitation and temperature across Eastern Africa and the Sahel, chap. 14 *in* Wardlow, B., Anderson, M., and Verdin, J., eds., *Remote sensing of drought—Innovative monitoring approaches*. London, UK: Taylor and Francis.

Füssel, H.-M. (2009). *Review and quantitative analysis of indices of climate change exposure, adaptive capacity, sensitivity, and impacts*. Background note to the World Development Report 2010. Washington, DC: World Bank.

Hinkel, J. (2011). "Indicators of vulnerability and adaptive capacity": Towards a clarification of the science–policy interface. *Global Environmental Change*, 21, 198-208.

Midgley, S. J. E., R. A. G. Davies & S. Chesterman. (2011). Climate risk and vulnerability mapping in southern Africa: status quo (2008) and future (2050). Report produced for the Regional Climate Change Programme for Southern Africa (RCCP), UK Department for International Development (DFID). Cape Town, South Africa: OneWorld Sustainable Investments.

OECD. (2008). *Handbook on constructing composite indicators: methodology and user guide*. Paris: Organization for Economic Co-operation and Development.

Thow, A., & M. de Blois. (2008). *Climate change and human vulnerability: Mapping emerging trends and risk hotspots for humanitarian actors*. Bath, UK and Geneva, Switzerland: Maplecroft, and CARE International.

Wikipedia. (2014). Kayes Region. Available at http://en.wikipedia.org/wiki/Kayes_Region.

Yusuf, A.A., & H. Francisco. (2009). *Climate Change Vulnerability Mapping for Southeast Asia.* Singapore: EEPSEA.

ANNEX I. FUTURE CLIMATE SCENARIOS

AI.1 RATIONALE FOR DOWNSCALING AND BIAS-CORRECTION

Future climate conditions are estimated using General Circulation Models (GCMs), which are state-of-the-art numerical representations of physical and chemical processes within the climate system. GCMs are used to simulate the effects of greenhouse gas emissions on atmospheric composition, and then to estimate the effects of changes in atmospheric composition on atmospheric and oceanic circulation, temperature, and rainfall. While those models represent the processes in the climatic system to the best of our current knowledge and technological capacity, they remain an imperfect representation of the system and better capture general characteristics of large climatic systems, such as monsoon systems, than climate conditions in a given location. In particular, it is well established that in their representation of the West African Monsoons, the main system driving the climate in West Africa, GCMs capture reasonably well the northward shift between May and October and southward retreat from November to April. But the exact amplitude and timing of this shift, and the exact amounts of rainfall produced, can be over- or under-estimated. This situation is partly due to a relatively coarse resolution of the models that cannot capture many of the local features such as water bodies, mountain ranges, and changes in land cover. In addition, in the Sahel, the models underestimate the inter-annual and decadal variability and are not able to capture the wet period during the 1950s or the drought in the 1970s and 1980s (Biasutti, 2013).

Therefore, it is usually recommended to correct such systematic biases *a posteriori* either by 1) using regional models that only cover small parts of the globe, have higher resolution, and capture many local features; or 2) by statistically adjusting rainfall amounts, average temperature, and other climate variables based on local observations. The latter method downscales changes in large-scale climate produced by the GCMs to any resolution/location, while regional models remain limited to resolutions above 10x10km and carry some of GCMs' systematic biases. In this study, we chose to use a statistical downscaling method to derive projections in climate characteristics (rainfall and temperature) for each of the grid cells of the initial observed historical rainfall and temperature data.

In addition to the downscaling, the analysis of projections involved the assessment of the uncertainty in the projections by considering outputs from several models, each having distinct characteristics and systematic biases.

AI.2 DATA AND METHODS

GCMs outputs at nominal resolution between 100x100km and 300x300km were obtained from the Coupled Model Intercomparison Project Phase 5 (CMIP5), the official archive of the latest IPCC assessment. We retrieved data from 10 different models and under two emission scenarios, the RCP4.5 (corresponding to a 'steady state' of current emission levels) and RCP8.5 (corresponding to increased emissions over time). Table A1-1 summarizes the models used. Projections of precipitation and temperature were retrieved for the period 2015–2065. These were further split into two 30-year periods, 2015–2045 and 2035–2065, with corresponding period midpoints of 2030 and 2050 respectively. Thirty-year periods are the standard for assessing average climate characteristics. In

addition, to project values, GCM values for the historical period 1971–2005 were also obtained and used in the bias correction and downscaling.

TABLE A1-1: GCMS USED TO DERIVE THE PROJECTIONS, INCLUDING THE COUNTRY AND THE INSTITUTION THAT DEVELOPED THE MODEL AND MODELS RESOLUTION

Model	CanESM2	CCSM4	CNRM-CM5	CSIRO-Mk3-6-0	GISS-E2-R	Had GEM 2-ES	MIROC-ESM	MIROC 5	MPI-ESM-LR	MRI-CGCM3
Lab	CCCMA	NCAR	CNRM-CERFACS	CSIRO-QCCCE	NASA GISS	MOHC	MIROC	MIROC	MPI	MRI
Country of origin	Canada	USA	France	Australia	USA	UK	Japan	Japan	Germany	Japan
Reso-lution in degrees (lat. x long.)	2.8x2.8	0.9x1.25	1.4x1.4	1.87x1.87	2x2.3	1.25x 1.87	2.81x2.81	1.4x1.4	1.8x1.8	1.125x 1.125

Note: At the equator, 1 degree latitude or longitude corresponds to 110 km.

FIGURE A1-1. ILLUSTRATION OF MODEL'S RESOLUTION: (A) IS A LOW-RESOLUTION MODEL, AND (B) IS A HIGH-RESOLUTION MODEL

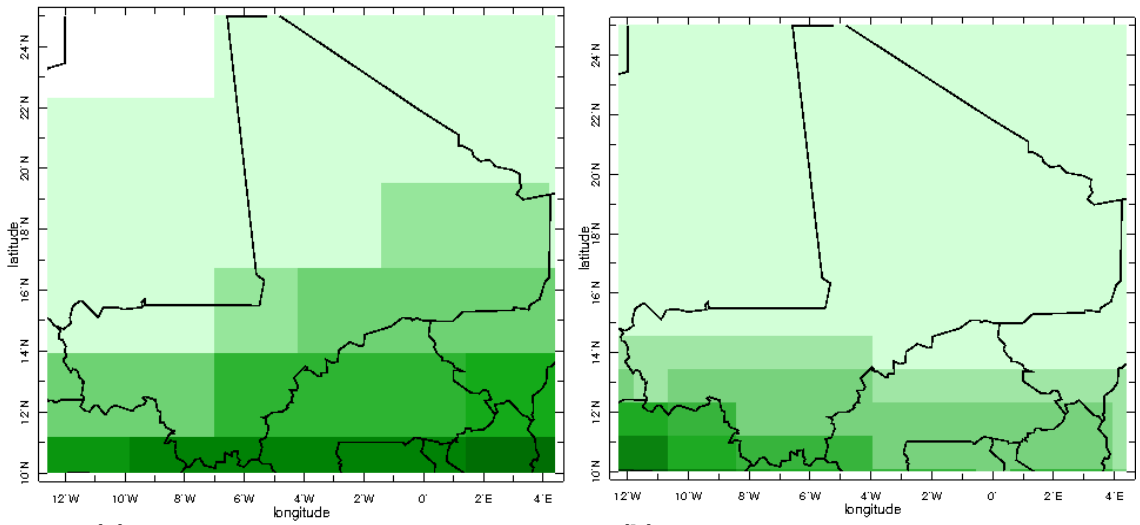

(a) **(b)**

Raw GCM outputs were statistically downscaled focusing on correcting the biases in the timing of the rainy season, magnitude of rainfall, temperature, and other variables as well as amplitude of their inter-annual variability (which the models tend to underestimate). To achieve this downscaling, a multistep procedure was applied using monthly records of rainfall and temperature observed in Mali from Funk et al. (2012):

1. For each grid point in the observations and each model, a grid point with the seasonal cycle of rainfall that best matches the average observed seasonal cycle was determined.
2. Linear regressions between monthly rainfall values observed and simulated in matching grid points over the historical period were then computed for each calendar month (January to December)

using ranked values.[10] Those regression equations were then used to predict bias-corrected values of projections, with raw projections used as predictor. In other words, rainfall and temperature projected by the GCMs are used as predictors to derive more realistic values based on predictive relationships established using observations and simulations of the historical climate. The bias-corrected historical average seasonal cycle using those regressions perfectly matches the average observed seasonal cycle (not shown).

A multi-model average is believed to be the most probable climate of the future (IPCC 2007). Therefore, average characteristics computed over the two 30-year periods centered on 2030 and 2050 were computed for the average of all models. Variations in projected conditions between models are shown as 'dry' and 'wet' models, ranking respectively as 2nd and 8th out of 10 models in terms of annual precipitations averaged over the box encompassing Mali. Only annual rainfall and temperature trends are presented. Other variables, such as the coefficient of variation or decadal variance, are not reliable in the models.

AI.3 RESULTS

Figure A1-2 at the end of this section provides the historical precipitation amounts and temperature trends for reference, while Figures A1-3 to A1-6 provide the map figures for the projection results for precipitation and temperature. Note that there is not always a simple association between driest and warmest models or wettest and coolest models. On one hand, the rain-producing phenomenon, the West African monsoon, is driven by the temperature difference between the ocean to the south (cooler) and the interior of the land (warmer). Its strength depends on the strength of this difference. On the other hand, rain cools land surface through evaporation and the shading effects of the clouds; so the wetter the rainy season, the cooler the temperature. Thus, some models may produce cooler temperatures because of stronger rainfall, while other models may produce stronger rainfall because of warmer inland temperatures. All of those pathways are possible and they should be interpreted as possible scenarios for rainfall and temperature evolution in Mali.

For rainfall, annual totals in mm/year are presented using the same scale as the observations. The overall structure of rainfall, decreasing from south to north, is projected to remain the same in the future; generally few changes are projected, irrespective of the emission scenario and time horizon. The spread among the models is not very large, especially for projected rainfall for the period represented by the 2030 midpoint. The differences between the 'dry' and the 'wet' models are more apparent for the period represented by the 2050 midpoint under both RCP scenarios.

As with the historical climate conditions, for temperatures, linear trends in degrees-Celsius increase per decade were computed. Under the RCP4.5 scenarios, the average trend over the next three decades is similar to current trends in amplitude and spatial patterns; it only slightly increases in the following decades. The driest model projects temperature increases that are slightly slower than the current rate, but the multimodel and the wet model point to a slightly faster increase. But even in those slowly warming conditions, the evapotranspirative demand on plants will increase, affecting the sustainability of agriculture especially in the fastest-warming zones in the north, which are also drier.

[10] GCMs are not expected to reproduce the exact historical time-series of rainfall, temperature, and other variables observed in a given location; only statistical characteristics such as average monthly rainfall and its standard deviation are expected to coincide with the observations. Thus regression models cannot be constructed by associating observed and simulated values in time. We chose here to construct the relationships based on values that were ranked from smallest to largest in the historical and simulated series. In that way, bias in the amplitude of the variability can also be corrected.

Under RCP8.5 scenarios, the projected warming is faster everywhere but especially so in the dry zones. The slowest warming rates are projected by the wettest model in the southern half of the country, where it is projected to warm at a rate similar to that of current trends. The driest regions, however, are projected to warm under this scenario faster than they warm under RCP4.5. The multi-model average suggests a warming rate three times the current rate in the 2050 period, with the northern parts warming faster than the south. The only exception is the model that projects the driest conditions in the 2050 period, with faster warming trends in the southern parts of the country probably due to drier conditions there. The wettest model, on the other hand, projects the slowest warming trends in the same areas; the spread between the results in the 2050s period under the RCP8.5 scenario is slightly higher than the spread for other wet and dry scenarios.

AI.4 CONCLUSIONS

Bias-corrected and downscaled outputs of 10 models of different resolution point to small changes in rainfall over Mali, with the wettest model projecting slightly wetter conditions and the driest model projecting slightly drier conditions. All models, however, project steady warming, with rates ranging from close to current rates to three times the current rates. In most cases, northern, drier regions are projected to warm the fastest. This occurrence may adversely impact agricultural production, because the evapotranspirative demand of crops may no longer be met. Moreover, the upper temperature limit may be reached for certain crops. Further studies might be needed to more precisely investigate the impact that the increase in temperature could have on agriculture in those areas.

AI.5 REFERENCES

Biasutti, M. (2013). Forced Sahel rainfall trends in the CMIP5 archive, *Journal of Geophysical Research on the Atmosphere*, 118, 1613–1623.

Funk, C., Michaelsen, J., and Marshall, M. (2012). Mapping recent decadal climate variations in precipitation and temperature across Eastern Africa and the Sahel, chap. 14 *in* Wardlow, B., Anderson, M., and Verdin, J., eds., *Remote sensing of drought—Innovative monitoring approaches*. London, UK: Taylor and Francis.

Intergovernmental Planel on Climate Change. (2007). *Climate Change 2007: The Physical Science Basis*. Contribution of Working Group I to the Fourth Assessment Report of the Intergovernmental Panel on Climate Change [Solomon, S., D. Qin, M. Manning, Z. Chen, M. Marquis, K.B. Averyt, M. Tignor, and H.L. Miller (eds.)]. Cambridge University Press, Cambridge, United Kingdom; and New York, NY, USA.

FIGURE A1-2. OBSERVED TOTAL ANNUAL RAINFALL AND TEMPERATURE TRENDS

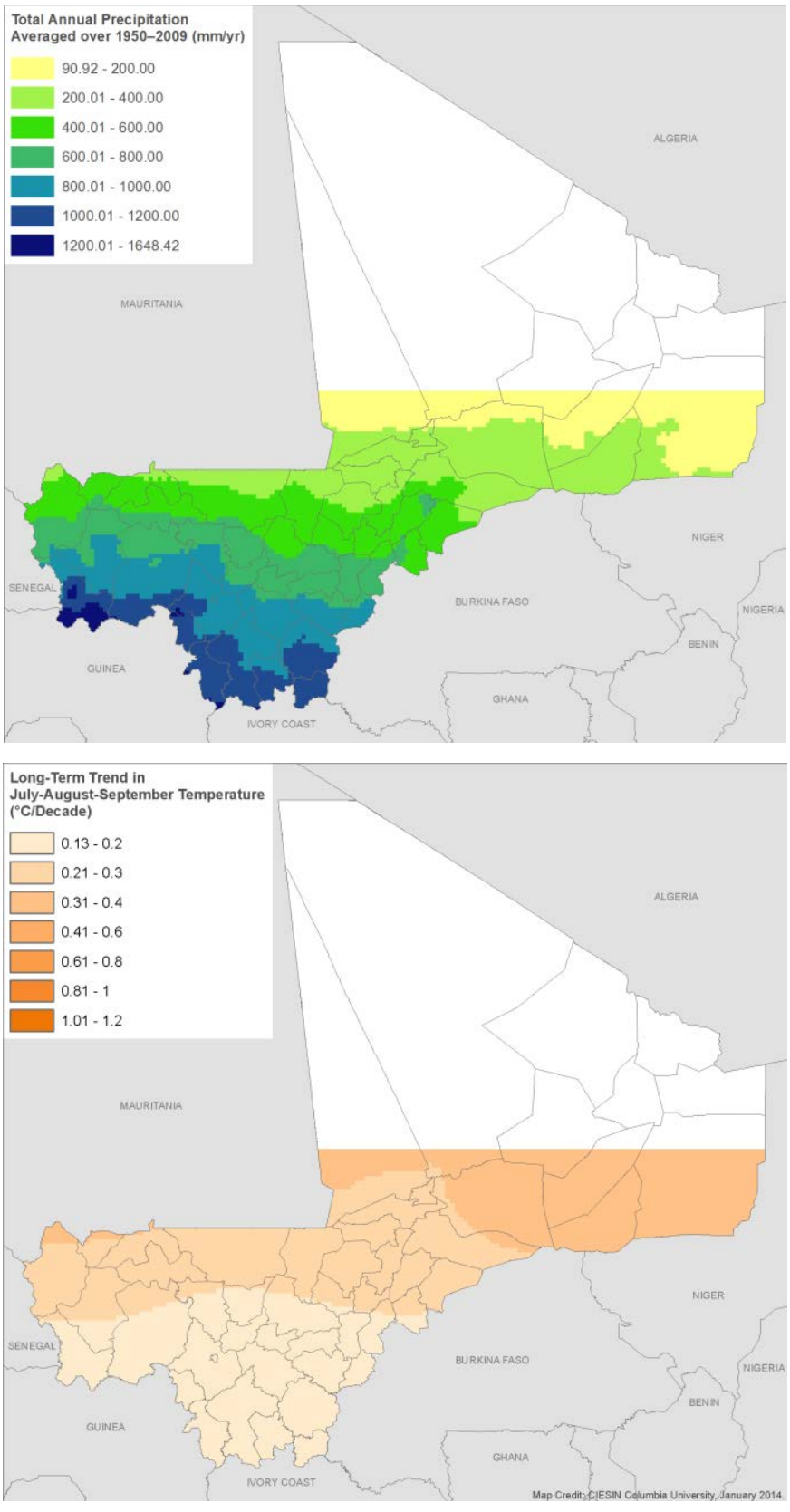

FIGURE AI-3: PROJECTED TOTAL ANNUAL RAINFALL AND TEMPERATURE TRENDS FOR 2030 (2015-2045) PERIOD UNDER RCP4.5 SCENARIO
(LEFT COLUMN: DRY MODEL; MIDDLE COLUMN: MULTIMODEL AVERAGE; RIGHT COLUMN: WET MODEL)

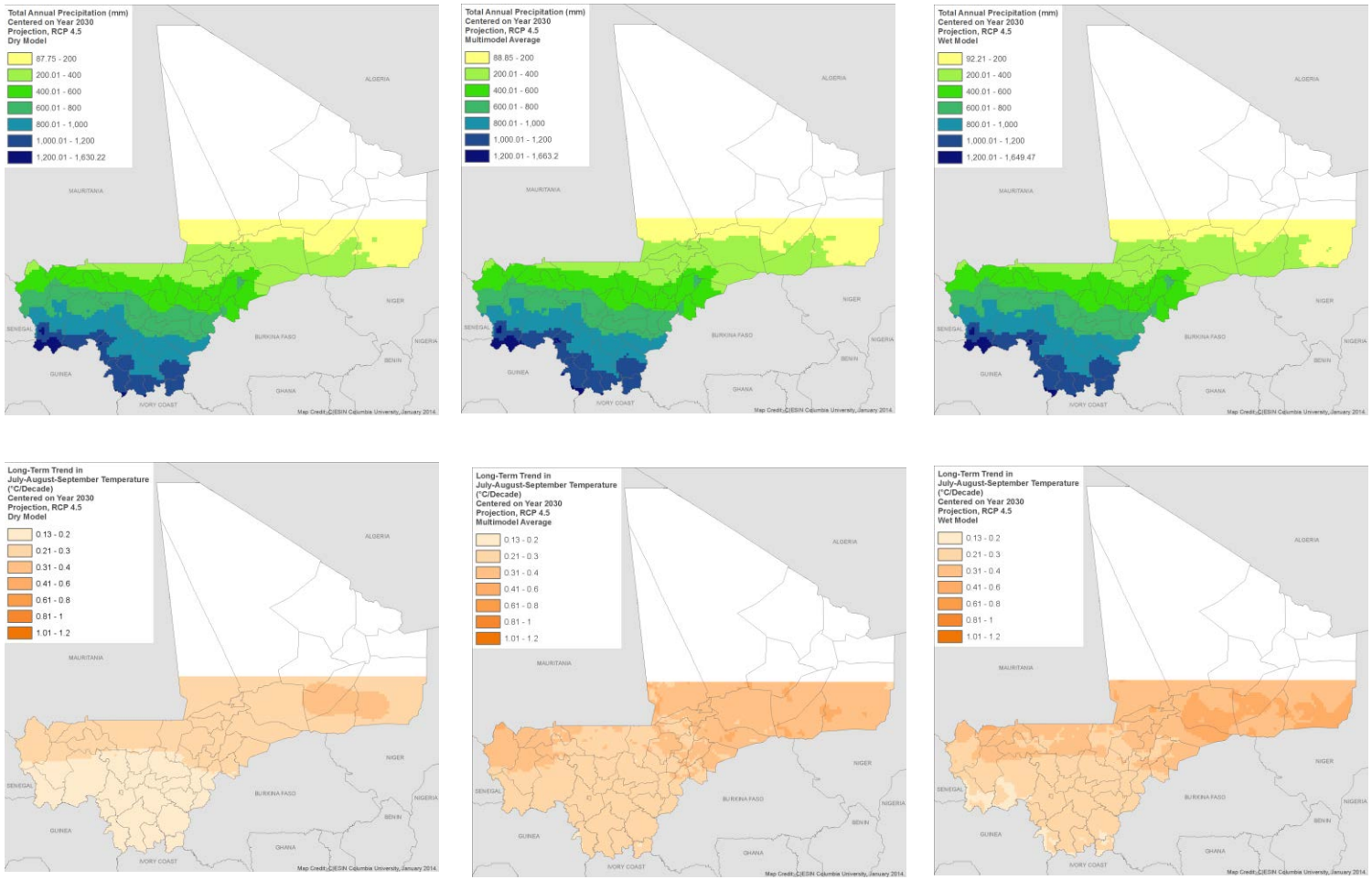

FIGURE AI-4. PROJECTED TOTAL ANNUAL RAINFALL AND TEMPERATURE TRENDS FOR 2050 (2045-2065) PERIOD UNDER RCP4.5 SCENARIO.
(LEFT COLUMN: DRY MODEL; MIDDLE COLUMN: MULTIMODEL AVERAGE; RIGHT COLUMN: WET MODEL)

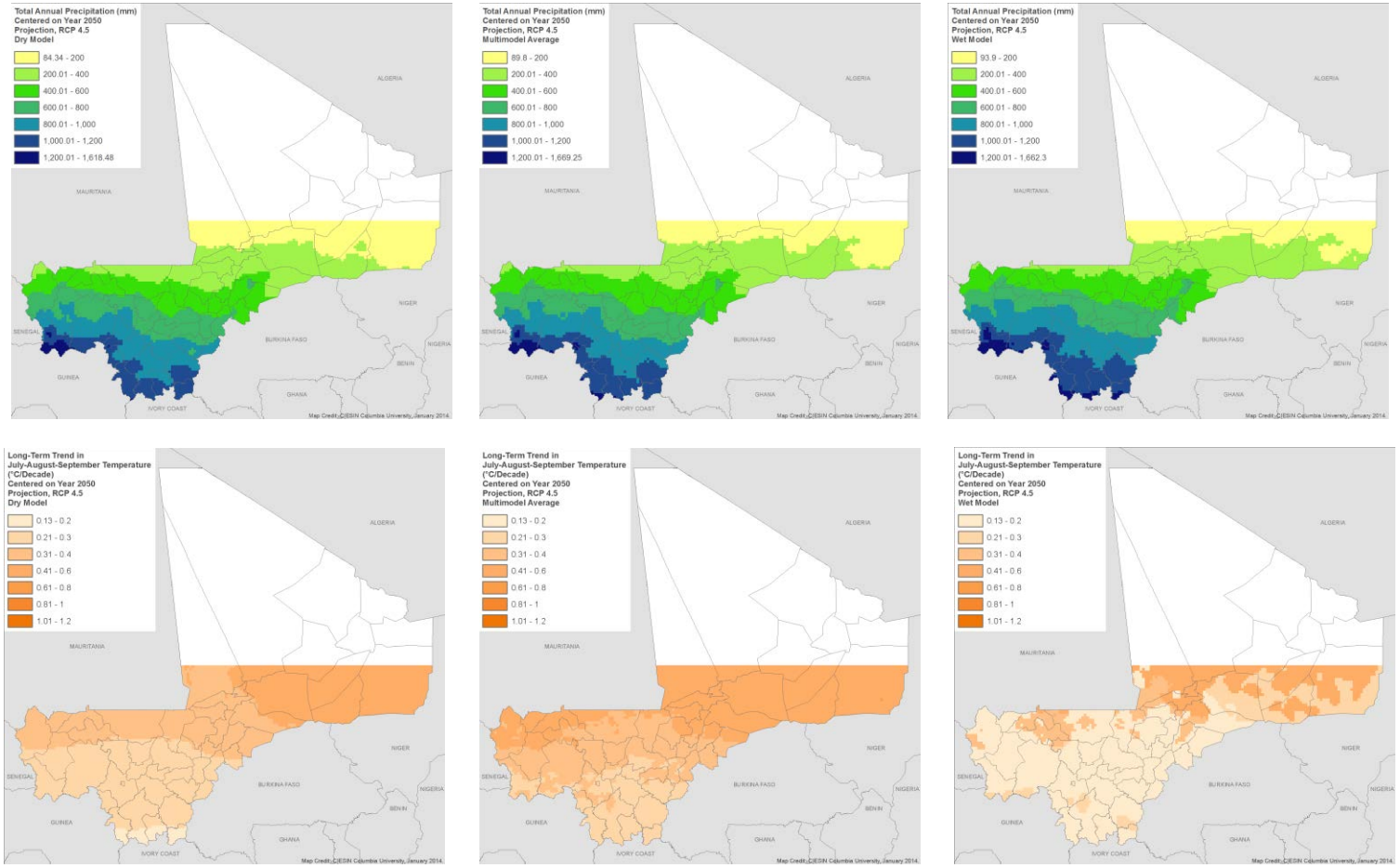

FIGURE A1-5. PROJECTED TOTAL ANNUAL RAINFALL AND TEMPERATURE TRENDS FOR 2030 (2015-2045) PERIOD UNDER RCP8.5 SCENARIO.
(LEFT COLUMN: DRY MODEL; MIDDLE COLUMN: MULTIMODEL AVERAGE; RIGHT COLUMN: WET MODEL)

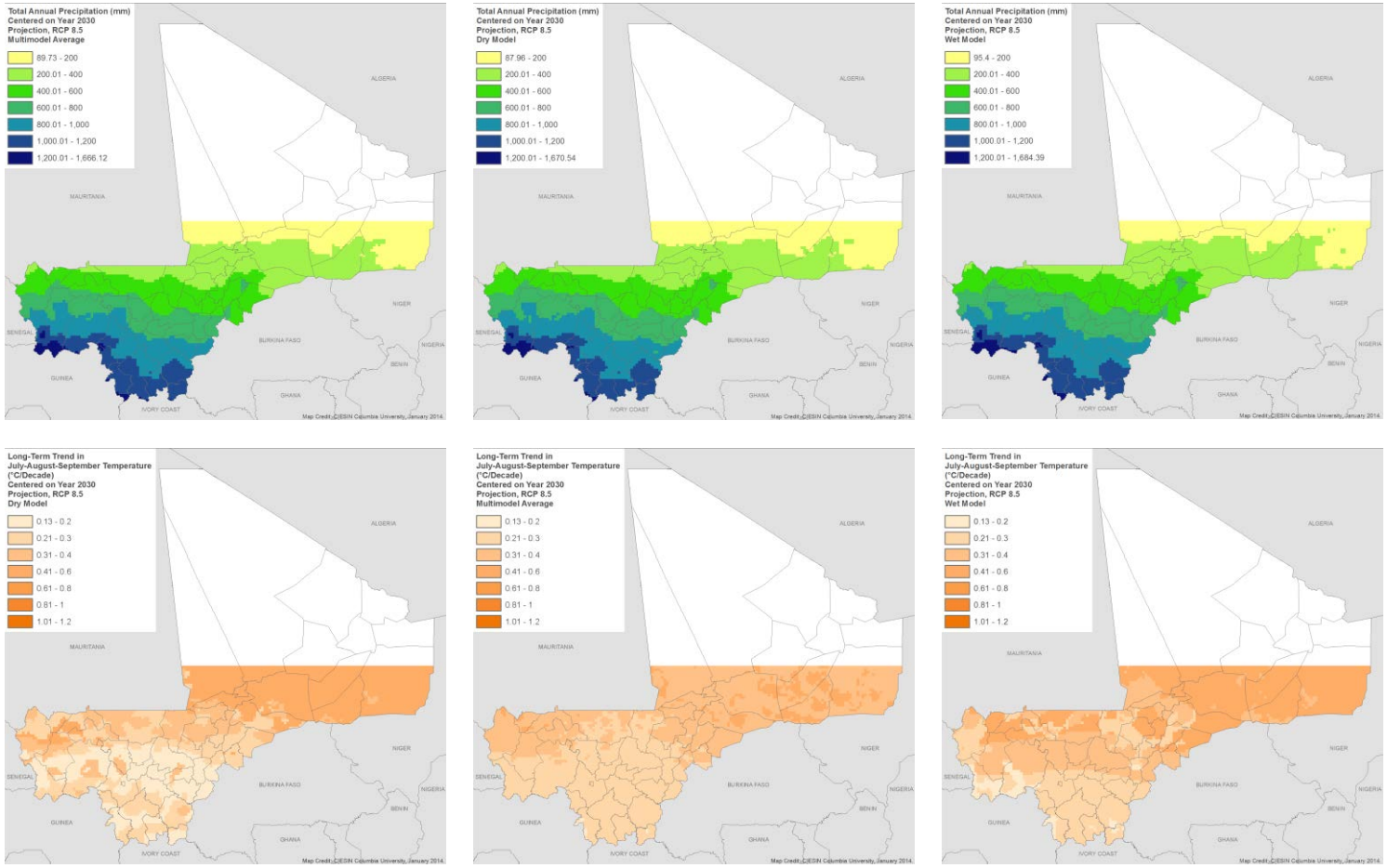

FIGURE A1-6. PROJECTED TOTAL ANNUAL RAINFALL AND TEMPERATURE TRENDS FOR 2050 (2045-2065) PERIOD UNDER RCP8.5 SCENARIO
(LEFT COLUMN: DRY MODEL; MIDDLE COLUMN: MULTIMODEL AVERAGE; RIGHT COLUMN: WET MODEL)

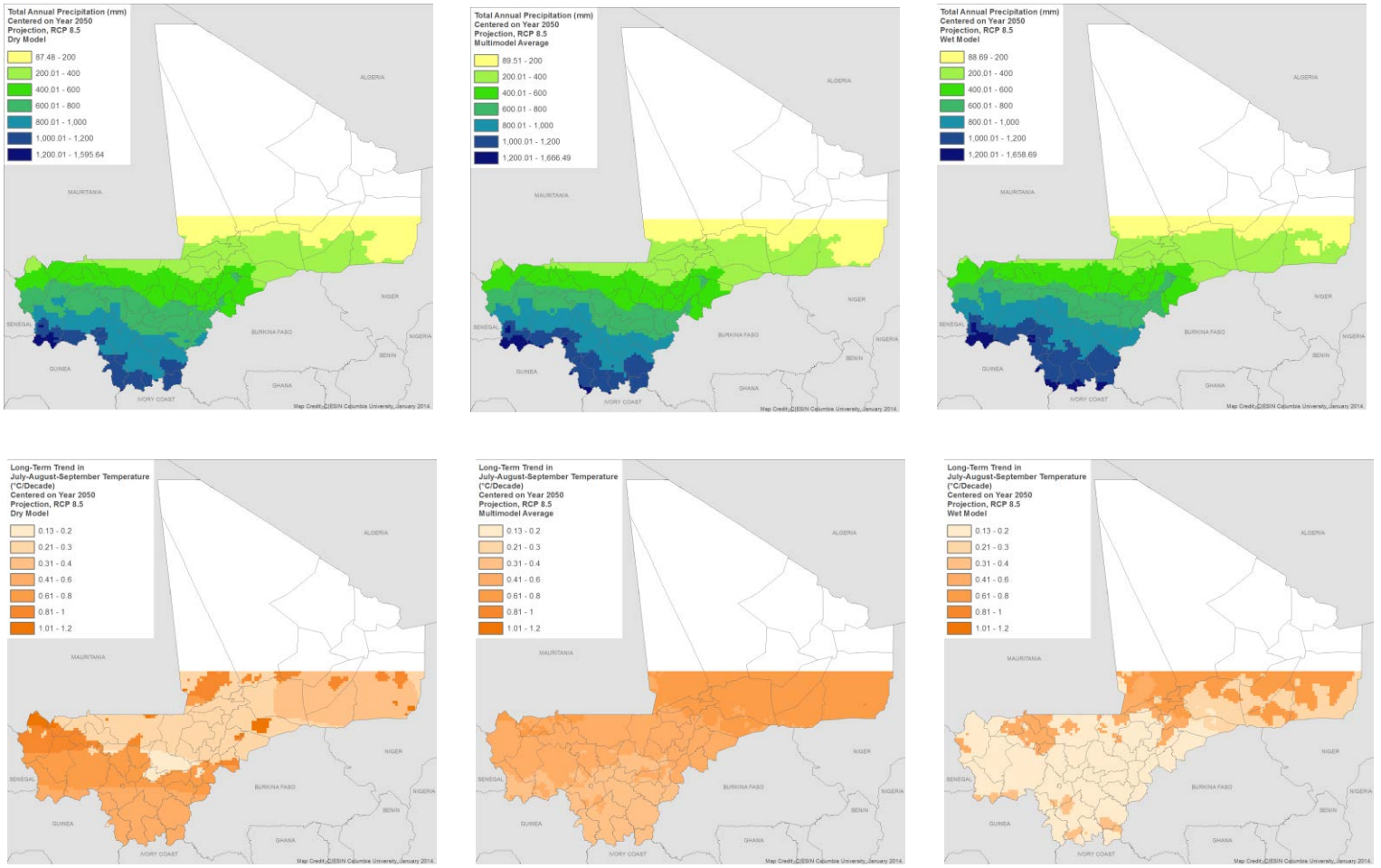

ANNEX II. PRINCIPAL COMPONENTS ANALYSIS

AII.1 OVERVIEW

The fundamental purpose of index construction is data reduction. As Abson et al. (2012:516) note, "indices reduce the amount and complexity of the information that must be communicated while simultaneously providing an indication of the interaction of multiple… indicators through a single aggregated vulnerability 'score'." A commonly used alternative to the additive approach is principal components analysis (PCA). In this approach, the indicators are not grouped *a priori* into components of vulnerability, but rather the statistical relationships among the indicators are used to group them according to similarity in their statistical (and therefore spatial) distributions. The idea is to break the n-dimensional cloud of relationships (where n = the number of indicators) among the indicators into a smaller set of uncorrelated principal components (PCs) that are linear combinations of the input variables. Because the PCs are uncorrelated, the scores associated with each PC encapsulate a unique aspect of the overall socio-ecological vulnerability represented by the original set of vulnerability indicators (Abson et al., 2012).

The number of PCs equals the number of variables, but each successive PC explains less of the overall total variation. Thus, the main information usually can be meaningfully captured by a few leading PCs. The developer needs to decide how many PCs to retain; a common method of component selection, the Keiser criterion, suggests keeping all components with an eigenvalue (which is output with other PCA statistics in common statistical packages) higher than 1.

Prior to running a PCA, the data are standardized as z-scores by subtracting the mean and dividing by standard deviation, so that all the variables are presented on the same scale with the standard deviation of each variable equal to 1. Hence, a z-score of 2 represents a value two standard deviations above the mean, and a z-score of -2 represents two standard deviations below the mean. Each PC, then, can be interpreted as a z-score, though the directionality (whether positive z-scores represents high or low vulnerability) needs to be tested against the underlying data. It is often appropriate, for reasons discussed below, to invert a PC before combining them.

One advantage of the PCA is that it can help illuminate the statistical relationships among the indicators used for a spatial vulnerability assessment. Each PC captures spatial covariance or correlation among the indicators, and different PCs reflect uncorrelated patterns. The indicators with the highest factor loadings (equivalent to correlation coefficients) for a given PC can be functionally grouped to describe that component. This approach allows the developer to identify where different aspects of vulnerability are most intensely present. While the additive approach does allow development of component sub-indices, the sub-indices are developed on the basis of theoretical rather than statistical relationships among the indicators. Thus, a PCA approach can be complementary to the additive/averaging approach, providing users with additional information.

AII.2 METHODS

We utilized all 18 indicators in a PCA, without regard to their assignment to particular components of vulnerability. We extracted six components that explain 68 percent of the total variation. Using a common method of component selection, Keiser criterion, we report the factor loadings of all components with an eigenvalue greater than 1(Table A2-1). The plots (Figure A2-1) show that the eigenvalues for the first six components exceed 1. While each indicator included in the PCA had a variance of 1 (because of the z-score standardization), the first component (PC1) has a variance six times as high (eigenvalue = 6.12), meaning that it captures substantially more variance in the n-dimensional cloud of relationships among the indicator values than the subsequent PCs (three times more than PC2 and almost six times more than PC3-PC6).

FIGURE A2-1. SCREE PLOT FOR THE PCS

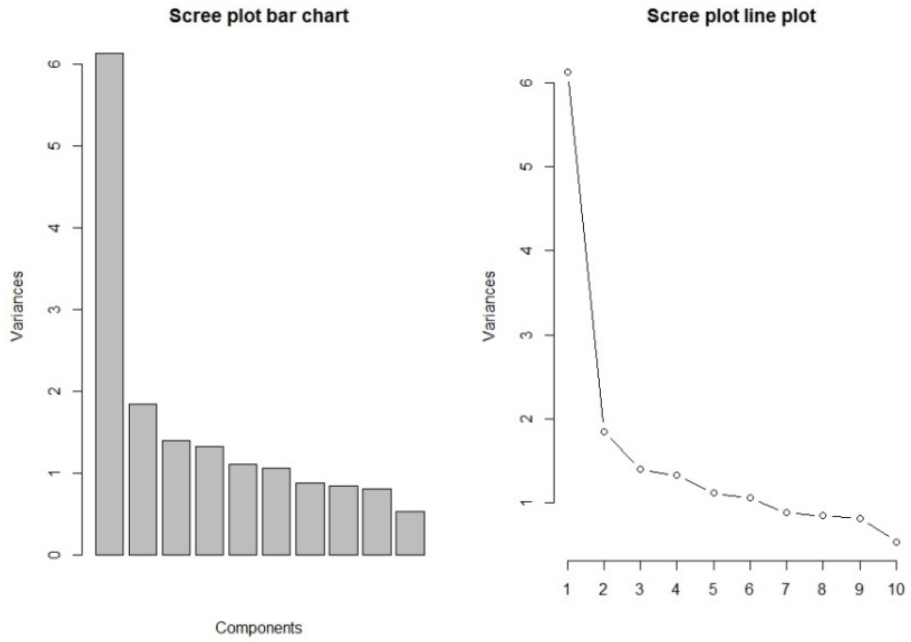

Table A2-1 shows the factor loadings of each indicator for each principal component. The loadings equate to correlation coefficients, such that higher values (negative or positive) correspond to higher correlations. We highlight the variables with high loadings for each component (above an absolute value of ~0.250). High positive loadings (indicators positively correlated with the PC) are in blue; high negative loadings (indicators negatively correlated with the PC) are in red. Loadings close to 0 are not significant.

In a next step, we use the highest factor loadings (in absolute value) to assign an interpretation to each PC. For PC1, given the very high negative loadings for four climate exposure indicators and soil organic carbon (which is strongly associated with precipitation levels), we call this a climate exposure component. Interestingly, the spatial pattern of high infant mortality is the inverse of these climate exposure metrics, suggesting that high infant mortality is found in areas with relatively higher rainfall and lower rainfall variability (as measured by the coefficient of variation of precipitation and NDVI), as well

as areas of higher malaria prevalence. In PCA it is legitimate to invert components where high negative loadings are associated with higher vulnerability.[11] We do this in the case of PC1 and map the resulting inverted principal component (Figure A2-2a), which shows the characteristic north-south gradient found in the exposure component of the additive approach.

PC2 (Figure A2-2b) is driven by two DHS indicators, household wealth and maternal education, both with loadings of >0.500. These, along with the poverty index (also strongly correlated with PC2), strongly link to household-level social vulnerability; thus, PC2 could represent either a sensitivity or adaptive capacity component.

TABLE A2-1. FACTOR LOADINGS BY PRINCIPAL COMPONENT (PC)

	PC1	PC2	PC3	PC4	PC5	PC6
PRCP - Average annual precipitation	-0.376	0.010	0.062	-0.216	0.045	0.019
IACV - Coefficient of variation (CV) of precipitation	-0.377	-0.026	-0.065	-0.036	0.074	-0.080
DCVAR - Decadal component precipitation	-0.113	-0.018	-0.593	-0.024	-0.159	0.267
NDVICV - CV of NDVI	-0.280	0.066	-0.078	-0.381	0.105	0.147
TTREND - Temperature trend	-0.367	0.040	-0.138	-0.218	-0.022	0.022
FLOOD - Flood frequency	0.049	-0.031	0.090	-0.368	-0.201	-0.491
HHWL - Household wealth	0.136	0.525	0.230	-0.115	-0.176	0.058
STNT - Child stunting	-0.117	-0.076	0.555	-0.013	-0.288	0.311
IMR - Infant mortality rate	0.247	0.146	0.194	-0.274	0.253	0.202
POVI - Poverty index	-0.082	0.241	0.162	-0.040	0.377	0.273
CONF - Conflict events	-0.058	-0.232	0.045	-0.087	-0.619	0.216
CARB - Soil organic carbon	-0.343	-0.103	0.123	-0.099	0.055	0.010
MALA - Malaria stability index	0.232	0.245	-0.285	-0.394	0.096	0.086
EDMO - Education level of mother	-0.055	0.578	-0.012	0.007	-0.375	-0.179
MARK - Market accessibility	-0.224	0.168	0.080	0.414	0.153	-0.376
HEALTH - Health infrastructure index	-0.259	0.333	-0.169	0.167	-0.125	-0.041
ANTH - Anthropogenic biomes	-0.305	0.052	0.208	-0.035	0.139	0.051
IRRI - Irrigated areas	-0.025	0.178	-0.075	0.400	-0.038	0.459

[11] According to the Social Vulnerability Index (SoVI), a widely used PCA-based metric for hazard risk assessment, adjustments can be made to the "components' cardinality (positive [+] or negative [-]) to insure that positive component loadings are associated with increased vulnerability, and negative component loadings are associated with decreased vulnerability." For more information, please visit the Hazards & Vulnerability Research Institute website at: http://webra.cas.sc.edu/hvri/products/sovi.aspx.

FIGURE A2-2. MAPS OF (A) PC1 (INVERTED) AND (B) PC2

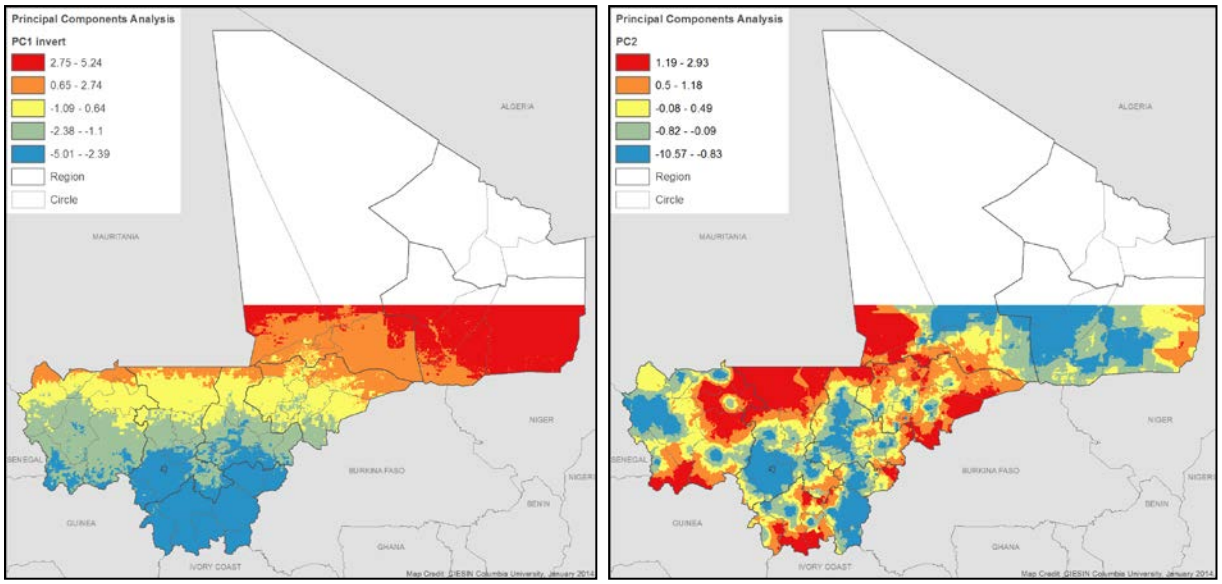

(a) **(b)**

PC3 (Figure A2-3a) is overwhelmingly driven by child stunting and looks almost identical to the child stunting map presented in Annex IV. Interestingly, the percentage of precipitation variance explained by the decadal component, which reflects persistent dry or wet conditions (DCVAR) that can have a high impact on food security, is negatively correlated with this PC. The DCVAR indicator points to higher exposure to persistent climatic anomalies, especially prolonged drought. We do not have a good explanation as to why a climate metric that would typically have a high correlation with child stunting is actually anti-correlated. It may be that since the DHS survey was conducted in 2006, and a period of average to above average rainfall preceded it, that the stunting metric from this survey simply is not reflecting climate variability. It could be that the intuitive association between stunting and persistence of sequences of bad or good years is not correct and that it is the regions that experience higher shocks in individual years that are more at risk of stunting. This is an example where more research into the causality of statistical relationships is required. PC4 (Figure A2-3b) has two strongly positive indicators — market accessibility and irrigation — but malaria, flood frequency, and the coefficient of variation of NDVI are all negatively correlated. It is not surprising that irrigation and flooded areas are co-located. On balance, this also appears to be an adaptive capacity indicator linked strongly to the river network (rivers also figure into market accessibility in Mali, with major boat traffic on the Niger).

FIGURE A2-3. MAPS OF (A) PC3 AND (B) PC4

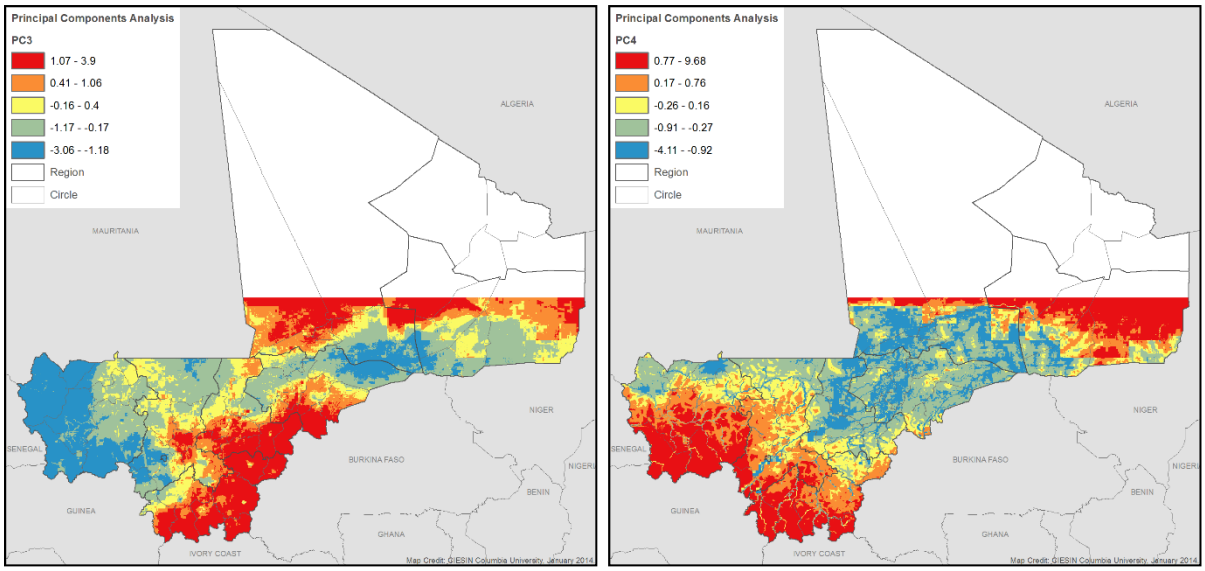

(a) **(b)**

FIGURE A2-4. MAPS OF (A) INVERTED PC5 AND (B) INVERTED PC6

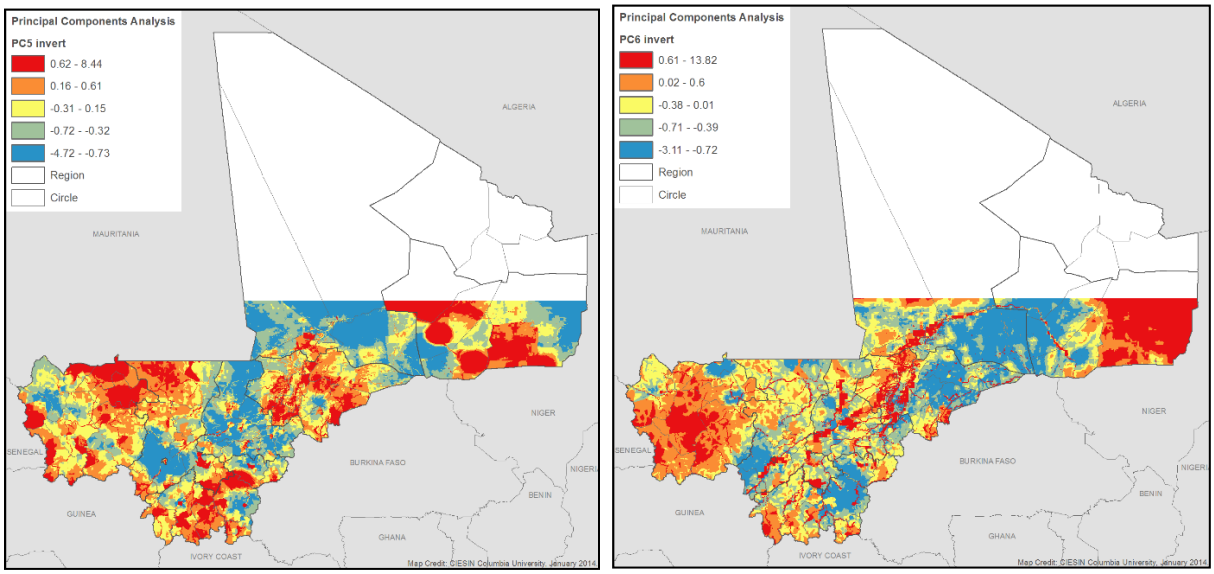

(a) **(b)**

For PCs 5 and 6, again we feel on a theoretical basis, and because of high negative loading for conflict events (PC5) and flood frequency (PC6), that these two components should be inverted. PC5 (Figure A2-4a) largely is a conflict-related measure, which interestingly is inversely correlated with the poverty index. PC6 (Figure A2-4b) is largely driven by flood vulnerability and low market accessibility.

Given their high eigenvalues, we averaged the first four PCs (doubling the weight of the inverted PC1 on the basis of its much higher eigenvalue) to create an overall PCA map of vulnerability (Figure A2-5).[12] It is interesting to overlay onto the overall PCA map the location of settlements and higher level roads (Figure A2-6); it becomes clear that the lowest vulnerability is associated with proximity to major settlements and roads, and the highest vulnerability is closely related to inaccessibility and climate stressors. When comparing the PCA results to the vulnerability map generated by the additive approach, we see that the distribution of vulnerability is broadly similar. In order to make the comparison more effective, we have remapped the vulnerability index (found in the main text Figure 5, page 12) in quintile categories (such that each category contains an equal number of pixels (Figure A2-7). This information is more directly comparable to the maps in Figures A2-5 and A2-6.

Overall, the PCA approach provides additional insight into the patterns of climate vulnerability in Mali based on correlations among indicators. It points out some interesting statistically derived groupings among indicators that were not foreseen *a priori* in the allocation of indicators to components, pointing out in some cases the potential dual nature of some indicators; i.e., contributing to both sensitivity and lack of adaptive capacity.

FIGURE A2-5. OVERALL PCA MAP OF VULNERABILITY

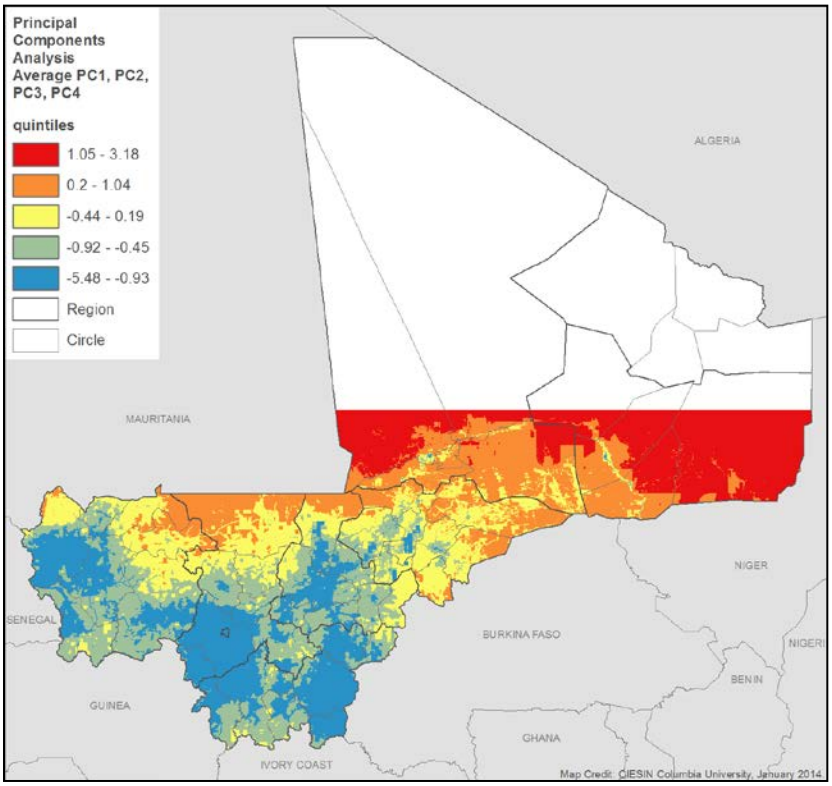

[12] We were also less convinced of the inversion of PCs 5 and 6 than the rationale we had for inverting PC1. Furthermore, the last two PCs have relatively low eigenvalues of 1.12 and 1.06, respectively. There is a drop in eigenvalues after the fourth PC, which contributed to our decision to only include the first four PCs in the overall vulnerability map. We did test the results of an aggregation using all six PCs, and the differences in the overall patterns of vulnerability were negligible.

FIGURE A2-6. OVERALL PCA-BASED MAP OF VULNERABILITY (WITH SETTLEMENTS AND ROAD NETWORKS)

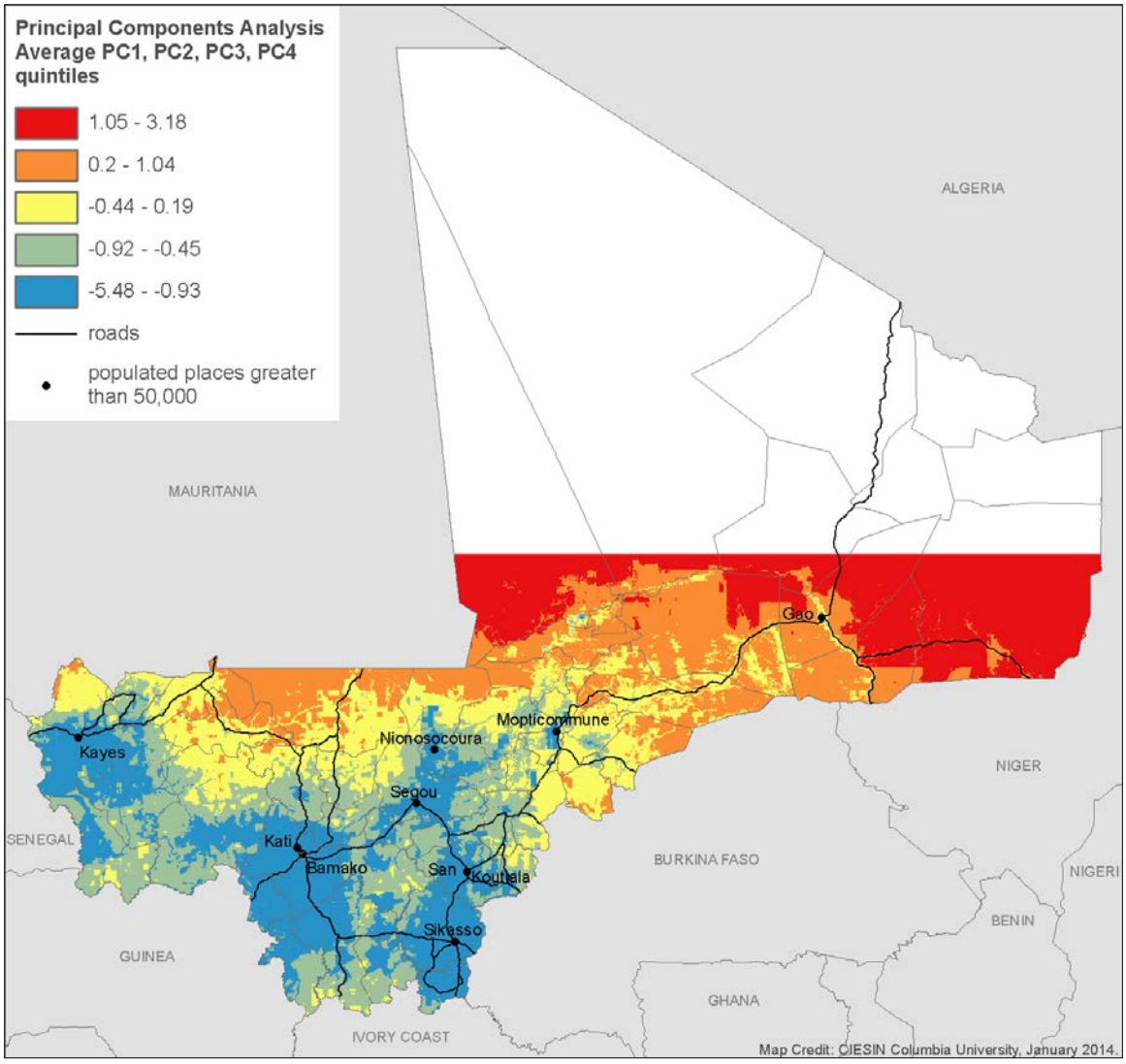

FIGURE A2-7. THE ADDITIVE VULNERABILITY MAP (REPRESENTED IN QUINTILES)

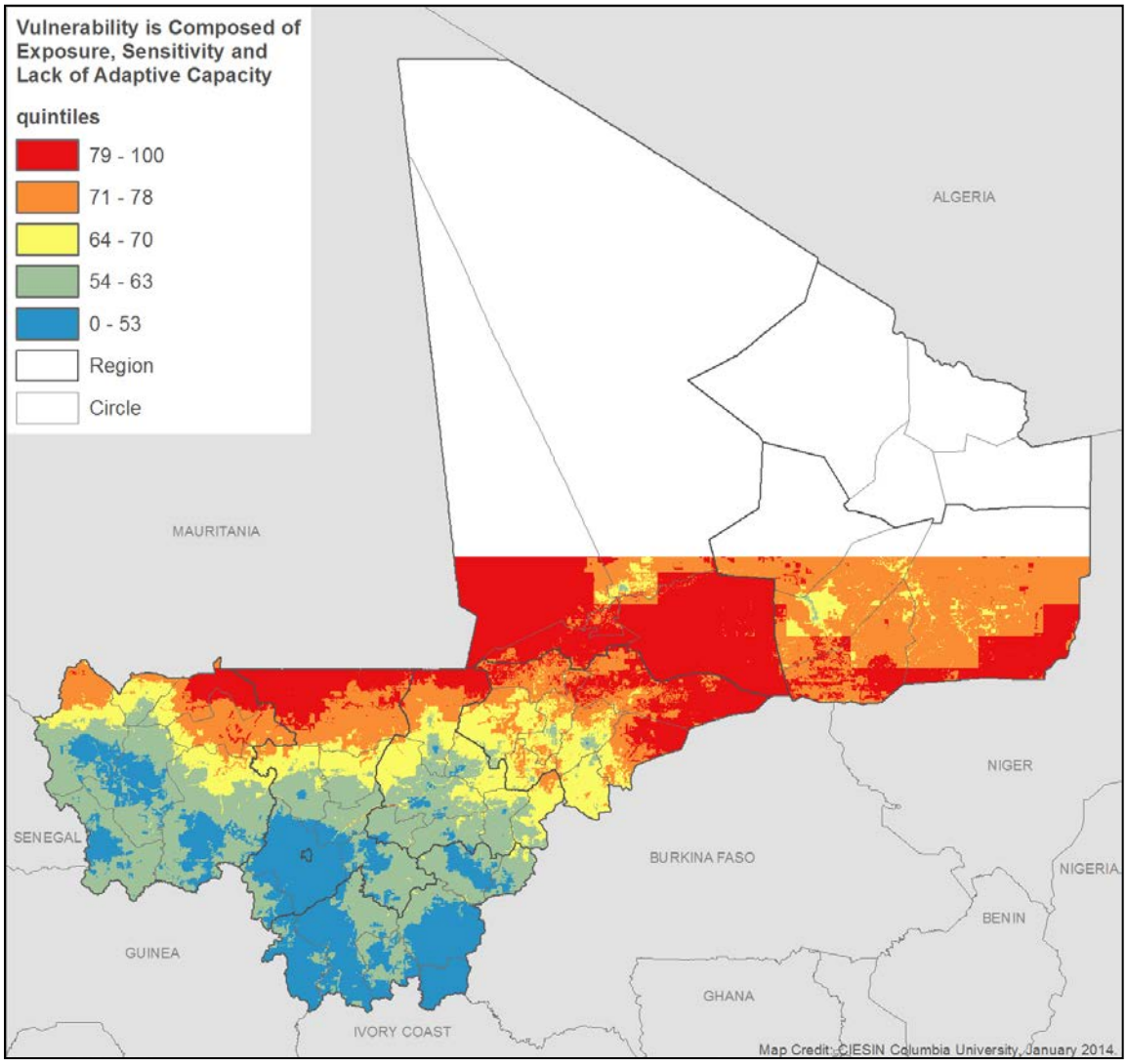

ANNEX III. SENSITIVITY ANALYSIS

AIII.1 INTRODUCTION

As discussed in the methods section, there are a number of subjective decisions that are made in the process of vulnerability index construction. Therefore, it is important to test the sensitivity of results to alternative index construction methodologies. The overall purpose of sensitivity analysis is to examine the robustness of index results to different assumptions regarding the construction of vulnerability, the relative contribution of individual indicators, and weighting and aggregation schemes.

We focused on two major sources of uncertainty: selection of weights and the inclusion of specific indicators. Differential weights often are used in index creation to account for the relative importance of the indicators; however, the sensitivity of results to differential weighting needs to be tested. In our analysis, we assign double weights for indicators collected from the 2006 DHS that were available at the cluster level (data from Jankowska et al., 2012) for a number of reasons. The primary reason is that these data are of high spatial accuracy and resolution, and have relatively lower levels of uncertainty compared to some of the other sensitivity and adaptive capacity metrics.[13] Secondly, the data are closely aligned proxies to the sensitivity and adaptive capacity components. In terms of indicator inclusion, we remove indicators one at a time to assess the impact of the removal of given indicators on results.

The aim of the analysis is to identify areas where the vulnerability index results increase or decline in percentage terms as a result of changes in methodology.

AIII.2 WEIGHTED VS. UNWEIGHTED

We evaluated the impact of differential weighting on vulnerability scores by subtracting the vulnerability index where equal weights were assigned to each indicator from our original vulnerability index constructed using differential weights. The unweighted version was constructed using a simple average of all indicators per component, rescaling (stretching) the component scores to 0-100, and then averaging the three components of exposure, adaptive capacity, and exposure.

The weighted vulnerability index was calculated using the average of three composites: adaptive capacity, sensitivity, and exposure.

$$\textit{Vulnerability Index weighted} = (\textit{Exposure} + \textit{Sensitivity} + \textit{Adaptive Capacity})/3$$

Exposure is a simple unweighted average of the six indicators: average annual precipitation, interannual precipitation CV, decadal precipitation variance, NDVI CV, trend in temperature, and flood frequency.

$$\textit{Exposure} = (\textit{average annual precipitation} + \textit{interannual precipitation CV} + \textit{decadal precipitation variance} + \textit{NDVI CV} + \textit{trend in temperature} + \textit{flood frequency})/6$$

[13] MEASURE/DHS has a widely recognized reputation for conducting survey research and data cleaning to the highest standards.

Sensitivity is calculated as a weighted average of seven variables: household wealth, child stunting, infant mortality rate, poverty index by commune, conflict events, soil organic carbon, and malaria stability index. We have doubled the values for child stunting and household wealth, resulting in a divisor of nine, as follows:

*Sensitivity = (household's wealth*2 + child stunting*2 + infant mortality rate + poverty index + conflict events+ soil organic carbon + malaria stability index)/9*

Adaptive capacity is generated by a weighted average of five variables: education level of the mother, market accessibility, health infrastructure index, anthropogenic biomes, and irrigated areas. The weight of the education level of the mother was doubled compared to the rest of the variables included in the composite, resulting in a divisor of six, as follows:

*Adaptive capacity = (education level of the mother*2 + market accessibility + health infrastructure index + anthropogenic biomes + irrigated areas)/6*

When we subtract the "equal weights" Vulnerability Index from our original weighted Vulnerability Index (i.e., Weighted Minus Unweighted Vulnerability Index), the maximum decline in vulnerability in a single pixel is 16.7 percent, and the maximum increase is 8 percent (Table A3-1). The average percent decline in vulnerability is 5.6 percent. The changes result from removing the additional weight (importance) assigned to the DHS indicators. The area differences are mapped in Figure A3-1. The weighted approach has the advantage (or disadvantage, depending on one's perspective) of presenting higher vulnerability in large regions of southern Mali where stunting and IMR are high, and mother's education and household wealth are low.

TABLE A3-1. SUMMARY OF DIFFERENCE (WEIGHTED *MINUS* UNWEIGHTED VULNERABILITY INDEX)

	Min.	1st Qu.	Median	Mean	3rd Qu	Max.
Equal weights	-8.034	2.853	5.579	5.183	7.592	16.700

FIGURE A3-1. RESULTS OF WEIGHTED *MINUS* UNWEIGHTED VULNERABILITY INDEX

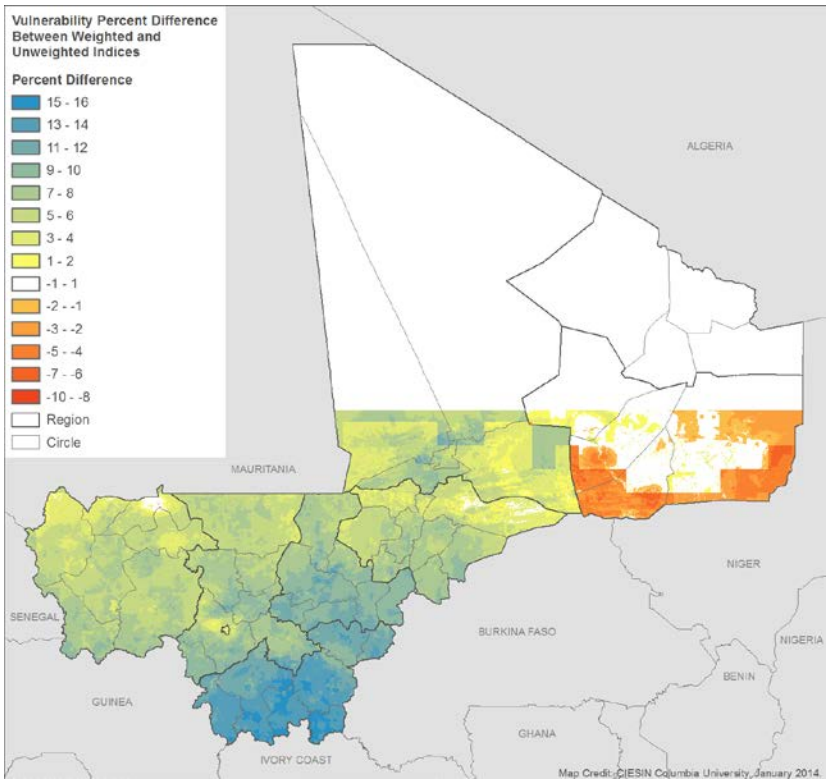

Note: orange to red areas indicate higher vulnerability in the unweighted index; yellow to blue areas indicate lower vulnerability in the unweighted index.

AIII.3 EXCLUSION OF INDICATORS

To test the impact of indicator exclusion on vulnerability, we removed one indicator at a time from the vulnerability index calculation, retaining the differential weights of our original index approach. Table A3-2 presents the minimum, first quartile, median, mean, third quartile, and maximum results for the country as a whole. We observe that the maximum impact (decrease) in the vulnerability index is made by removal of child stunting (~14 percent), and large declines are also observed with the removal of education of the mother. Both of these indicators received double weights in the original vulnerability index. In addition, removing flood frequency (~13 percent) and household wealth (~10 percent) also result in declines in the vulnerability index. On the other hand, an increase in the vulnerability index is observed by the removal of soil carbon and irrigated areas (~9 percent). Figure A3-2 presents the percent difference maps for four versions of the vulnerability index. There are relatively strong differences when the following indicators are removed: child stunting, irrigated areas, and soil carbon.

It is important to note that these are just values, and that most of the grids have small differences (evidenced by regions in white in Figure A3-2). As expected, the largest average differences (see Mean column in Table A3-2) are observed for removed variables with double weights: education of the mother and household wealth. In general the mean changes are modest (on the order of 2 to 4 percent) while the maximum observed changes of 14 percent (decreased vulnerability as a result of removal) and minimum of -9 percent (increased vulnerability as a result of removal) suggest that at most

a given pixel can decline or increase by one vulnerability class. These sensitivity tests suggest relatively robust methods and results.

TABLE A3-2. SUMMARIES FOR DIFFERENCES IN VULNERABILITY INDEX AFTER EXCLUDING ONE INDICATOR AT THE TIME

	Min.	1st Qu.	Median	Mean	3rd Qu	Max.
no anth	-6.575	-3.254	-2.199	-2.418	-1.572	3.131
no carb	-9.172	-3.899	-2.864	-2.153	0.534	5.083
no conf	-0.665	-0.312	-0.198	-0.018	-0.096	8.218
no dcvar	-4.163	-0.355	0.871	0.796	1.864	5.854
no edmo	-4.054	2.252	4.544	4.083	5.897	12.910
no flood	-1.991	-0.147	0.875	1.132	2.132	12.480
no health	-6.864	0.123	1.282	0.865	2.024	4.537
no hhwl	-7.362	1.241	2.904	2.795	4.574	10.440
no iacv	-3.259	-0.988	-0.284	-0.187	0.354	3.906
no imr	-7.544	-0.839	0.576	0.042	1.969	6.363
no irri	-9.448	0.000	0.000	-0.048	0.000	0.000
no mala	-5.368	1.193	2.378	1.195	2.815	4.343
no mark	-4.482	-2.346	-1.849	-1.536	-1.09	5.184
no ndvicv	-6.931	-2.365	-1.400	-1.433	-0.484	3.434
no povi	-5.254	0.017	0.8822	0.937	1.754	5.619
no prcp	-5.714	-1.040	-0.1399	-0.275	0.481	3.479
no stnt	-4.502	-0.538	0.5516	0.965	2.056	14.330
no ttrend	-4.428	-0.050	1.031	0.760	1.746	3.278

In conclusion, while the results show some sensitivity to these modifications on the order of average percent changes of +/-5 percent (and up to +/-10 percent for individual pixels), we feel that the results of the overall vulnerability index are relatively robust to changes in the index construction.

FIGURE A3-2. PERCENT CHANGE IN VULNERABILITY INDEX SCORE (A) WITHOUT STUNTING; (B) WITHOUT HOUSEHOLD WEALTH; (C) WITHOUT IRRIGATED AREAS; AND (D) WITHOUT SOIL CARBON

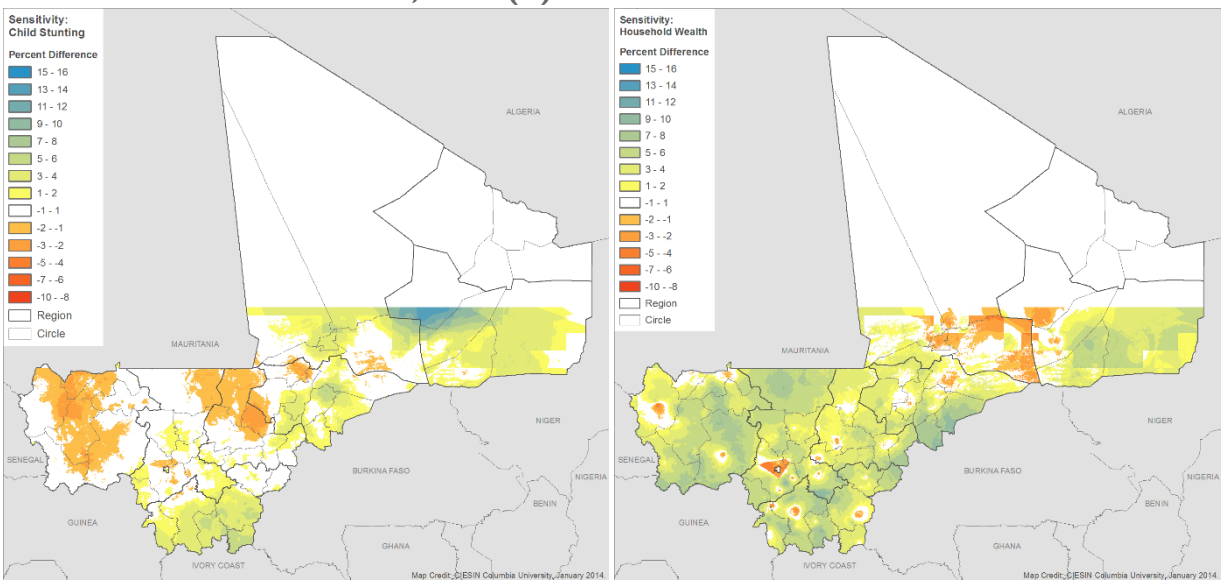

(a) **(b)**

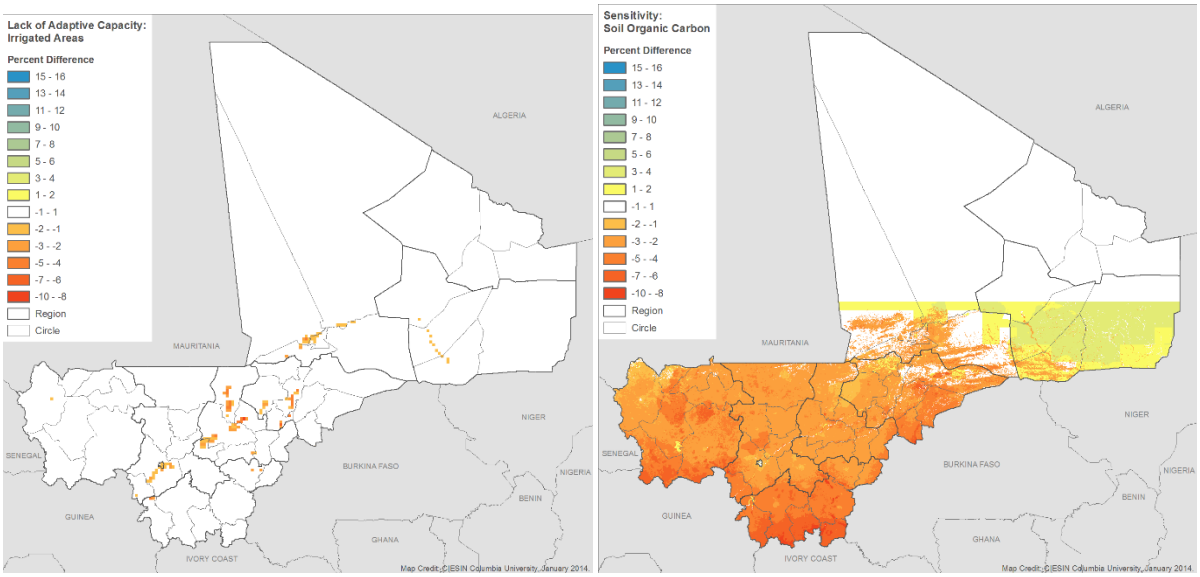

(c) **(d)**

Note: orange to red areas indicate higher vulnerability without the indicator; yellow to blue areas indicate lower vulnerability without the indicator.

AIII.4 REFERENCES

Jankowska, M., D. Lopez-Carr, C. Funk, G.J. Husak, Z.A. Chafe. (2012). Climate change and human health: Spatial modeling of water availability, malnutrition, and livelihoods in Mali, Africa. *Applied Geography*, 33:4-15.

ANNEX IV. INDICATOR METADATA

This section includes the following for each indicator:

- Maps of the indicator in its "raw" form (on the left) and as a transformed indicator on the 0-100 scale (on the right). The indicator maps are produced with equal interval categories using break points of 20, 40, 60, and 80 so as to better to represent the contribution that that indicator makes to the overall vulnerability score.
- Histograms representing the statistical distribution on the raw scale (left) and on the transformed indicator scale (right).
- A table describing the original source data and any performed processing steps.

AIV.1 EXPOSURE INDICATORS

Average Annual Total Precipitation

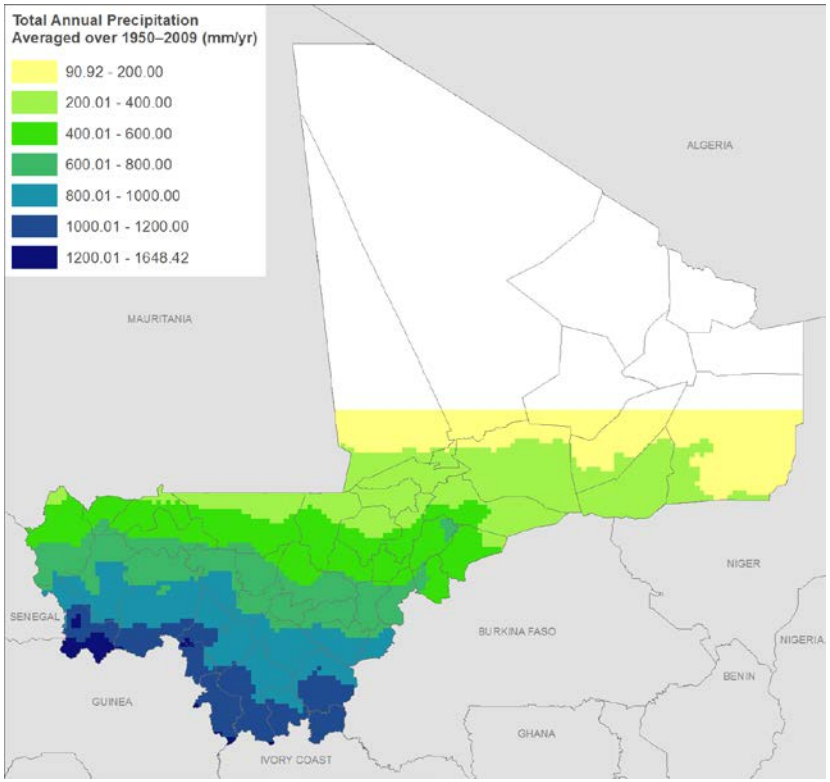

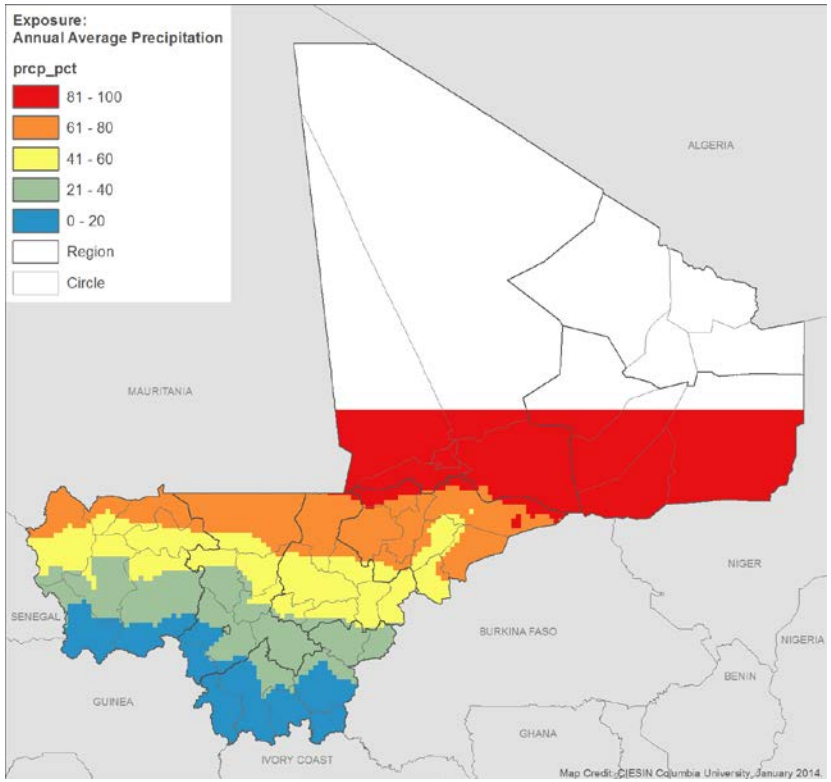

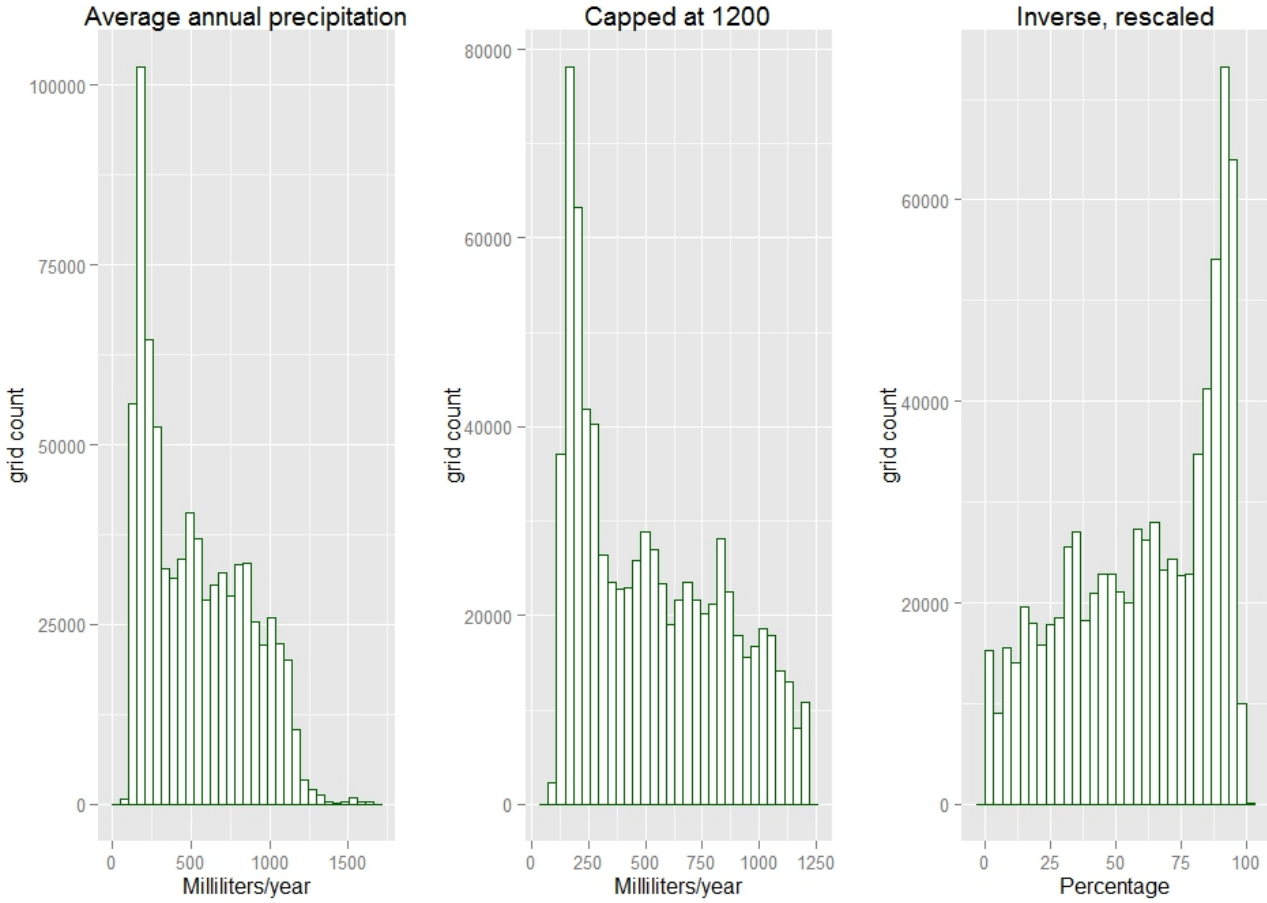

Title:	**Average annual total precipitation**
Indicator Code:	PRCP
Component:	exposure
Rationale:	This indicator describes how much rainfall is annually received. The amount of rainfall indicates suitability for agriculture,

	with lower rainfall generally representing a limiting factor for agriculture. For reference purposes, 450mm is generally the threshold for millet, the most drought-resistant of Mali's crops; 800mm is the threshold for cash crops such as cotton.
Source Data Set:	This is a long-term climatology of the total annual average computed for the 1950-2009 period. It is based on a high-resolution FEWSNET precipitation data set, FEWSNET FCLIM_TS (original time period of 1901-2009; original grid resolution of 0.1x0.1 degree). Data courtesy of FEWSNET. The following is the methodological publication: Funk, C., Michaelsen, J., and Marshall, M. (2012). Mapping recent decadal climate variations in precipitation and temperature across Eastern Africa and the Sahel, chap. 14 in Wardlow, B., Anderson, M., and Verdin, J., eds., *Remote sensing of drought—Innovative monitoring approaches*. London, UK: Taylor and Francis.
Units:	millimeters/year
Computation:	Original grid is 0.1x0.1 degree; it has been resampled by CIESIN to a 1km resolution by simply attributing the value of the larger grid cell to each smaller cell nested within it.
Statistics for raw data:	Min=90.92, Max=1648, Median=483.30, Mean=532.70, Standard Deviation=318.44 [computed for all of Mali below 17.2 degrees N latitude]
Scoring system:	Data vales were winsorized at 1,200 millimeters per year. Data has then been transformed into 0-100, with 0 corresponding to high rainfall (low exposure) and 100 to low rainfall (high exposure).
Statistics for transformed data:	Min=0, Max=100, Median=64.62, Mean=60.30, Standard Deviation=28.37 [computed for all of Mali below 17.2 degrees N latitude].
Limitations:	This variable has been generated using the FEWSNET gridded dataset, which was produced by interpolating (kriging) meteorological station data from public sources (there is relatively sparse station coverage over most of the area). Additional station data for Permanent Interstate Committee for Drought Control in the Sahel (CILSS) countries were obtained from AGRHYMET.
Spatial Extent:	Original data set 12S-25N, 20W-52E; here only the area 12N-25N and 12.3W-4.45E used.
Spatial Resolution:	Original 0.1x0.1 degree
Year of Publication:	2012
Time Period:	Original length 1901-2009; here only data from 1950 to 2009 used.
Additional Notes:	
Date:	10/08/2013
Format:	Excel file
File Name:	climate_fishnet_10082013.xls
Contact person:	FEWSNET: Chris Funk; CIESIN: Sylwia Trzaska

Interannual Coefficient of Variation in Precipitation (July-August-September)

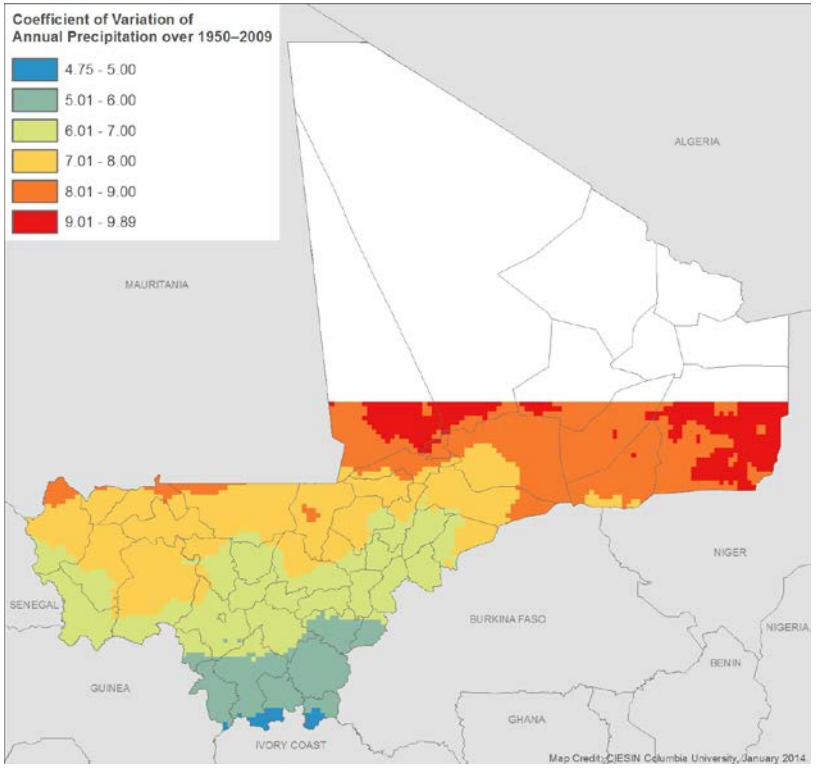

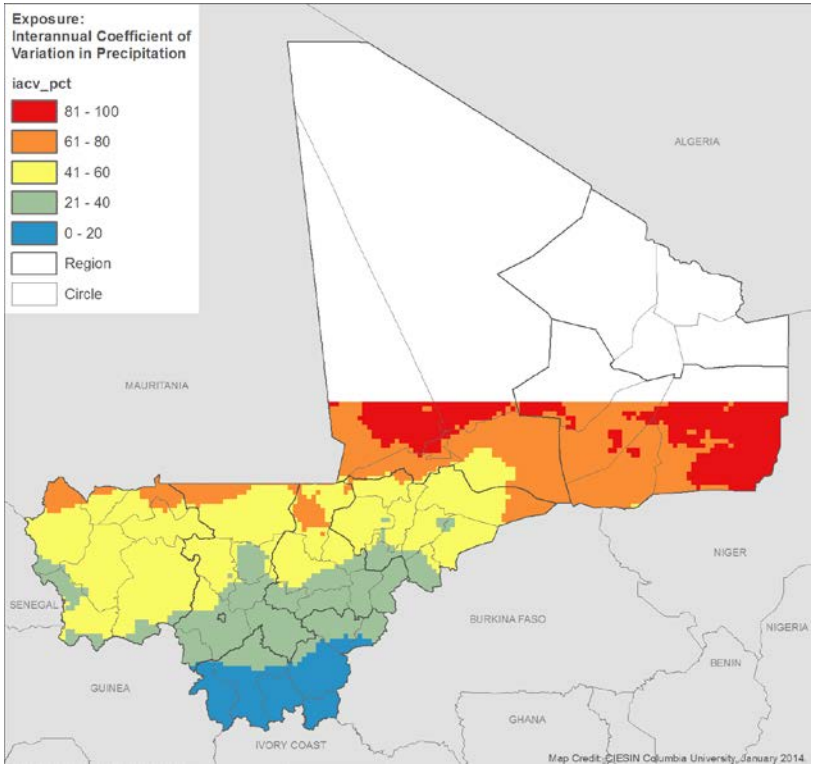

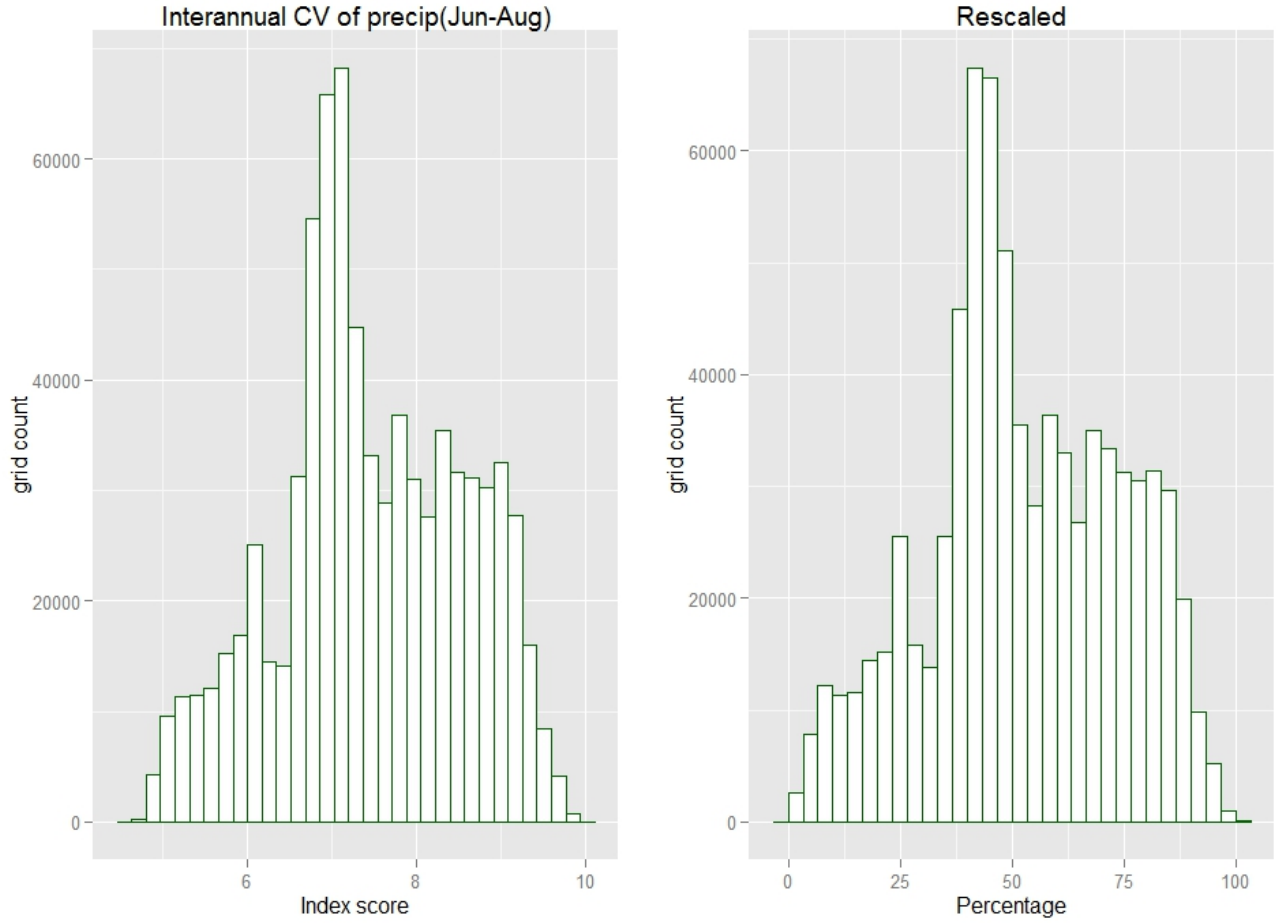

Title:	**Interannual Coefficient of Variation in Precipitation (July-August-September)**
Indicator Code:	IACV
Component:	exposure
Rationale:	Indicates how much rainfall varies in a given location relative to the annual total. High relative variability indicates higher volatility of conditions suitable for agriculture. We focus on the peak rainy season, when crops depend most on rainfall.

Source Data Set:	This is a long-term coefficient of variation, i.e., a standard deviation of annual totals divided by average total annual rainfall computed during the 1950-2009 period using the same data set as the PRCP indicator: FEWSNET FCLIM_TS (original length 1901-2009; original grid resolution 0.1x0.1 degree). See source information in the PRCP indicator metadata. Data courtesy of FEWSNET. The following is the methodological publication: Funk, C., Michaelsen, J., and Marshall, M. (2012). Mapping recent decadal climate variations in precipitation and temperature across Eastern Africa and the Sahel, chap. 14 in Wardlow, B., Anderson, M., and Verdin, J., eds., *Remote sensing of drought—Innovative monitoring approaches*. London, UK: Taylor and Francis.
Units:	Coefficient of variation
Computation:	Original grid is 0.1x0.1 degree; it has been resampled by CIESIN to 1km resolution by simply attributing the value of the larger grid cell to each smaller cell nested within it.
Statistics for raw data:	Min=4.75, Max=9.89, Median=7.32, Mean=7.45, Standard Deviation=1.10 [computed for all of Mali below 17.2 degrees N latitude]
Scoring system:	Data has been transformed to 0-100 scores, with 0 corresponding to low CV (low exposure) and 100 to high CV (high exposure).
Statistics for transformed data:	Min=0, Max=100, Median=50.01, Mean=52.53, Standard Deviation=21.40 [computed by Vali for all of Mali below 17.2 degrees N latitude].
Limitations:	This variable has been generated using the FEWSNET gridded dataset, which was produced by interpolating (kriging) meteorological station data from public sources (there is relatively sparse station coverage over most of the area). Additional station data for CILSS countries were obtained from AGRHYMET.
Spatial Extent:	Original data set 12S-25N, 20W-52E; here only area 12N-25N and 12.3W-4.45E used
Spatial Resolution:	Original 0.1x0.1 degree
Year of Publication:	2012
Time Period:	Original length 1901-2009; here only data from 1950 to 2009 used
Additional Notes:	
Date:	10/08/2013
Format:	Excel file
File Name:	climate_fishnet_10082013.xls
Contact person:	FEWSNET: Chris Funk; CIESIN: Sylwia Trzaska

Percentage of Precipitation Variance Explained by Decadal Component

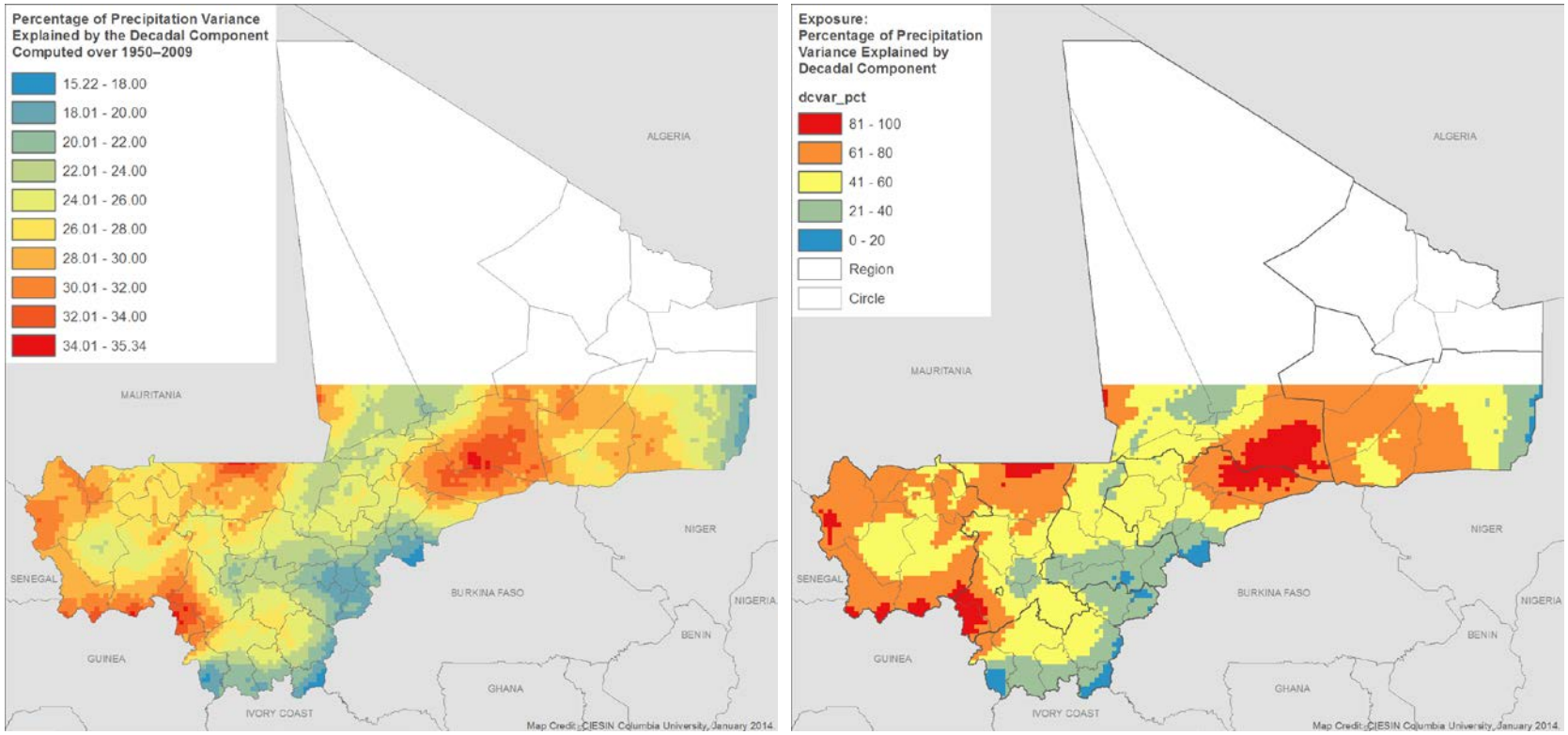

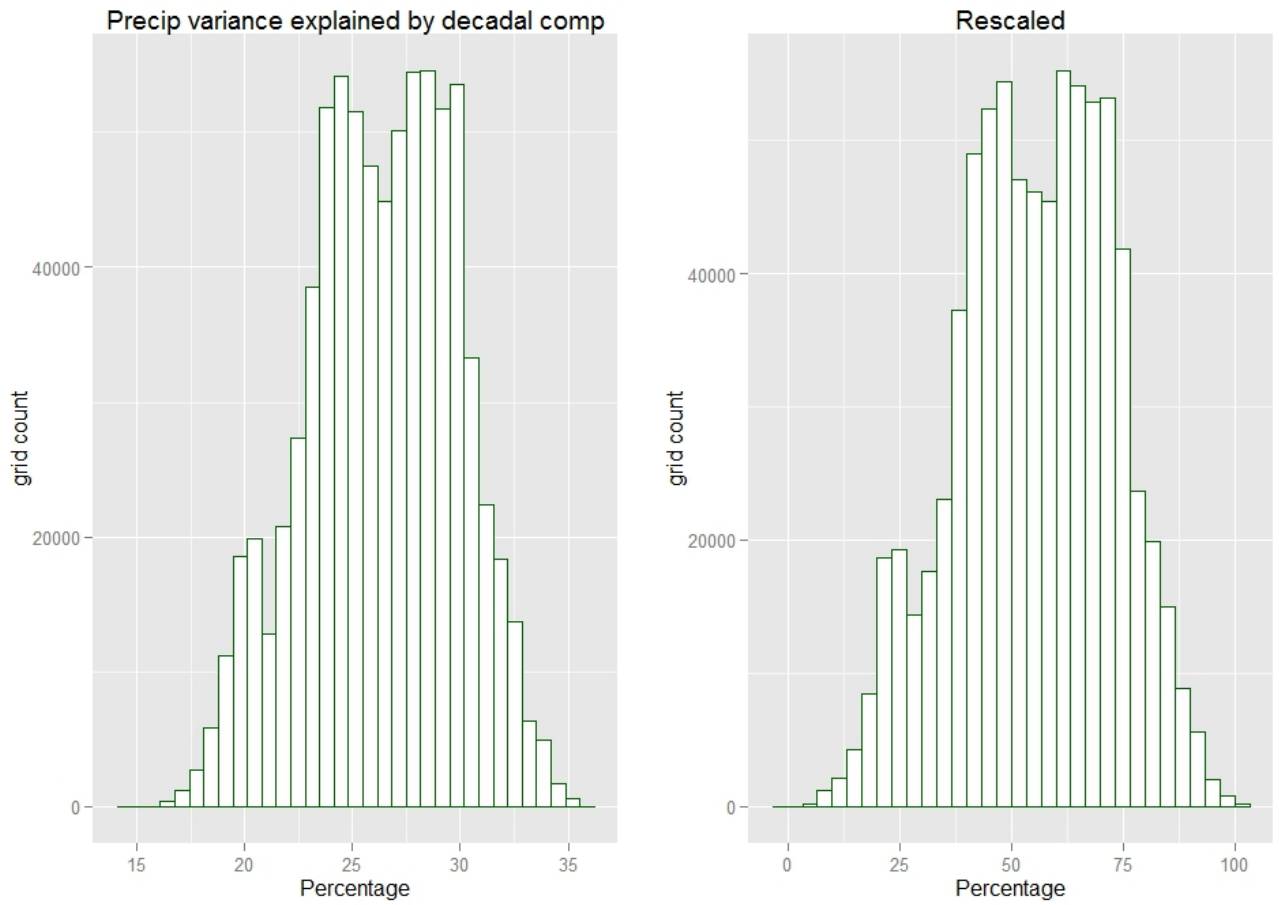

Title:	**Percentage of Precipitation Variance Explained by Decadal Component**
Indicator Code:	DCVAR
Component:	exposure
Rationale:	This indicator shows how much of total rainfall variability can be accounted for by decadal variations. Decadal variations reflect persistent dry or wet conditions and have a high impact on agriculture and food security, since cumulative effects

	of repeated droughts can be devastating for livelihoods. A high percentage of variance in the decadal band indicates a higher role of decadal variability in the area as well as higher exposure to persistent climatic anomalies.
Source Data Set:	This is a ratio between the variance in the decadal band and the total variance of rainfall, both computed over 1950-2009 period based on the FEWSNET FCLIM_TS data set. See source information in the PRCP indicator metadata. Data courtesy of FEWSNET. The following is the methodological publication: Funk, C., Michaelsen, J., and Marshall, M. (2012). Mapping recent decadal climate variations in precipitation and temperature across Eastern Africa and the Sahel, chap. 14 in Wardlow, B., Anderson, M., and Verdin, J., eds., *Remote sensing of drought—Innovative monitoring approaches*. London, UK: Taylor and Francis.
Units:	Percentages
Computation:	Original grid is 0.1x0.1 degree; has been resampled by CIESIN to 1km resolution by simple attributing the value of the larger grid to each smaller cell.
Statistics for raw data:	Min=15.20, Max=35.34, Median=26.50, Mean=26.34, Standard Deviation=3.47 [computed by Vali for all of Mali below 17.2 degrees N latitude].
Scoring system:	Data has been transformed into 0-100, with 0 corresponding to a low percentage of decadal variance (low exposure) and 100 corresponding to a high percentage of decadal variance (high exposure).
Statistics for transformed data:	Min=0, Max=100, Median=56.09, Mean=55.29, Standard Deviation=17.26 [computed by Vali for all of Mali below 17.2 degrees N latitude]
Limitations:	This variable has been generated using the FEWSNET gridded dataset, which was produced by interpolating (kriging) meteorological station data from public sources (there is relatively sparse station coverage over most of the area). Additional station data for CILSS (Permanent Interstate Committee for Drought Control in the Sahel) countries were obtained from AGRHYMET. .
Spatial Extent:	Original data set 12S-25N, 20W-52E; here only area 12N-25N and 12.3W-4.45E used
Spatial Resolution:	Original 0.1x0.1 degree
Year of Publication:	2012
Time Period:	Original length 1901-2009; here only data from 1950 to 2009 used
Additional Notes:	
Date:	10/08/2013
Format:	Excel file
File Name:	climate_fishnet_10082013.xls
Contact person:	FEWSNET: Chris Funk; CIESIN: Sylwia Trzaska

Coefficient of Variation of NDVI

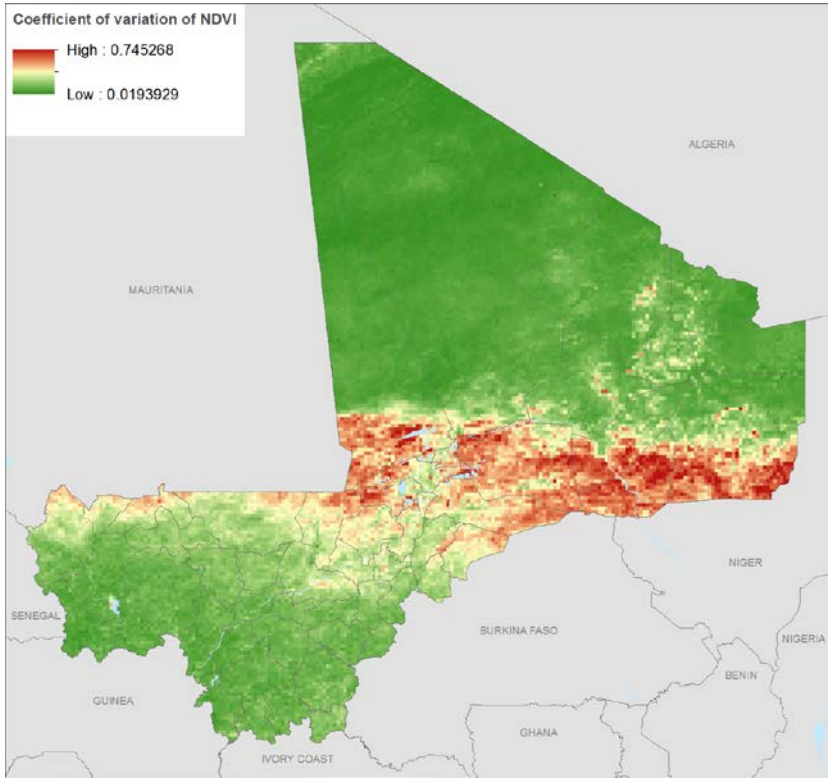

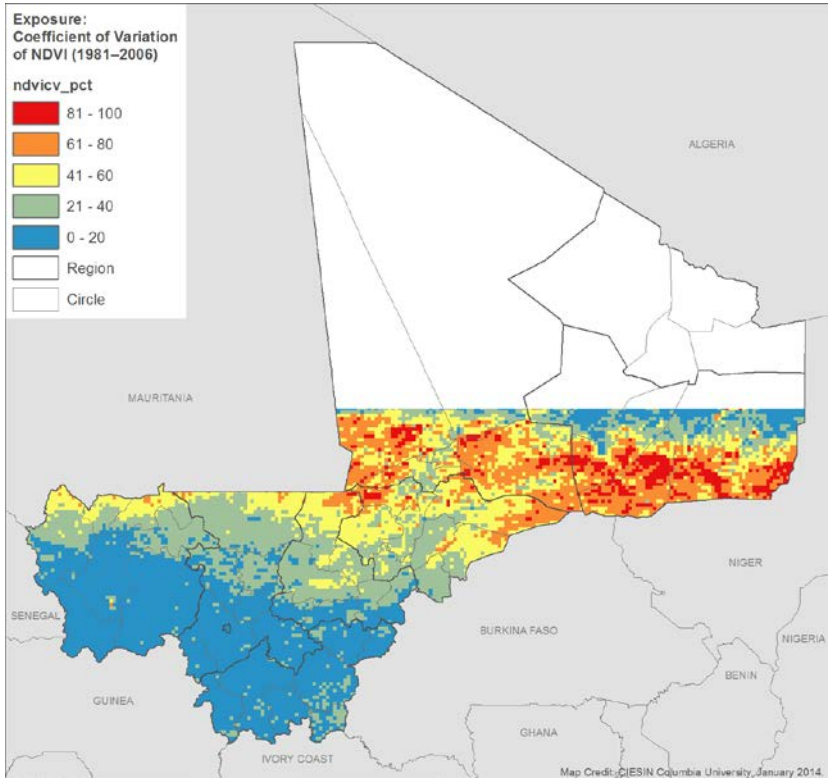

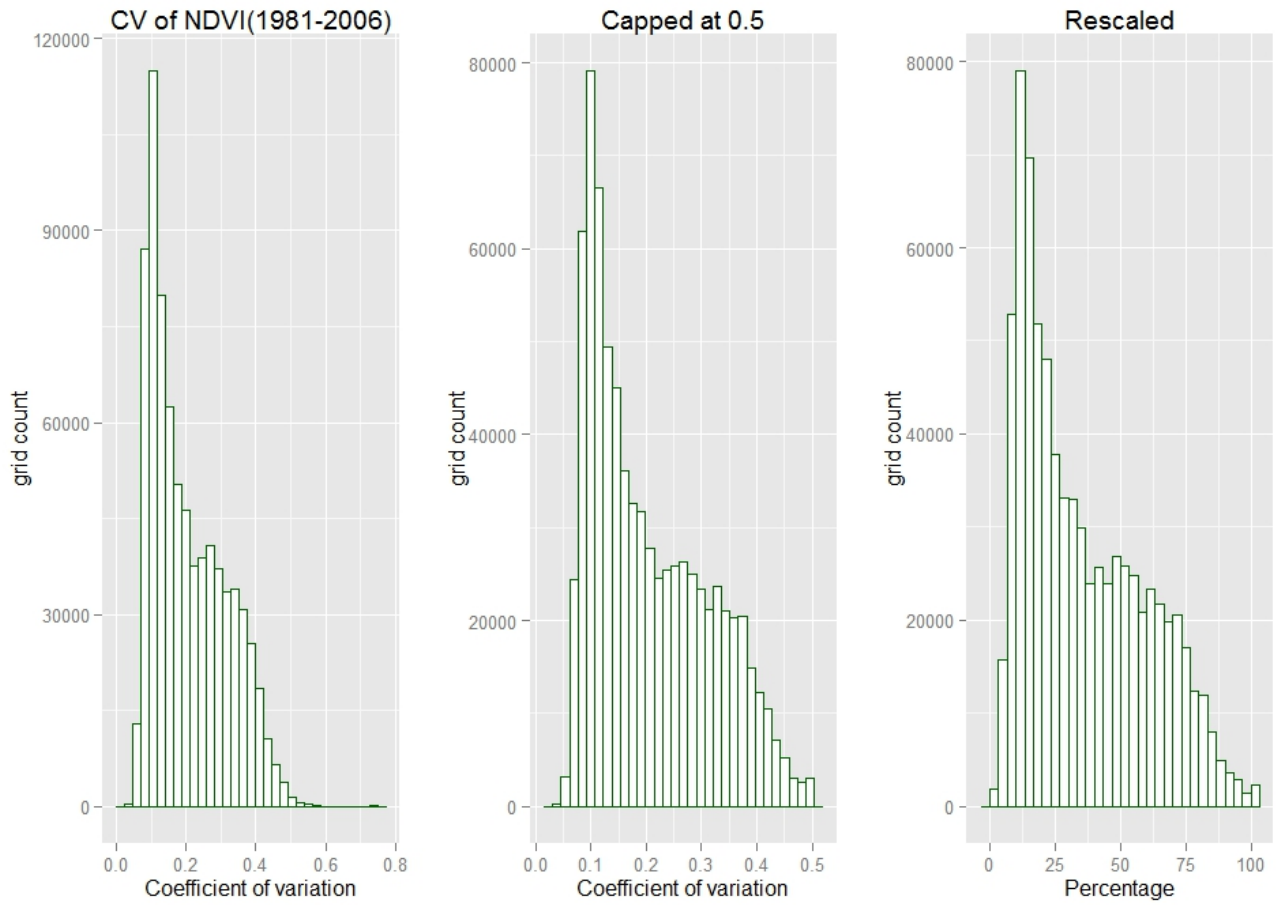

Title:	**Coefficient of Variation of Normalized Difference Vegetation Index (NDVI) (1981-2006)**
Indicator Code:	NDVICV
Component:	Exposure
Rationale:	Precipitation variability can only be tracked to the extent that there are relatively dense meteorology station networks. This indicator supplements the Interannual Coefficient of Variation in Precipitation (July-August-September) indicator by providing

	higher spatial resolution data based on satellite observations of greenness for the month of August for a 25-year period.
Source Data Set:	Global Inventory Modeling and Mapping Studies (GIMMS) (glcf.umd.edu/data/gimms/). The GIMMS (Global Inventory Modeling and Mapping Studies) data set is a normalized difference vegetation index (NDVI) product available for a 25-year period spanning from 1981 to 2006. The data set is derived from imagery obtained from the Advanced Very High Resolution Radiometer (AVHRR) instrument onboard the NOAA satellite series 7, 9, 11, 14, 16, and 17. This is an NDVI dataset that has been corrected for calibration, view geometry, volcanic aerosols, and other effects not related to vegetation change. NDVI values are 0 to 1; -0.1 is water; and -0.05 is "Null." Citation: Tucker, C.J., Pinzon, J.E., and Brown, M.E. (2004), Global Inventory Modeling and Mapping Studies, 2.0, Global Land Cover Facility, University of Maryland, College Park, Maryland. Copyright University of Maryland; Department of Geography; use is free to all if acknowledgement is made. UMD holds ultimate copyright. Data subset and downloaded from the IRI data library, available at: http://iridl.ldeo.columbia.edu/expert/SOURCES/.UMD/.GLCF/.GIMMS/.NDVIg/.global/.ndvi/
Units:	Coefficient of variation
Computation:	Bi-monthly values of NDVI are averaged for the months of August from 1981 to 2006, and the August coefficient of variation is computed as the ratio of standard deviation to mean. The tabular data set was converted to an 8km raster. This was subset to the Mali national boundary extent using ArcGIS Extract by Mask tool and a 30 arc-second raster mask generated from a 30 arc-second fishnet. Raster values were extracted using ArcGIS Extract Values to Points tool and the 30 arc-second fishnet centroids. The output was exported to a .csv table for re-coding and statistical analysis.
Statistics for raw data:	Min=0.04, Max=0.7453, Median=0.18, Mean=0.21, Standard Deviation=0.11 [computed for all of Mali below 17.2 degrees N latitude]
Scoring system:	Data vales were winsorized at a 0.5 coefficient of variation. Data has been transformed into 0-100, with 0 corresponding to low coefficient of variation (low exposure), and 100 corresponding to high coefficient of variation (high exposure)
Statistics for transformed data:	Min=0, Max=100, Median=29.72, Mean=35.79, Standard Deviation=23.35 [computed for all of Mali below 17.2 degrees N latitude]
Limitations:	NDVI readings are less reliable for sparsely vegetated areas where rainfall is less than 450mm per year.
Spatial Extent:	Global

Spatial Resolution:	8km
Year of Publication:	2006
Time Period:	1981 to 2006
Additional Notes:	IRI Data Library data set documentation: http://iridl.ldeo.columbia.edu/SOURCES/.UMD/.GLCF/.GIMMS/.NDVIg/.global/.dataset_documentation.htmlAssociated peer-reviewed publications: Pinzon, J., Brown, M.E. and Tucker, C.J., (2005). Satellite time series correction of orbital drift artifacts using empirical mode decomposition. In: N. Huang (Editor), Hilbert-Huang Transform: Introduction and Applications, pp. 167-186. Tucker, C.J., J. E. Pinzon, M. E. Brown, D. Slayback, E. W. Pak, R. Mahoney, E. Vermote and N. El Saleous (2005), An Extended AVHRR 8-km NDVI Data Set Compatible with MODIS and SPOT Vegetation NDVI Data. International Journal of Remote Sensing, Vol 26:20, pp 4485-5598.
Date:	Downloaded from IRI data library on 10/2/13.
Format:	Downloaded as TSV, then converted to raster.
File Name:	ndvi_cv_aug.xlsx
Contact person:	Alessandra Giannini

Long-term Trend in July-August-September Temperature

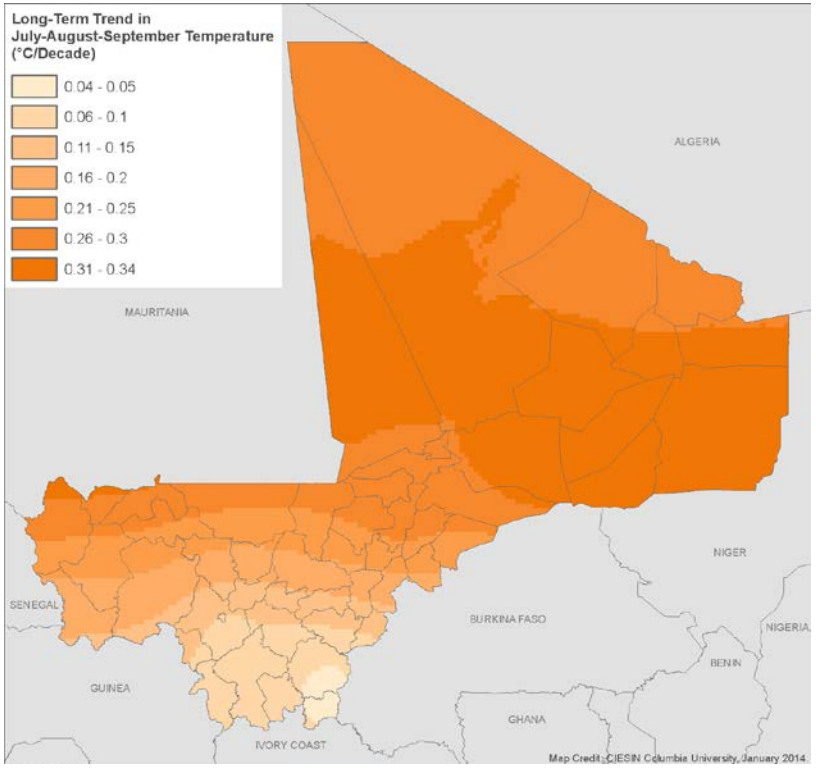

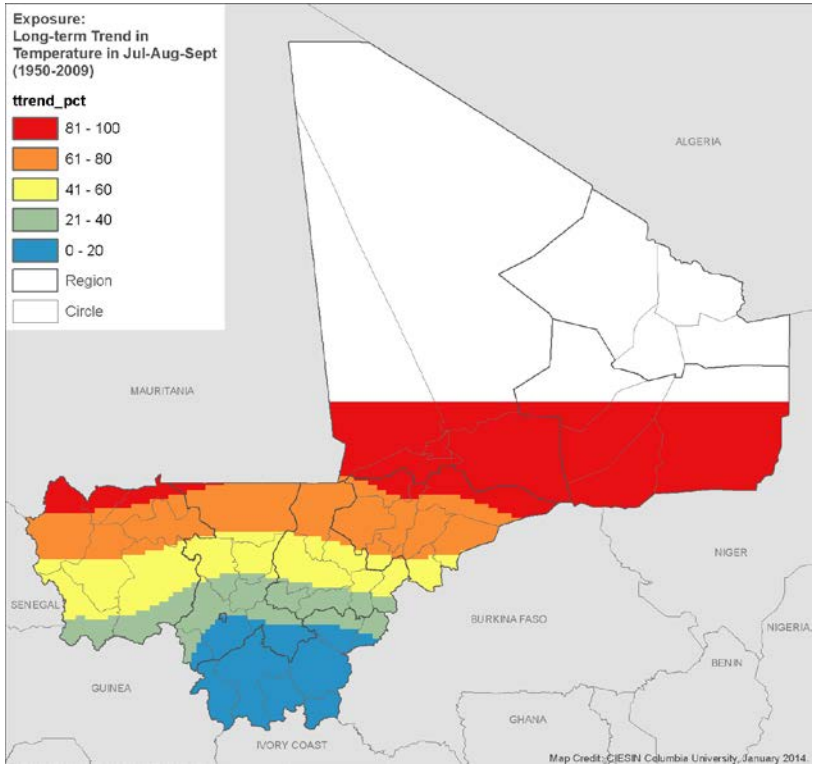

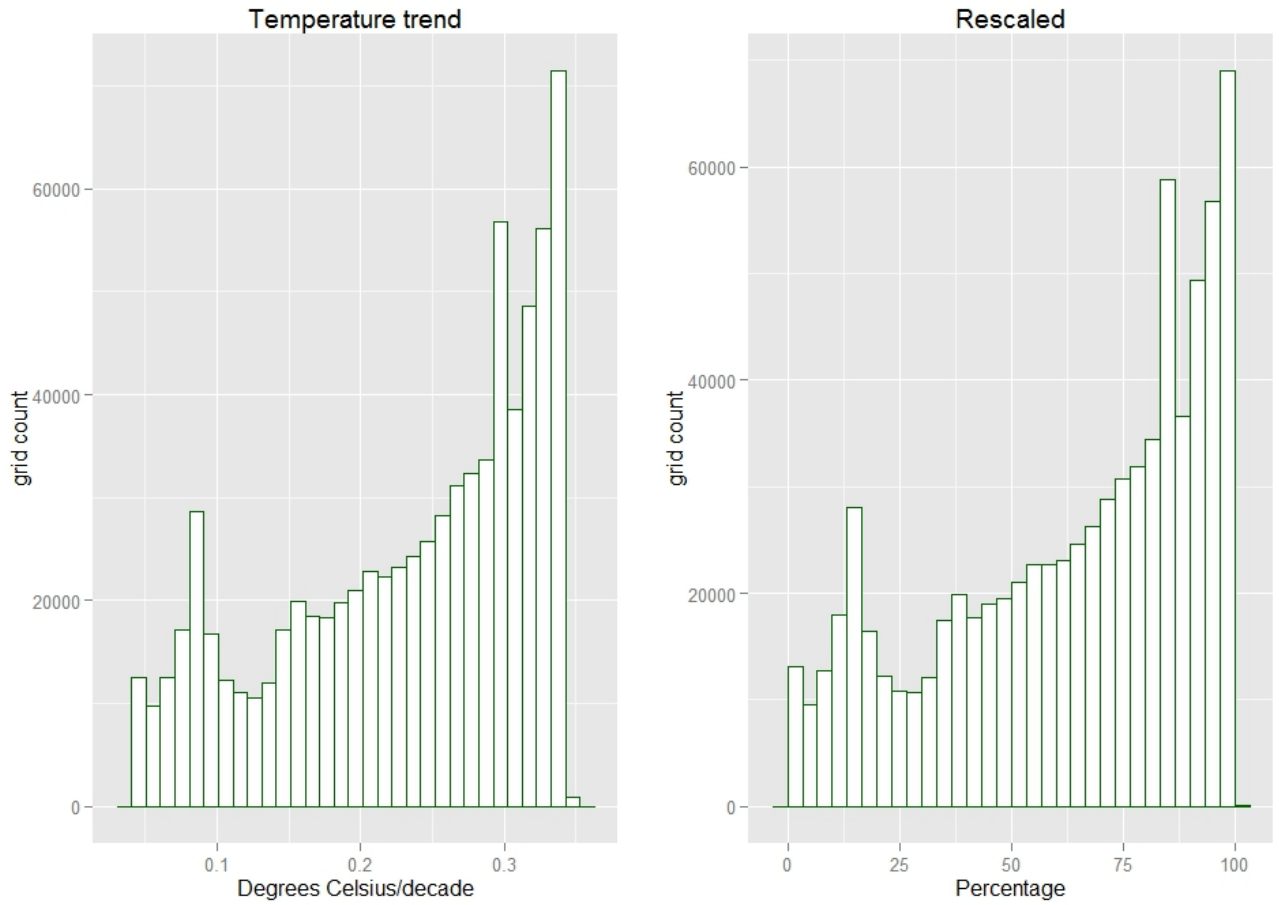

Title:	**Long-term Trend in July-August-September Temperature**
Indicator Code:	TTREND
Component:	exposure
Rationale:	The trend in temperature indicates an increase in temperature. In semi-dry areas, increases in temperature will increase evapotranspiration and hence increase the demand on water and water stress. Regions with the highest increase in

	temperature have experienced the highest changes in water demand and stress. Here only average temperature during the general growing season, July to September, is considered.
Source Data Set:	Calculated from the same FEWSNET data set as PRCP. Data courtesy of FEWSNET. The following is the methodological publication: Funk, C., Michaelsen, J., and Marshall, M. (2012). Mapping recent decadal climate variations in precipitation and temperature across Eastern Africa and the Sahel, chap. 14 in Wardlow, B., Anderson, M., and Verdin, J., eds., *Remote sensing of drought—Innovative monitoring approaches*. London, UK: Taylor and Francis.
Units:	Degrees Celsius/decade
Computation:	Original grid is 0.1x0.1 degree; has been resampled by CIESIN to 1km resolution by simply attributing the value of the larger grid cell to each smaller cell nested within it. The trend was obtained by adjusting a linear trend to temperature time-series in each cell.
Statistics for raw data:	Min=0.04, Max=0.34, Median=0.26, Mean=0.23, Standard Deviation=0.09 [computed for all of Mali below 17.2 degrees N latitude]
Scoring system:	Data has been transformed into 0-100, with 0 corresponding to lowest (possibly negative) trend (low exposure) and 100 to highest positive number (highest increase in temperature - high exposure)
Statistics for transformed data:	Min=0, Max=100, Median=71.24, Mean=63.74, Standard Deviation=28.74 [computed for all of Mali below 17.2 degrees N latitude]
Limitations:	This variable has been generated using FEWSNET gridded dataset produced by interpolating (kriging) station data from public sources, i.e., sparse coverage over most of the area. Additional come data from Agrhymet and National Meteorology Agency Ethiopia in CILSS countries and Ethiopia. Therefore, there is higher confidence in those areas. FEWSNET warns that: 'The data should not be used outside these nations: Burkina Faso, Burundi, Chad, Djibouti, Ethiopia, Eritrea, Gambia, Guinea Bissau, Guinea, Kenya, Mauritania, Mali, Niger, Rwanda, Sudan, Somalia, Sudan, Tanzania and Uganda." The temperature data are only available as anomalies from baseline temperatures in an original data set to which CIESIN did not have access. This meant that we could calculate trends per decade but not absolute temperatures.
Spatial Extent:	Original data set 12S-25N, 20W-52E; here only area 12N-25N and 12.3W-4.45E used
Spatial Resolution:	Original 0.1x0.1 degree
Year of Publication:	2011
Time Period:	Original length 1901-2009; here only data from 1950 to 2009 used
Additional Notes:	
Date:	10/08/2013

Format:	Excel file
File Name:	climate_fishnet_10082013.xls
Contact person:	FEWSNET: Chris Funk; CIESIN: Sylwia Trzaska

Flood Frequency

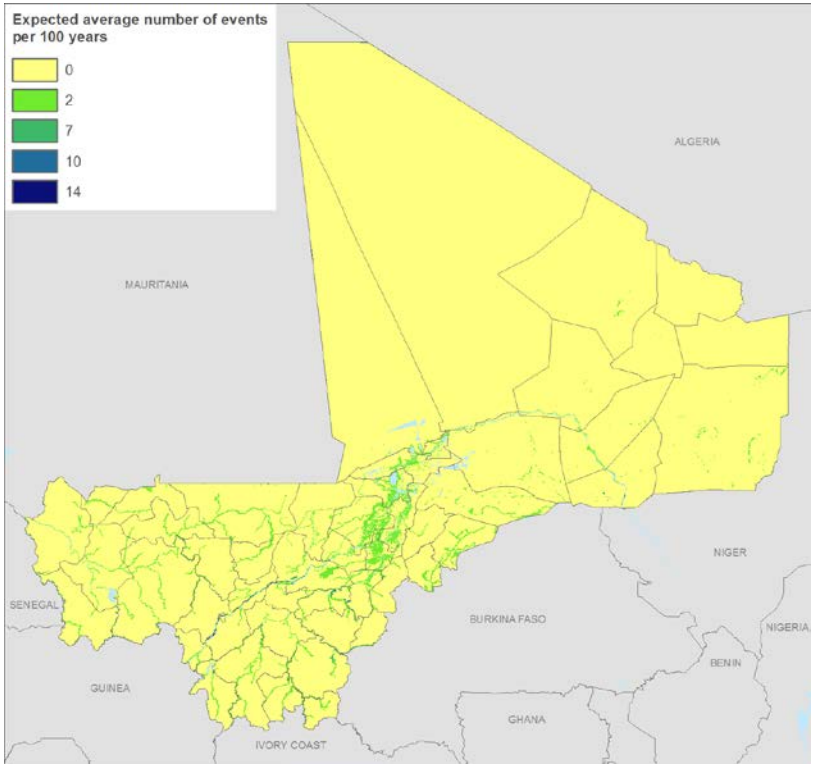

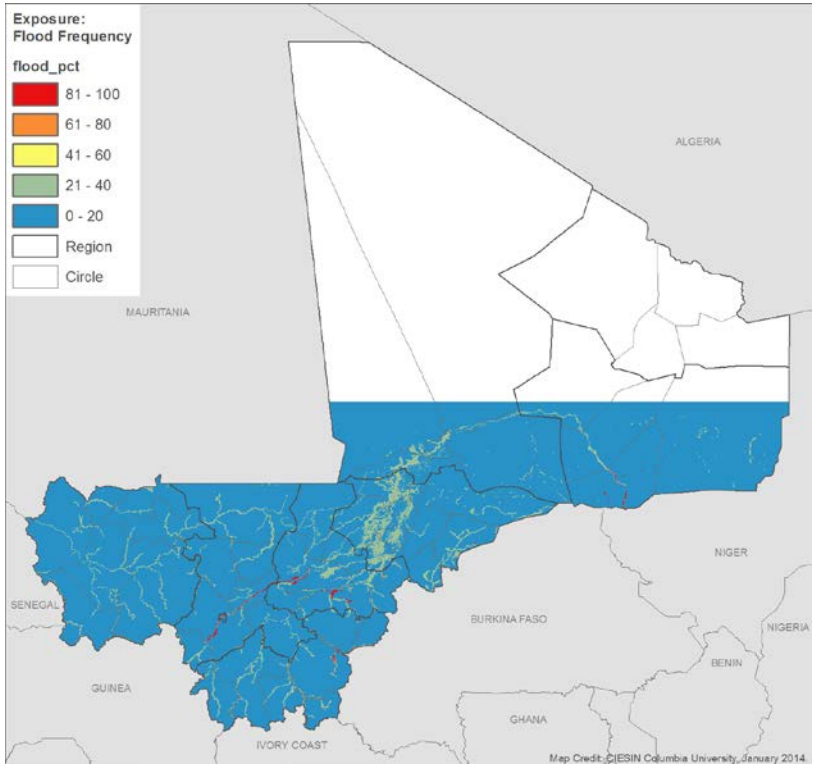

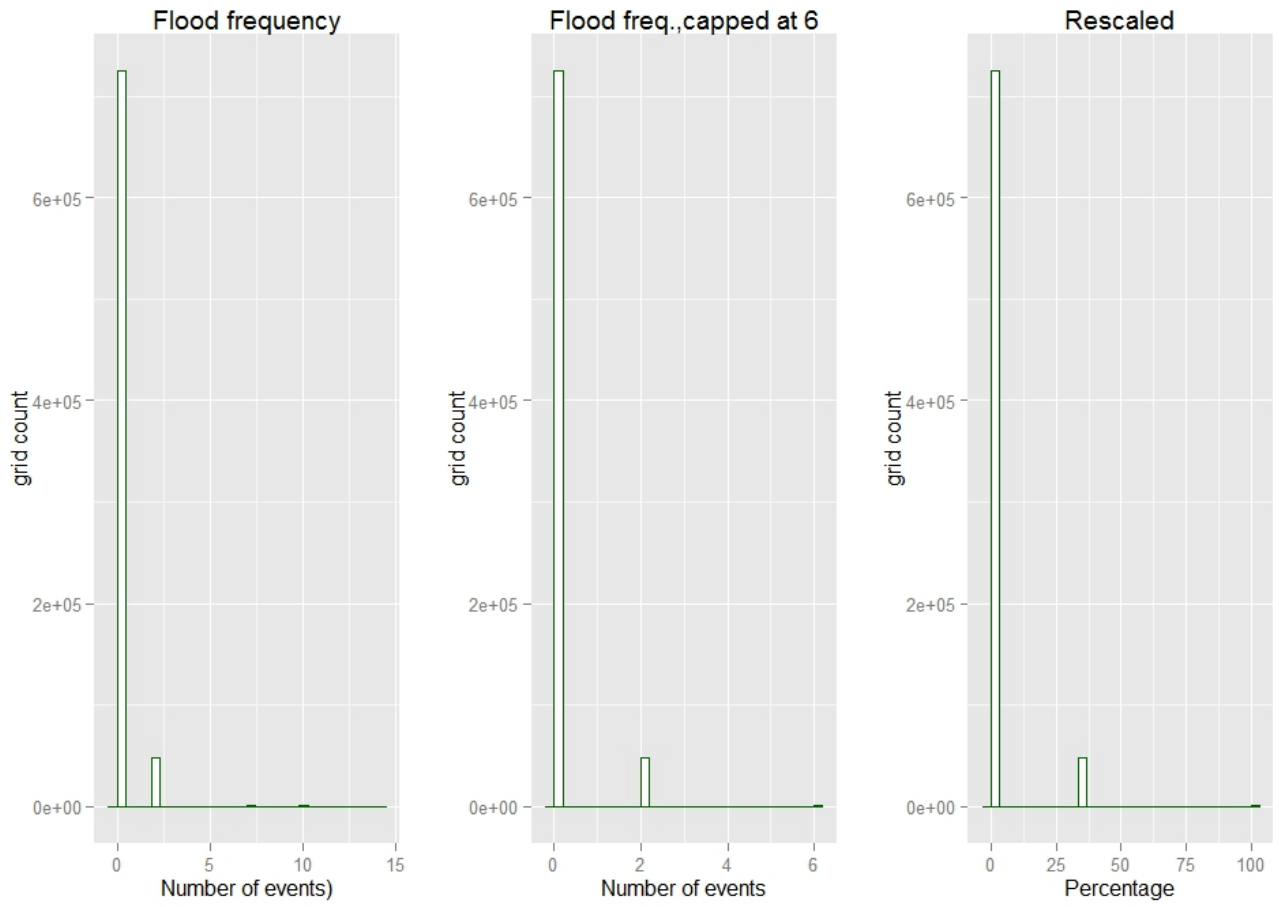

Title:	Flood frequency
Indicator Code:	FLOOD
Component:	Exposure
Rationale:	Floods can have adverse impacts on crops and livelihoods, and can result in human morbidity and mortality.

Source Data Set:	This dataset includes an estimate of flood frequency. It is based on three sources: 1) A GIS modeling using a statistical estimation of peak-flow magnitude and a hydrological model using HydroSHEDS dataset and the Manning equation to estimate river stage for the calculated discharge value. 2) Observed flood from 1999 to 2007, obtained from the Dartmouth Flood Observatory (DFO). 3) The frequency was set using the frequency from UNEP/GRID-Europe PREVIEW flood dataset. In the area where no information was available, it was set to 50 years returning period. Unit is expected average number of events per 100 years. This product was designed by UNEP/GRID-Europe for the Global Assessment Report on Risk Reduction (GAR). It was modeled using global data. Credit: GIS processing UNEP/GRID-Europe, with key support from USGS EROS Data Center, Dartmouth Flood Observatory 2008. • UNEP/DEWA/GRID-Europe • United National Environment Program Division of Early Warning and Assessment Global Resource Information Database • Downloaded from PREVIEW Global Risk Data Platform
Units:	Expected average number of events per 100 years
Computation:	The flood frequency data were subset to the Mali national boundary extent using ArcGIS Extract by Mask tool and a 30 arc-second raster mask generated from a 30 arc-second fishnet. Raster values were extracted using ArcGIS Extract Values to Points tool and the 30 arc-second fishnet centroids. The output was exported to a .csv table for statistical analysis.
Statistics for raw data:	Min=0, Max=14, Median=0, Mean=0.14, Standard Deviation=0.65 [computed for all of Mali below 17.2 degrees N latitude]
Scoring system:	Data values were winsorized at six events. Flood frequency was then transformed such that six events in 100 years results in a score of 100, ranging down to 0 events, which results in a score of 0.
Statistics for transformed data:	Min=0, Max=100, Median=0, Mean=2.3, Standard Deviation=9.29 [computed for all of Mali below 17.2 degrees N latitude]
Limitations:	This dataset was generated using a global dataset; it should not be used for local applications (such as land planning). The only purpose was to identify flood areas at the global level and to identify areas where more detailed data should be collected. Some flooded areas are clearly underestimated – for example in coastal areas or large flood plains. This analysis was conducted using global datasets, the resolution of which is not relevant for in-situ planning and should not be used for life-and-death decisions. UNEP and collaborators should in no case be liable for misuse of the presented results. The designations employed and the presentation of material on the maps do not imply the expression of any opinion whatsoever on the part of UNEP or the Secretariat of the United Nations concerning the legal status of any country, territory, city or area or of its authorities, or concerning the delimitation of its frontiers or boundaries.
Spatial Extent:	Global
Spatial Resolution:	0.0833 decimal degrees (~10 km)
Year of Publication:	2009
Time Period:	Observed flood from 1999 to 2007

Additional Notes:	Downloaded from PREVIEW Global Risk Data Platform: http://preview.grid.unep.ch/index.php?preview=data&events=floods&evcat=2&lang=eng Metadata: http://geonetwork.grid.unep.ch/geonetwork/srv/en/iso19115to19139.xml?id=70
Date:	Downloaded on 29 August 2013
Format:	GeoTiff
File Name:	Fl_frequency
Contact person:	

AIV.2 SENSITIVITY INDICATORS

Household Wealth Index

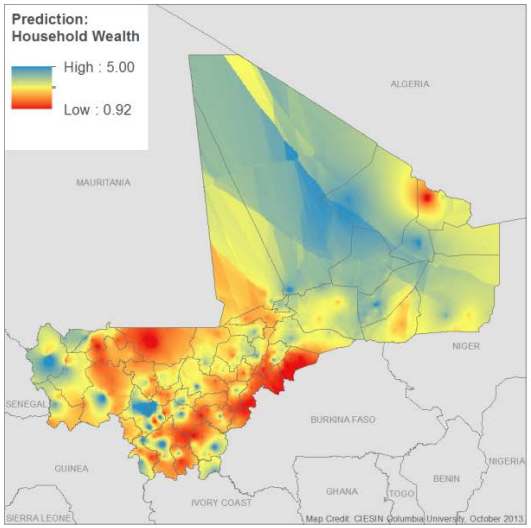

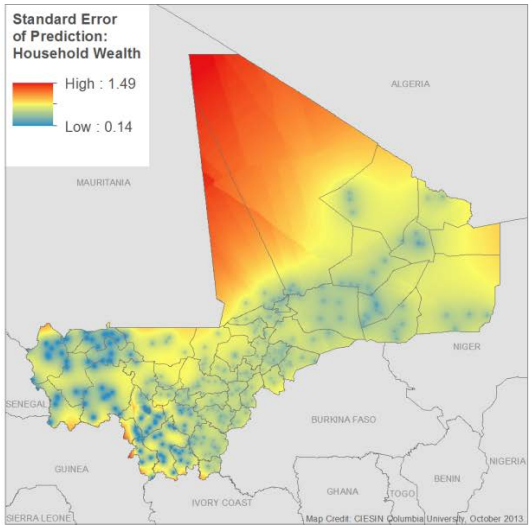

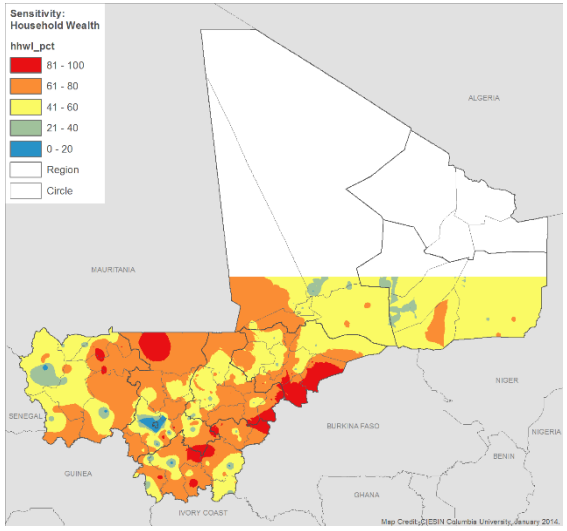

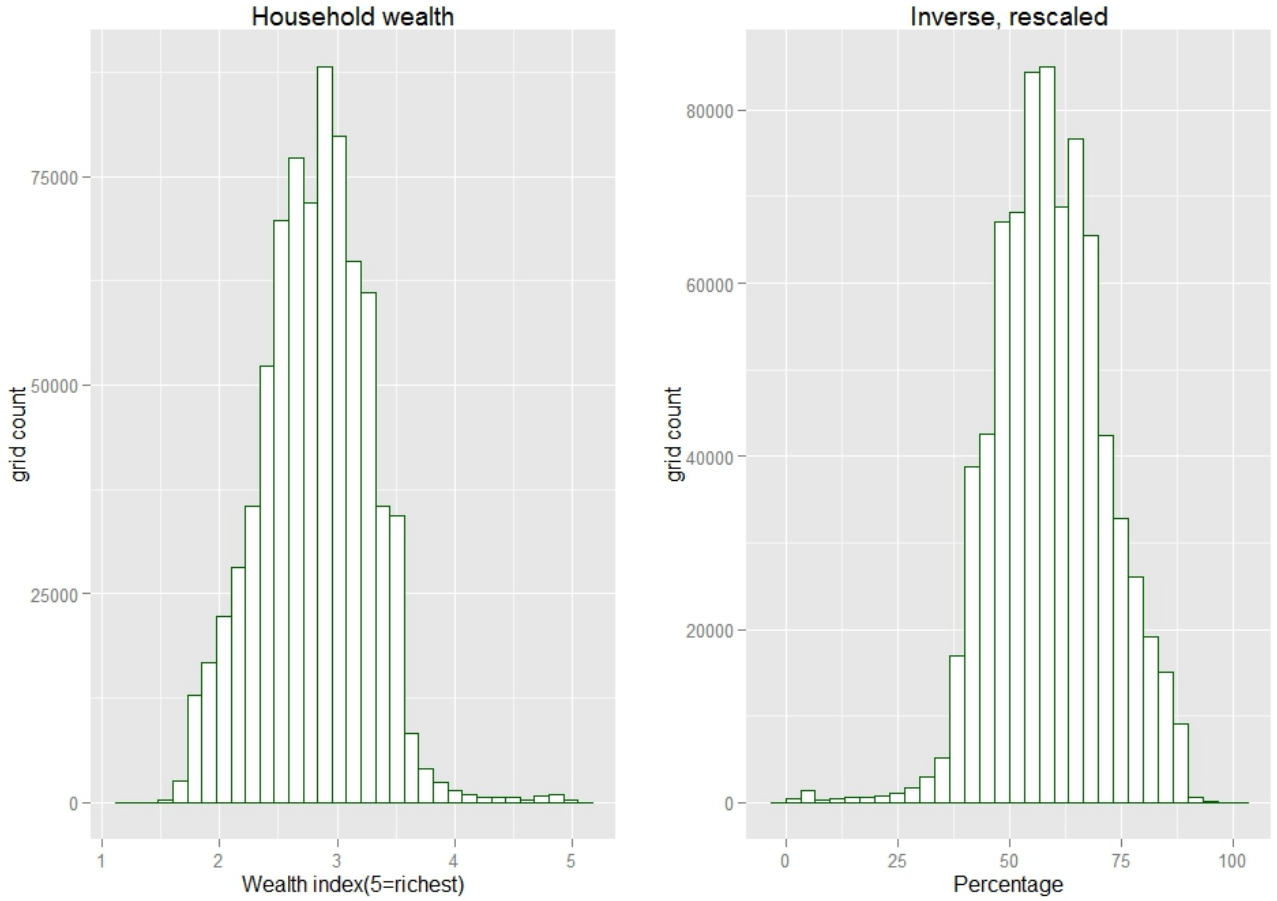

Title:	Household Wealth Index
Indicator Codes:	HHWL
Component:	Sensitivity
Rationale:	High levels of household wealth are assumed to contribute to greater resilience, while low levels of household wealth are assumed to lead to greater sensitivity to climate shocks, with a greater likelihood that households will need to sell assets

	or migrate during periods of prolonged stress.
Source Data Set:	The DHS wealth index is a composite measure of a household's cumulative living standard. The wealth index is calculated using easy-to-collect data on a household's ownership of selected assets, such as televisions and bicycles, materials used for housing construction, and types of water access and sanitation facilities. Generated with a statistical procedure known as principal components analysis, the wealth index places individual households on a continuous scale of relative wealth. DHS separates all interviewed households into five wealth quintiles to compare the influence of wealth on various population, health, and nutrition indicators. The wealth index is presented in the DHS Final Reports and survey datasets as a background characteristic. The cluster-level household wealth index data were kindly provided by Marta Jankowska and were used in the following paper. Citation: Jankowska, M., D. Lopez-Carr, C. Funk, G.J. Husak, Z.A. Chafe. (2012). Climate change and human health: Spatial modeling of water availability, malnutrition, and livelihoods in Mali, Africa. *Applied Geography*, 33:4-15
Units:	Index of 1-5 (with 5 being richest)
Computation:	To create a surface from the cluster points, we followed the proceeding steps. We created 30 arc-second (0.00833 degrees; ~1km) *prediction* and *prediction standard error* surfaces from the cluster point data using ArcGIS's Empirical Bayesian Kriging tool. The rasters were subset to the Mali national boundary extent using ArcGIS Extract by Mask tool and a 30 arc-second raster mask generated from a 30 arc-second fishnet. Raster values were extracted using ArcGIS Extract Values to Points tool and the 30 arc-second fishnet centroids. The outputs were exported to .csv tables for re-coding and statistical analysis. Because the data are spatially interpolated, the standard error helps us to understand the levels of uncertainty in the data presented in the left-hand map. In general, confidence levels are highest where the cluster points are closest together. Confidence is lowest in the northernmost sections of Mali, which were excluded from the present mapping activity.
Statistics for raw data:	*Min=1.30, Max=5, Median=2.83, Mean=2.81, Standard Deviation=0.46* [computed for all of Mali below 17.2 degrees N latitude]
Scoring system:	Raster values were re-scaled to 0-100, with high household wealth representing low sensitivity.
Statistics for transformed data:	*Min=0, Max=100, Median=58.68, Mean=59.26, Standard Deviation=12.45* [computed for all of Mali below 17.2 degrees N latitude]
Limitations:	For limitations, see the DHS Data Quality and Use page, available at: https://www.measuredhs.com/data/Data-Quality-and-Use.cfm.
Spatial Extent:	Mali

Spatial Resolution:	The spatial resolution of the areas represented by each cluster point varies based on the density of cluster points. The resulting grid was at 30 arc-seconds.
Year of Publication:	2007
Time Period:	2006
Additional Notes:	Two records in the cluster dataset were lacking latitude and longitude information. These were removed from the shapefile prior to generating the surfaces. Regarding the general use of cluster data from the DHS, geographic information is collected in the DHS and AIDS Indicator Survey (AIS) surveys. All survey data are presented both nationally and by sub-national reporting areas. These reporting areas are often, but not always, provinces or groups of provinces; they are included in all recoded datasets. But one can obtain higher levels of spatial precision by using the cluster data. The cluster dataset has one record for every cluster in which the survey was conducted. This type of file includes the latitude and longitude of the center of the sample cluster. Further information can be found at: https://www.measuredhs.com/data/File-Formats.cfm#CP_JUMP_8037
Date:	Downloaded 8/28/13 from http://www.measuredhs.com/
Format:	esri shapefile and dbf
File Name:	child_clusters.dbf child_clust.shp
Contact person:	N/A

Child Stunting

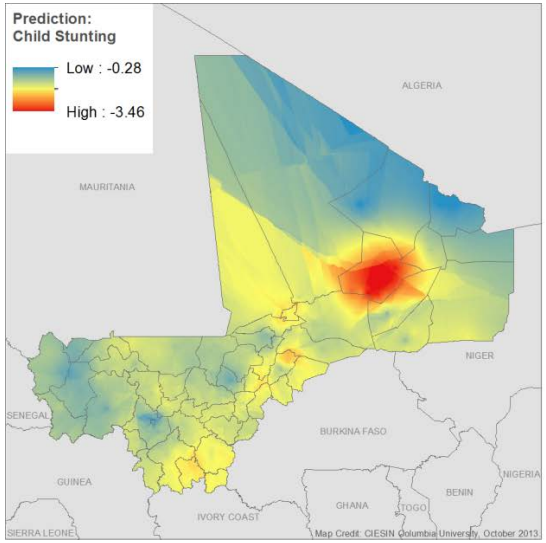

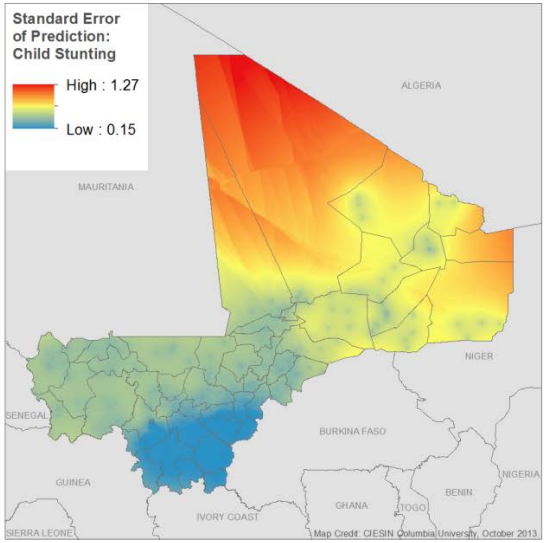

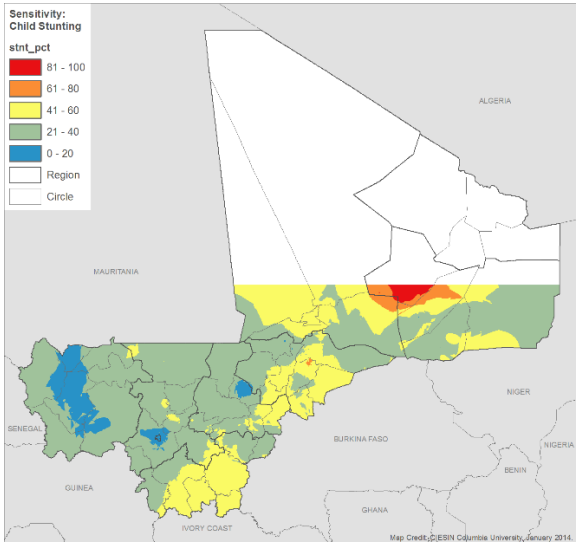

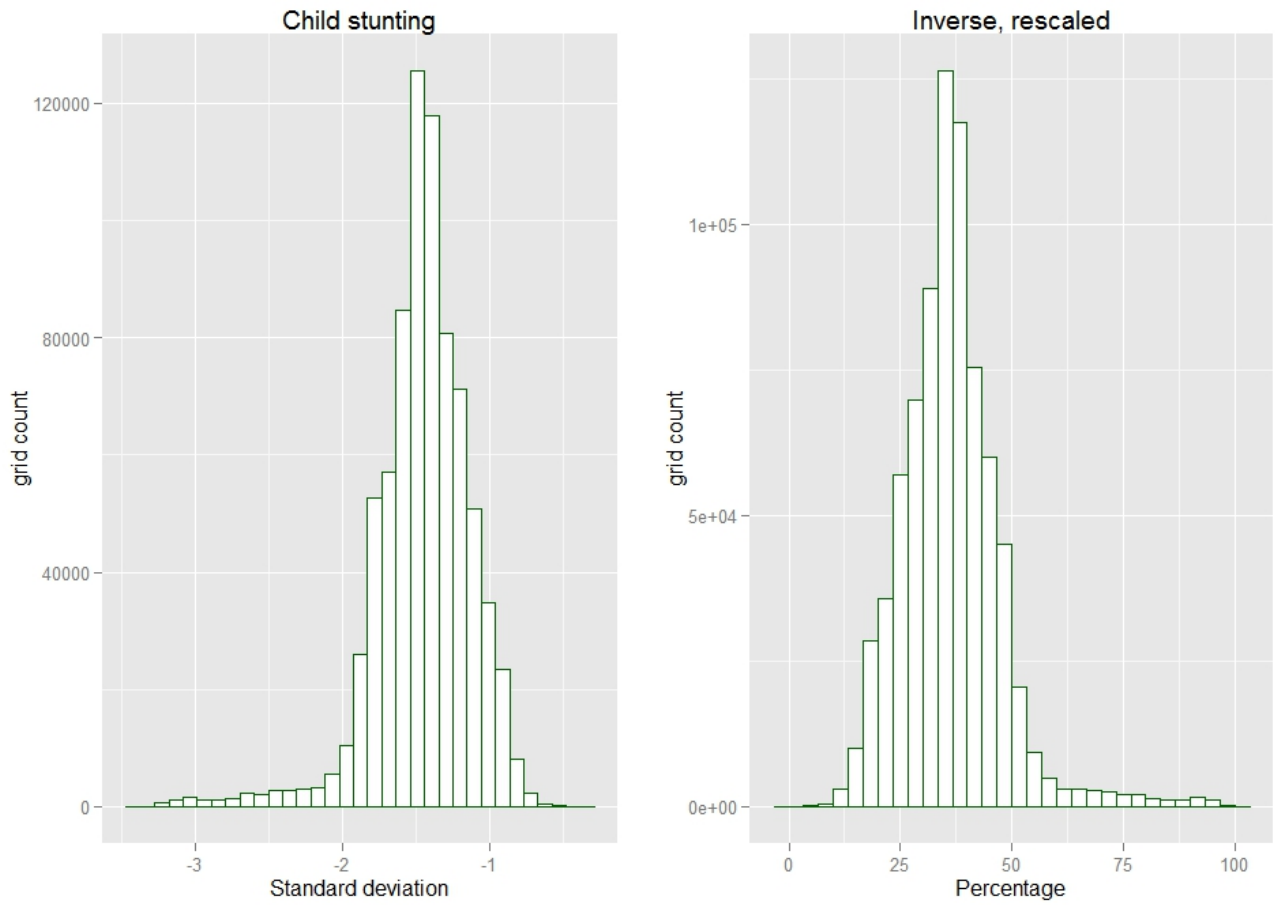

Title:	Child Stunting
Indicator Codes:	STNT
Component:	Sensitivity
Rationale:	Children that are already suffering the impact of long-term malnutrition will be more sensitive to climate stressors.

Source Data Set:	Stunting is defined as having a height (or length)-for-age more than two standard deviations below the median of the National Center for Health Statistics (NCHS)/World Health Organization (WHO) growth reference population. Stunting represents the effects of long-term malnutrition. The cluster level data were kindly provided by Marta Jankowska, and were used in the following paper. Citation: Jankowska, M., D. Lopez-Carr, C. Funk, G.J. Husak, Z.A. Chafe. (2012). Climate change and human health: Spatial modeling of water availability, malnutrition, and livelihoods in Mali, Africa. *Applied Geography*, 33:4-15
Units:	Z-scores (0 equals the mean, -1 equals one standard deviation below the international reference population; note that all scores in Mali are *below* the reference population)
Computation:	To create a surface from the cluster points, we followed the following steps. We created 30 arc-second (0.00833 degree; ~1km) *prediction* and *prediction standard error* surfaces from the cluster point data using ArcGIS's Empirical Bayesian Kriging tool. The rasters were subset to the Mali national boundary extent using ArcGIS Extract by Mask tool and a 30 arc-second raster mask generated from a 30 arc second fishnet. Raster values were extracted using ArcGIS Extract Values to Points tool and the 30 arc-second fishnet centroids. The outputs were exported to .csv tables for re-coding and statistical analysis. Because the data are spatially interpolated, the standard error helps us to understand the levels of uncertainty in the data presented in the left-hand map. In general, confidence levels are highest where the cluster points are closest together. Confidence is lowest in the northernmost sections of Mali, which were excluded from the present mapping activity.
Statistics for raw data:	Min=-3.30, Max-0.41, Median=-1.45, Mean=-1.46, Standard Deviation=0.32 [computed for all of Mali below 17.2 degrees N latitude]
Scoring system:	Raster values were re-scaled to 0-100, with high stunting equating to high sensitivity.
Statistics for transformed data:	Min=0, Max=100, Median=35.90, Mean=36.36, Standard Deviation=11.18 [computed for all of Mali below 17.2 degrees N latitude]
Limitations:	For limitations, see the DHS Data Quality and Use page, available at: https://www.measuredhs.com/data/Data-Quality-and-Use.cfm.
Spatial Extent:	Mali
Spatial Resolution:	The spatial resolution of the areas represented by each cluster point varies depending on the density of cluster points. The resulting grid was at 30 arc-seconds.
Year of Publication:	2007
Time Period:	2006
Additional Notes:	Two records in the cluster dataset were lacking latitude and longitude information. These were removed from the

	shapefile prior to generating the surfaces. Further information on the use of cluster data can be found in the Additional Notes section of the Household Wealth metadata.
Date:	Downloaded 8/28/13 from http://www.measuredhs.com/
Format:	Esri shapefile and dbf
File Name:	Mali CV Mapping_FINAL.docxchild_clust.shp
Contact person:	Marta Jankowska, University of California San Diego

Infant Mortality Rate

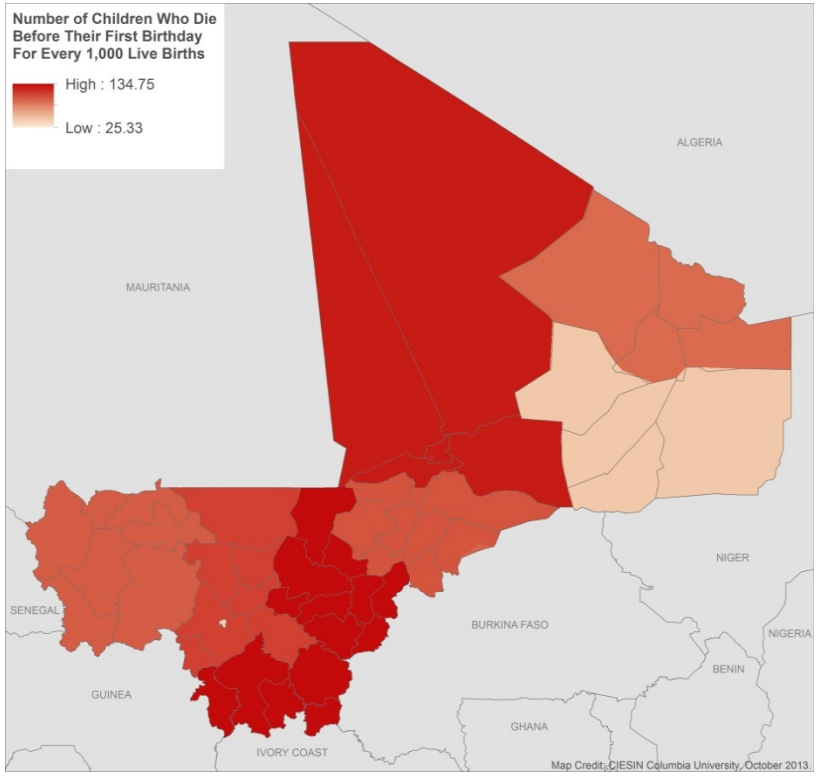

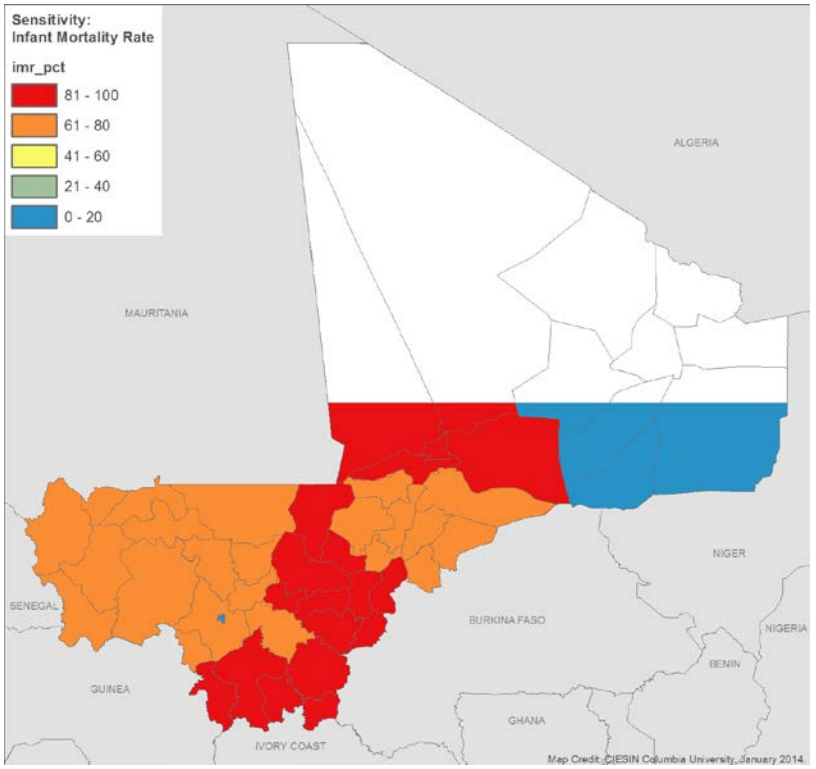

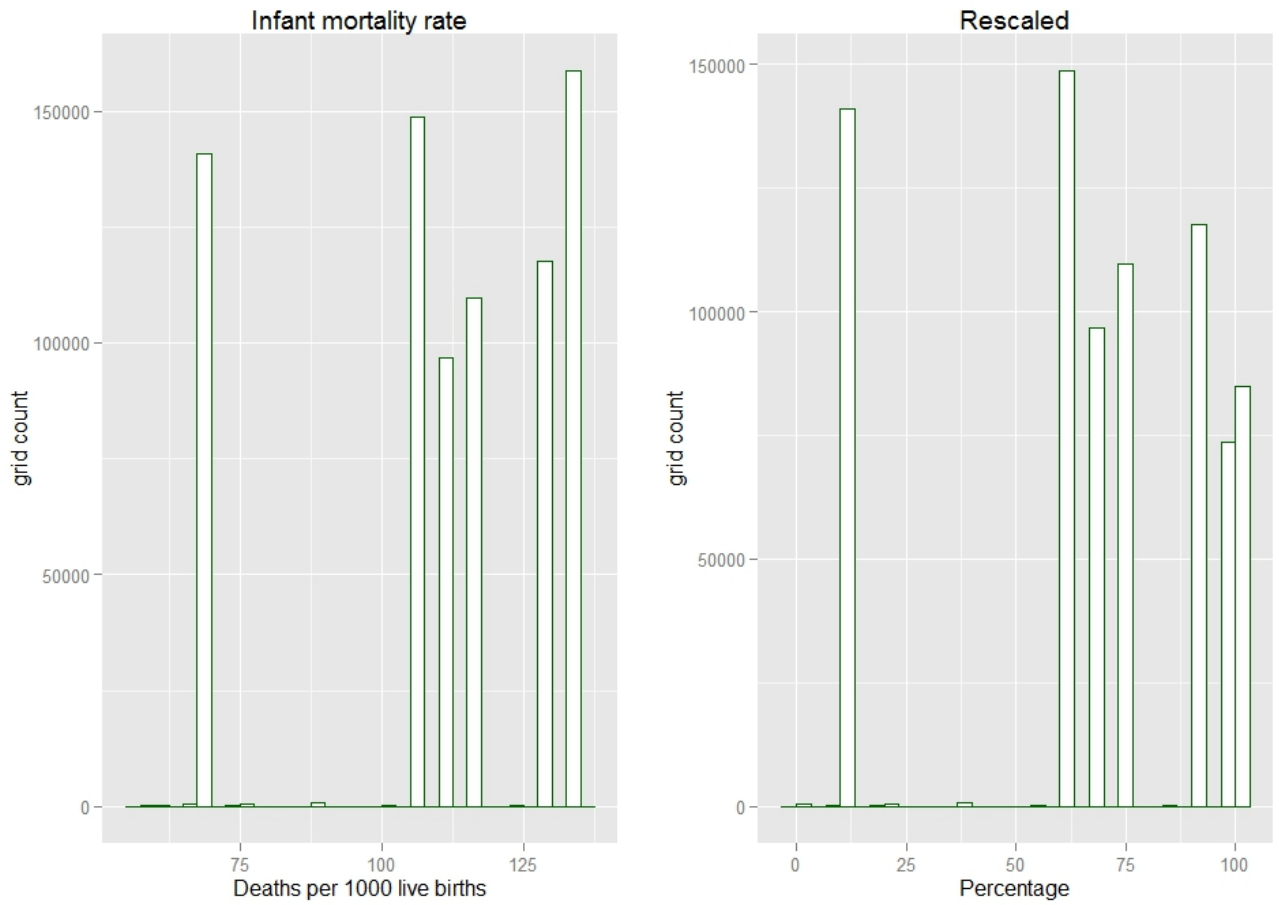

Title:	Infant Mortality Rate
Indicator Code:	IMR
Component:	Sensitivity
Rationale:	Infant mortality, which is measured in deaths per live births, is associated with a number of human wellbeing measures such as income and health indicators. High infant mortality suggests higher sensitivity to climate hazards.

Source Data Set:	Global Sub-National Infant Mortality Rate Database 2008, EI&W Version 1: November 2010 adjusted to 2011. The data set includes 2006 baseline data for Mali from DHS. This data set is an updated version of the following. Citation: Center for International Earth Science Information Network (CIESIN)/Columbia University. (2005). *Poverty Mapping Project: Global Subnational Infant Mortality Rates*. Palisades, NY: NASA Socioeconomic Data and Applications Center (SEDAC). http://sedac.ciesin.columbia.edu/data/set/povmap-global-subnational-infant-mortality-rates.
Units:	The infant mortality rate for a region or country is defined as the number of children who die before their first birthday for every 1,000 live births.
Computation:	Mali 2006 data adjusted using 2011 UNICEF national-level estimates. The global IMR data were subset to the Mali national boundary extent using ArcGIS Extract by Mask tool and a 30 arc-second raster mask generated from a 30 arc-second fishnet. Raster values were extracted using ArcGIS Extract Values to Points tool and the 30 arc-second fishnet centroids. The output was exported to a .csv table for statistical analysis.
Statistics for raw data:	Min=59.79, Max=134.80, Median=110.20, Mean=110.70, Standard Deviation=21.99 [computed for all of Mali below 17.2 degrees N latitude]
Scoring system:	Raster values were re-scaled to 0-100 based with high values representing high sensitivity.
Statistics for transformed data:	Min=0, Max=100, Median=67.32, Mean=67.93, Standard Deviation=29.34[computed for all of Mali below 17.2 degrees N latitude]
Limitations:	Mali 2006 data adjusted using 2011 UNICEF national-level estimates.
Spatial Extent:	Global
Spatial Resolution:	0.00833 decimal degrees (~1 kilometer)
Year of Publication:	unpublished
Time Period:	2011 (baseline data from 2006 were adjusted to be consistent with United Nations Children's Fund [UNICEF] reported national rates for 2011)
Additional Notes:	
Date:	Obtained on 28 August 2013
Format:	img
File Name:	imr_2011_adjusted
Contact person:	Kytt MacManus, CIESIN

Poverty Index

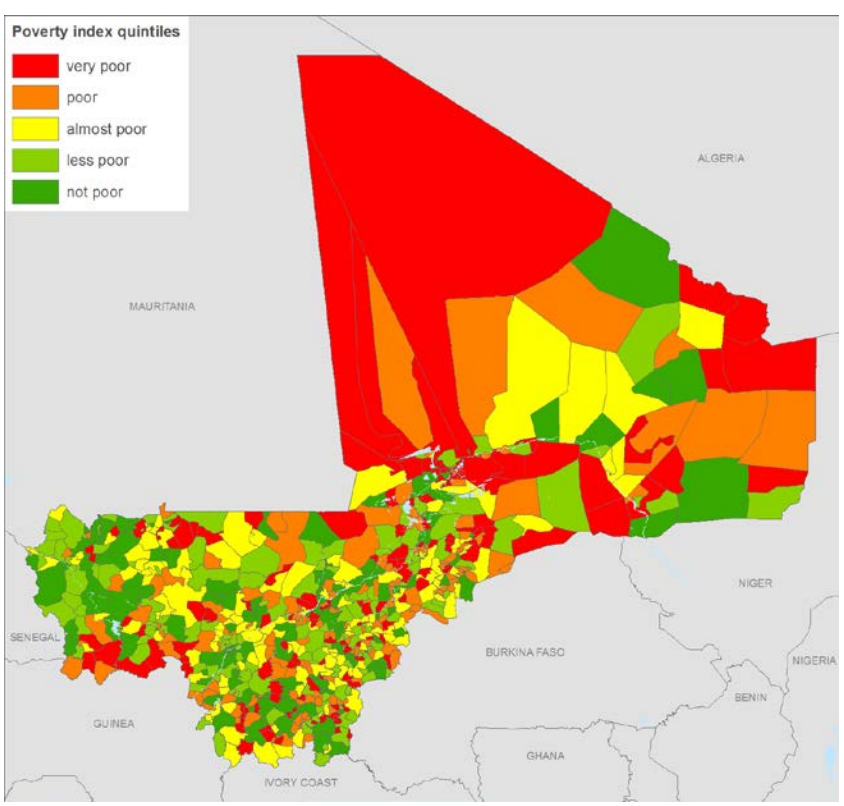

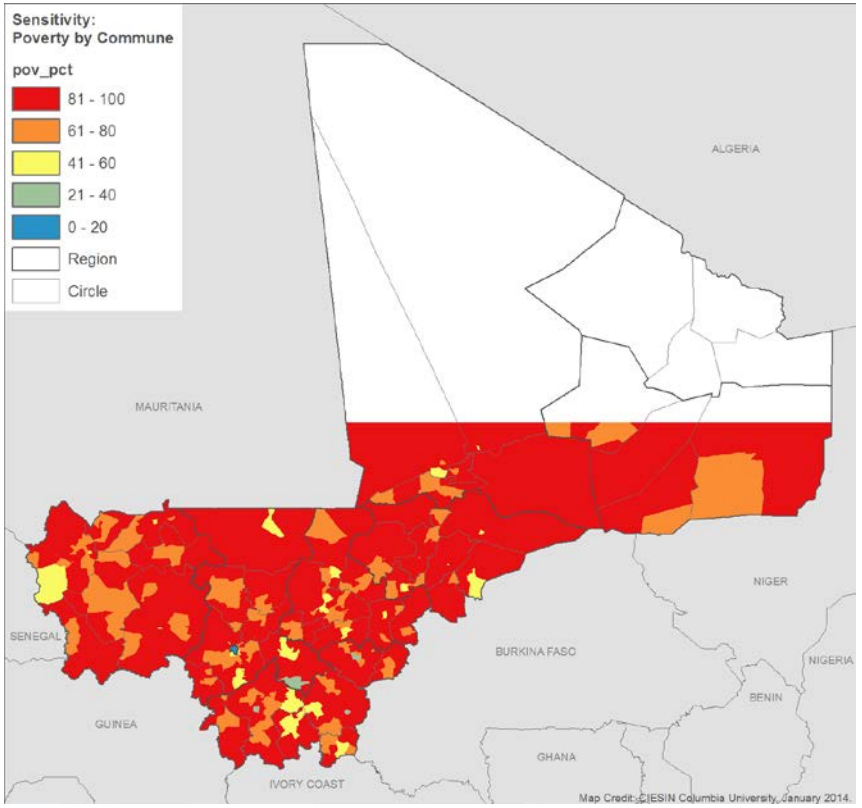

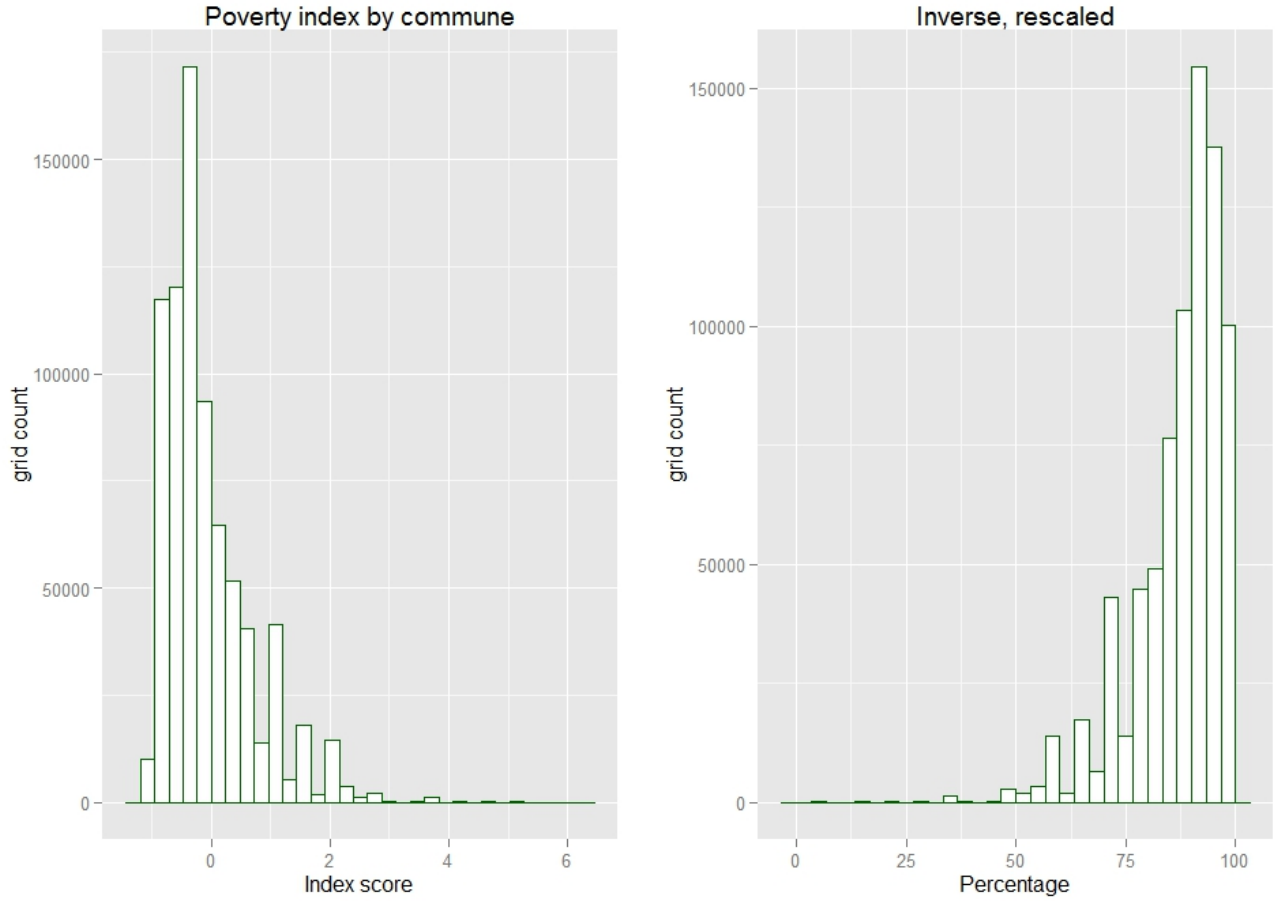

Title:	Poverty Index
Indicator Code:	POVI
Component:	Sensitivity
Rationale:	High poverty rates are likely to be associated with higher sensitivity to climate hazards.

Source Data Set:	The data on Poverty Index by Commune were collected in 2008 by *Observatoire du Developpement Durable Humain* (ODHD) and integrated in its 2010 report. The original French field names were renamed as follows: • Indice_de_pauvrete_communale [IPC] - POV_LEVEL (ranges from -1.00606 to 6.18484) • Groupe_de_pauvrete_communale - POV_GROUP ("very poor" to "not poor") The NTILES_IPC field is the POV_LEVEL (poverty index) field mapped to percentiles (it ranges from 1 to 5). We used POV_LEVEL to create this indicator.
Units:	Poverty scores
Computation:	The tabular data were matched to the GPW4 boundaries using the commune name as the field upon which the join was made. A spatial join was used to add the attributes from the boundary dataset to a centroids layer and the final point file output. This was exported to a .csv file for statistical analysis.
Statistics for raw data:	Min=-0.99, Max=6.185, Median=-0.28, Mean=-0.07, Standard Deviation=0.75 [computed for all of Mali below 17.2 degrees N latitude]
Scoring system:	Raster values were rescaled to 0-100 based on percentiles, high percentage values in the transformed variable representing high vulnerability.
Statistics for transformed data:	Min=0, Max=100, Median=90.08, Mean=87.10, Standard Deviation=10.43 [computed for all of Mali below 17.2 degrees N latitude]
Limitations:	Poverty index data are only available at the commune level; therefore, they do not capture sub-commune variation in poverty rates.
Spatial Extent:	Mali
Spatial Resolution:	Commune level
Year of Publication:	2010
Time Period:	2008
Additional Notes:	
Date:	Received from Amadou Diakité on 9/9/2013
Format:	Tabular data set
File Name:	Mali Poverty_ODHD_2008.xlsx
Contact person:	Amadou Diakité, Program Information Management Specialist, USAID Mali / PRM

Conflict (Political Violence)

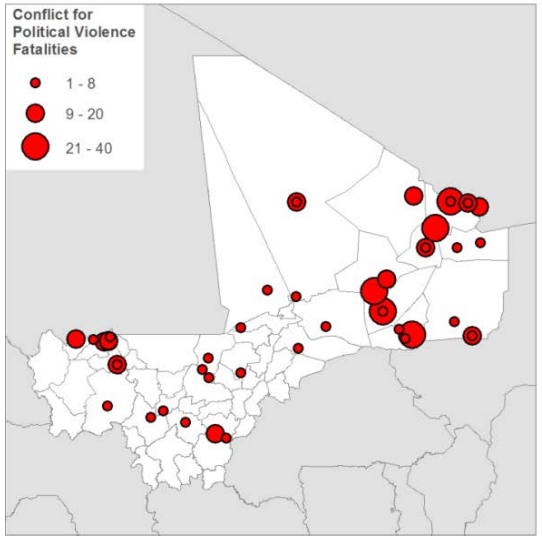

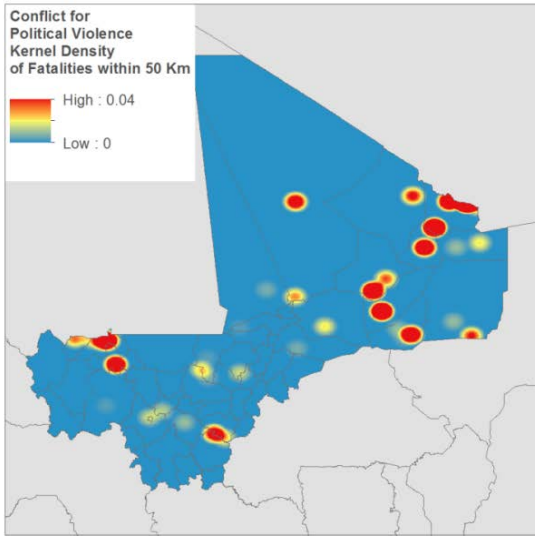

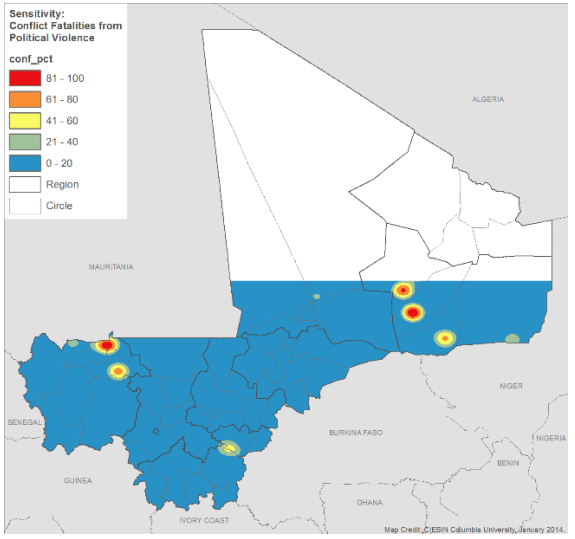

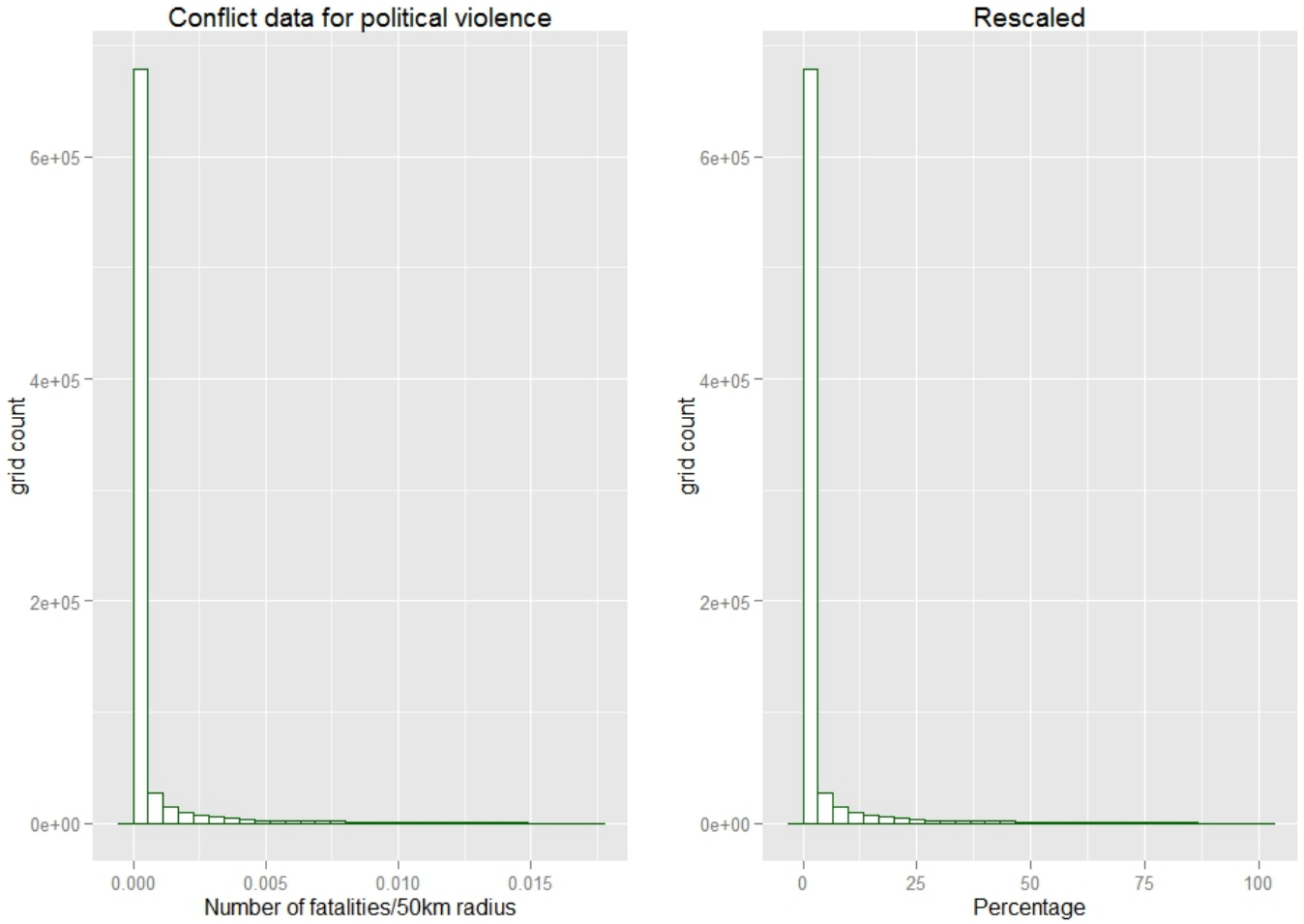

Title:	Conflict (Political Violence)
Indicator Code:	CONF
Component:	Sensitivity

Rationale:	Armed conflict reduces human security and increases the sensitivity of populations to climate stressors.
Source Data Set:	Armed Conflict Location and Event Dataset (ACLED), downloaded from: http://www.acleddata.com/data/africa/. Citation: Raleigh, Clionadh, Andrew Linke, Håvard Hegre and Joakim Karlsen. (2010). Introducing ACLED-Armed Conflict Location and Event Data. Journal of Peace Research 47(5) 1-10.
Units:	Number of fatalities per unit area within a 50km radius
Computation:	Only locations with conflict fatalities were assessed (points with zero fatalities were removed). A kernel density grid was created, weighted by the number of fatalities. The pixels of the kernel density grid represent the number of fatalities per unit area from the location of the conflict site within a 50-km radius. The output was exported to a .csv table for statistical analysis.
Statistics for raw data:	Min=0, Max=0.017, Median=0, Mean=0.0005, Standard Deviation=0.0017 [computed for all of Mali below 17.2 degrees N latitude]
Scoring system:	Conflict levels, as determined by a surface created from the original points data where severity was measured by fatalities, were transformed to a percentile scale in which high conflict results in high sensitivity.
Statistics for transformed data:	Min=0, Max=100, Median=0, Mean=0, Standard Deviation=9.76 [computed for all of Mali below 17.2 degrees N latitude]
Limitations:	Event data are derived from a variety of sources, including reports from developing countries and local media, humanitarian agencies, and research publications. Gaps in the record are possible.
Spatial Extent:	Mali
Spatial Resolution:	points
Year of Publication:	2012
Time Period:	1997 to 2012
Additional Notes:	
Date:	Downloaded on 08/29/2013
Format:	Shapefile
File Name:	XYMali.shp
Contact person:	

Soil Organic Carbon

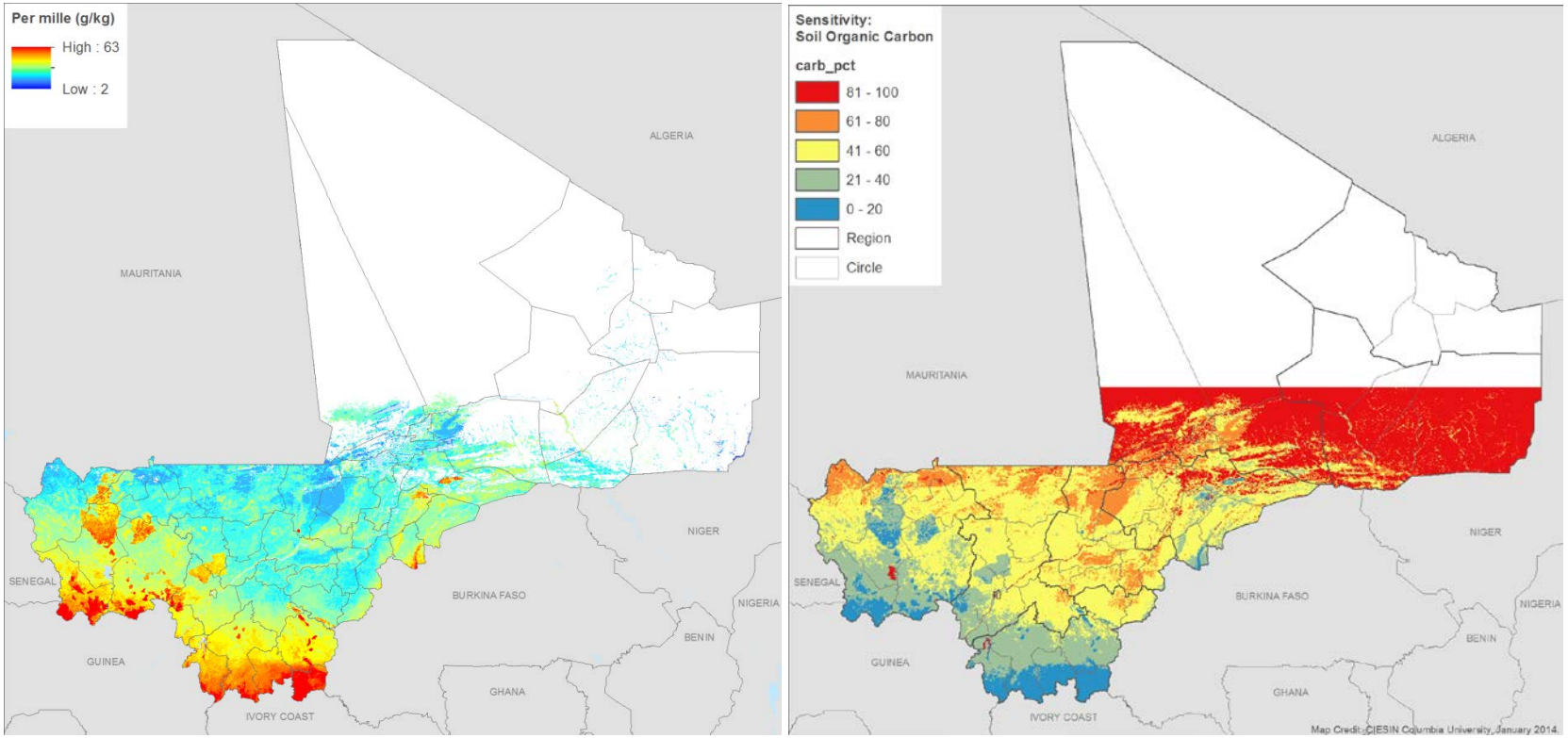

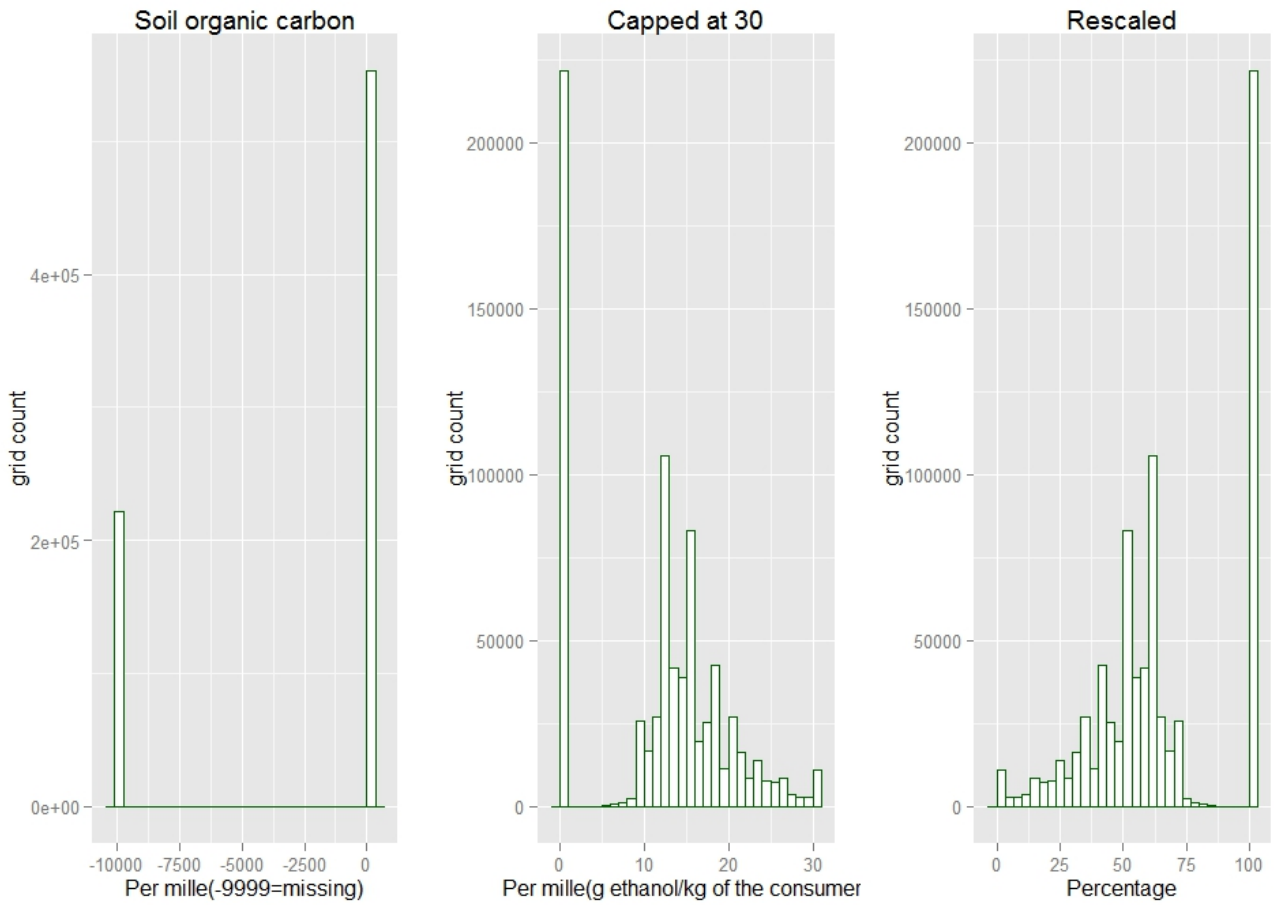

Title:	Soil organic carbon predicted mean
Indicator Code:	CARB
Component:	Sensitivity
Rationale:	Soil organic matter is generally associated with higher crop yields and greater soil moisture retention, thus making areas with higher soil organic matter more resilient to climate variability and change.

Source Data Set:	International Soil Reference and Information Centre (ISRIC) – World Soil Information, 2013. Soil property maps of Africa at 1 km. Available for download at www.isric.org.
Units:	Per mille (g of ethanol/kg of consumer)
Computation:	The soil organic carbon predicted mean for the 1st standard depth (0–5cm), 2nd standard depth (5–15cm) and 3rd standard depth (15–30cm) were summed for an approximation of the soil organic carbon in top soil, which is 0–20cm. The soil organic carbon data were subset to the Mali national boundary extent using ArcGIS Extract by Mask tool and a 30 arc-second raster mask generated from a 30 arc-second fishnet. Raster values were extracted using ArcGIS Extract Values to Points tool and the 30 arc-second fishnet centroids. The output was exported to a .csv table for statistical analysis.
Statistics for raw data:	With missing values: Min=-9999, Max=63, Median=12, Mean=-2850, Standard Deviation=4526.21 [computed for all of Mali below 17.2 degrees N latitude] Without missing values: Min=0, Max=63, Median=12, Mean=11.22, Standard Deviation=8.32 [computed for all of Mali below 17.2 degrees N latitude]
Scoring system:	Missing values in northern Mali were recoded to 0 organic carbon on the assumption that these areas have very sandy soils with sparse vegetation and low organic carbon. The data were winsorized at value 30, as the areas with values of 30 or more were considered highly vulnerable. Data values were inverted and re-scaled from 0-100 based on the percentile distribution of the raw data, such that high soil carbon is associated with low vulnerability and vice versa.
Statistics for transformed data:	Min=0, Max=100, Median =60, Mean=62.81, Standard Deviation=27.13 [computed for all of Mali below 17.2 degrees N latitude]
Limitations:	The accuracy of the maps has been assessed using five-fold cross-validation and has been derived as 1-MSE/sigma, where MSE is the mean square error at validation points, and sigma is the total variance for the target variable. The percent of variance explained always has been derived in the transformed (trans-Gaussian) space and should be considered as an approximation of the true map accuracy only. The true accuracy of the resulting maps depends on the quality of the input data and the interpolation method used. The legacy dataset may seem large, but in fact 12,000 profiles for the whole of Africa (18.3M pixels) means that one point has been used to predict about 1500 pixels (or about 10 times worse than standard for this scale; see Hengl [2006] for more details); and interpolations over large distances occur, also because the data locations are fairly clustered with large gaps for some parts of Africa. The covariate data can partly compensate for this because they exploit the relationship between soil property and covariates, but the goodness-of-fit of the multiple regressions ranged between 18 percent and 48 percent. Thus, these soil property maps should be only considered as a first step in a process toward more accurate soil property mapping for Africa, which should incorporate a much denser dataset and possibly additional soil information such as that contained in legacy soil type maps.
Spatial Extent:	Africa
Spatial Resolution:	0.00833 decimal degrees (~1 kilometer)
Year of Publication:	2013
Time Period:	Approximately 1950-2005

Additional Notes:	More information available at: http://www.isric.org/data/soil-property-maps-africa-1-km and at ftp://africagrids.net/1000m/ISRIC/ORCDRC/ORCDRC_README.txt
Date:	Obtained data on 09/23/2013 from Jen Mulvey
Format:	GeoTiff
File Name:	ORCDRC_sd1_M, ORCDRC_sd2_M, ORCDRC_sd3_M,
Contact person:	Jen Mulvey

Malaria Stability Index

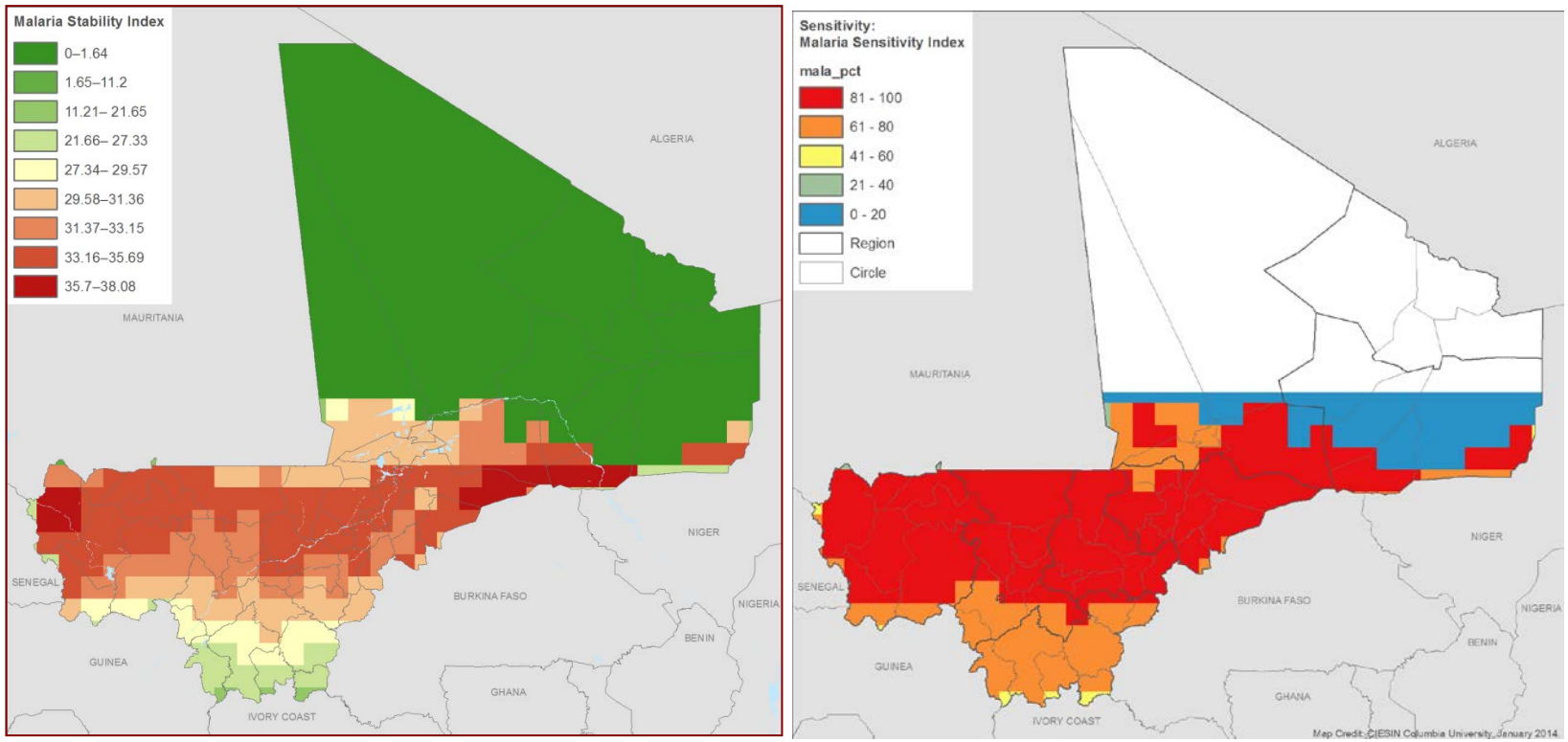

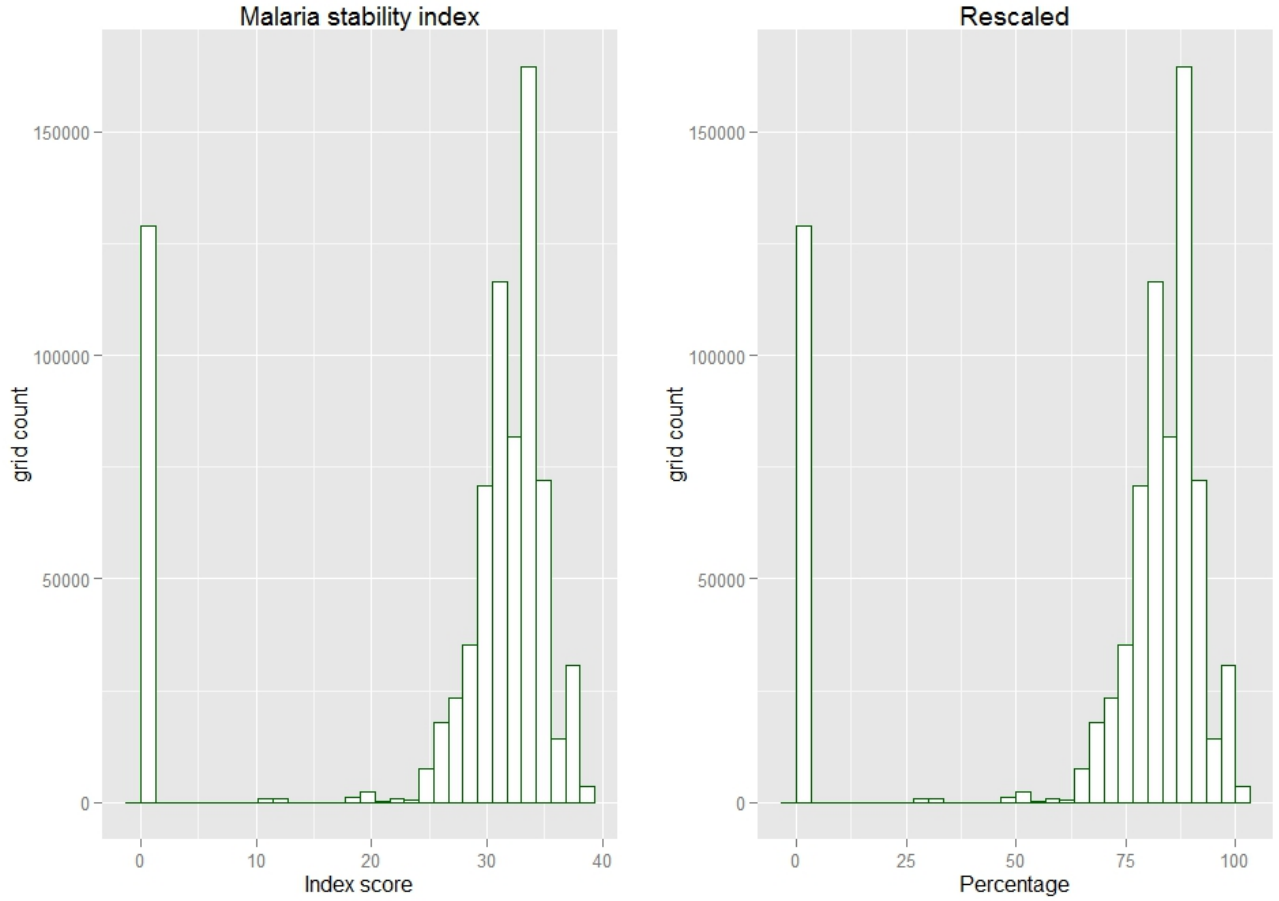

Title:	Malaria Stability Index
Indicator Code:	MALA
Component:	Sensitivity
Rationale:	Populations living in areas of high malaria transmission are more vulnerable to malaria. Malaria also increases sensitivity to other health threats, including those brought about by changing climatic conditions.

Source Data Set:	Citation: Kiszewski, A., Mellinger, A., Spielman, A., Malaney, P., Sachs, S.E., Sachs, J. (2004). A global index representing the stability of malaria transmission. *American Journal of Tropical Medicine and Hygiene*. 2004 May; 70(5):486-98. PMID: 15155980
Units:	Units range from 0.00–39.00 and represent the stability of malaria transmission based on regionally dominant vector mosquitos and 0.5 degrees gridded temperature and precipitation data set.
Computation:	The malaria data were subset to the Mali national boundary extent using ArcGIS Extract by Mask tool and a 30 arc-second raster mask generated from a 30 arc-second fishnet. Raster values were extracted using ArcGIS Extract Values to Points tool and the 30 arc-second fishnet centroids. The output was exported to a .csv table for statistical analysis.
Statistics for raw data:	Min=0, Max=38.08, Median=31.47, Mean=26.70, Standard Deviation=12.26 [computed for all of Mali below 17.2 degrees N latitude]
Scoring system:	Raster values were re-scaled to 0-100 based on percentiles, with high malaria stability translating to higher sensitivity.
Statistics for transformed data:	Min=0, Max=100, Median=82.64, Mean=70.11, Standard Deviation=32.21 [computed for all of Mali below 17.2 degrees N latitude]
Limitations:	Sources of error and bias. The diverse methods that have been used to estimate mosquito survival tend to bias comprehensive longevity estimates. Mark-release recapture methods appear to be most conservative, possibly because mosquitoes are damaged when they are captured and held prior to release. Estimates derived from laboratory-reared mosquitoes, held in population cages, tend to exceed those derived in other ways, reflecting perhaps the absence of such natural hazards as predators. These biases are most apparent in the case of vectors that are poorly represented in the literature. The disproportionate effect of vector longevity on the index further exacerbates the effect of such aberrations. The results of the version of our index based on feeding habit alone are more consistent with clinical experience than is the index that includes both longevity and human-biting habit. The anomaly introduced by the longevity parameter appears to derive more from measurement error, sample size, and inconsistent methodology than any biologic property. For the purpose of the present global analysis, therefore, we chose to substitute a fixed value for longevity. The methodology generally used for defining the blood-feeding habit of a mosquito is considerably less diverse and apparently more consistent than are methods used for estimating survival. Such estimates generally derive from precipitin resting, a method that has been used since the early 1920s and that has resulted in a considerable body of information on many of the dominant vectors. Because the precipitin test shows a relative lack of sensitivity, such results tend to be less determinate than are those based on gel diffusion or gene amplification. However, this diversity in the methods used for discriminating between blood sources appears not to introduce bias.
Spatial Extent:	Global
Spatial Resolution:	0.5 degrees
Year of Publication:	2004
Time Period:	unknown
Additional Notes:	

Date:	
Format:	Grid
File Name:	stxv5
Contact person:	

AIV.3 ADAPTIVE CAPACITY

Education Level of Mothers

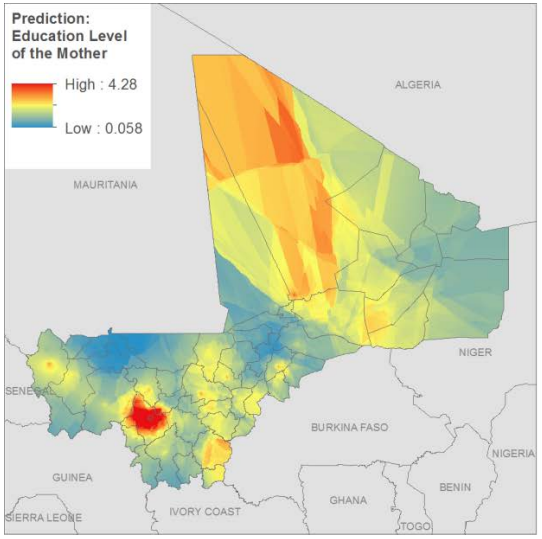

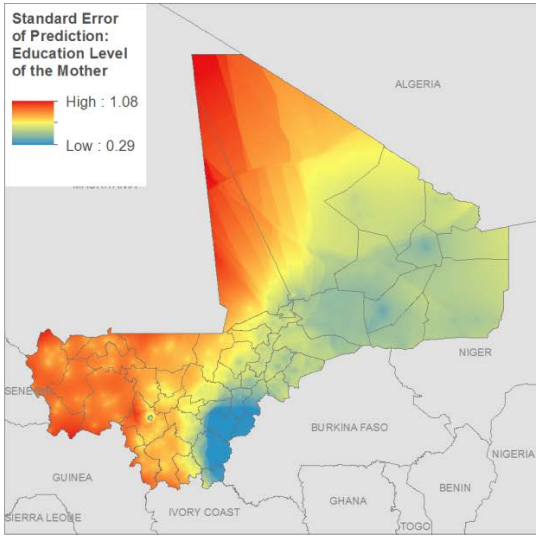

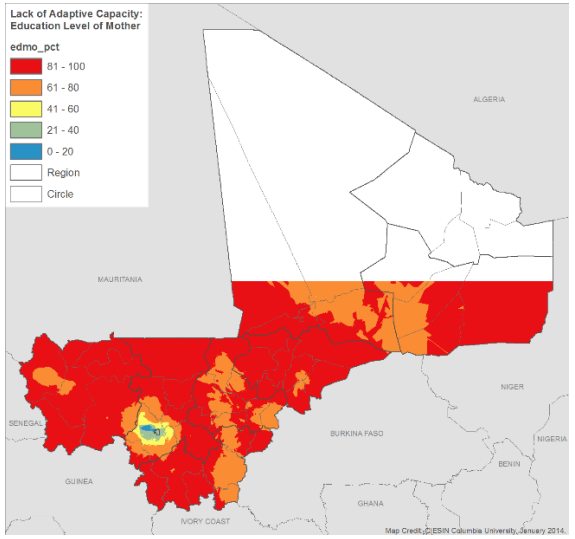

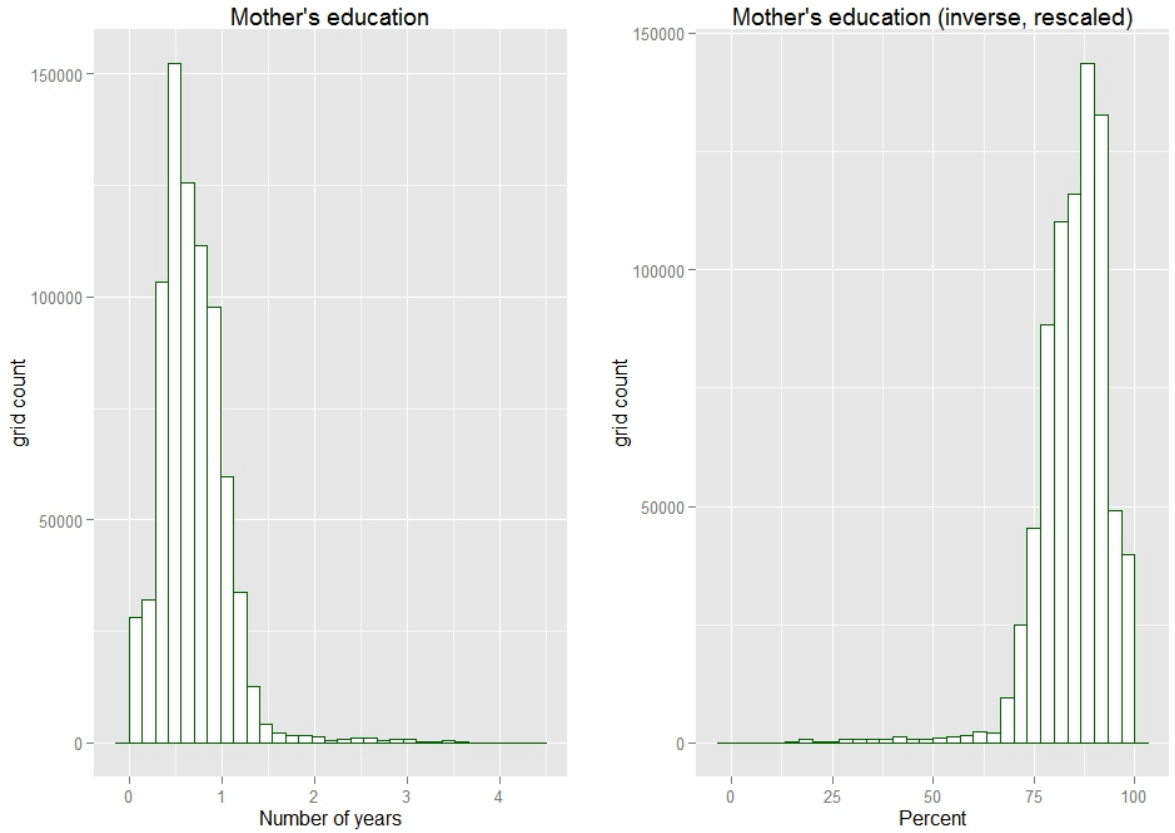

Title:	Education Levels of Mothers
Indicator Codes:	EDMO
Component:	Adaptive Capacity
Rationale:	Adaptive capacity is at least partly a function of awareness and education, and education of mothers addresses the education level of a relatively disadvantaged people group within Mali with major responsibility for the wellbeing of children. According to the DHS website, education is a key background indicator in the DHS that helps contextualize a country's health and development situation. There is a strong association between a mother's education and improved health, higher levels of knowledge, and increased levels of empowerment of women.

Source Data Set:	The cluster-level data were kindly provided by Marta Jankowska, and were used in the following paper: Jankowska, M., D. Lopez-Carr, C. Funk, G.J. Husak, Z.A. Chafe. (2012). Climate change and human health: Spatial modeling of water availability, malnutrition, and livelihoods in Mali, Africa. *Applied Geography*, 33:4-15
Units:	Years of formal education
Computation:	To create a surface from the cluster points, we followed the proceeding steps. We created 30 arc-second (0.00833 degrees; ~1km) *prediction* and *prediction standard error* surfaces from the cluster point data using ArcGIS's Empirical Bayesian Kriging tool. The rasters were subset to the Mali national boundary extent using ArcGIS Extract by Mask tool and a 30 arc-second raster mask generated from a 30 arc-second fishnet. Raster values were extracted using ArcGIS Extract Values to Points tool and the 30 arc-second fishnet centroids. The outputs were exported to .csv tables for re-coding and statistical analysis.
Statistics for raw data:	Min=0.05, Max=4.28, Median=0.64, Mean=0.69, Standard Deviation=0.37 [computed for all of Mali below 17.2 degrees N latitude]
Scoring system:	Raster values were re-scaled to 0-100, with high levels of mother's education equating to low levels of "lack of adaptive capacity"
Statistics for transformed data:	Min=0, Max=100, Median=86.07, Mean=84.94, Standard Deviation=8.74 [computed for all of Mali below 17.2 degrees N latitude]
Limitations:	For limitations, see the DHS Data Quality and Use page, available at: https://www.measuredhs.com/data/Data-Quality-and-Use.cfm.
Spatial Extent:	Mali
Spatial Resolution:	The spatial resolution of the areas represented by each cluster point varies depending on the density of cluster points. The resulting grid was at 30 arc-seconds.
Year of Publication:	2007
Time Period:	2006
Additional Notes:	Two records in the cluster dataset were lacking latitude and longitude information. These were removed from the shapefile prior to generating the surfaces. Further information on the use of cluster data can be found in the Additional Notes section of the Household Wealth metadata.
Date:	
Format:	
File Name:	child_clust.shp
Contact person:	Marta Jankowska, University of California San Diego

Market Accessibility

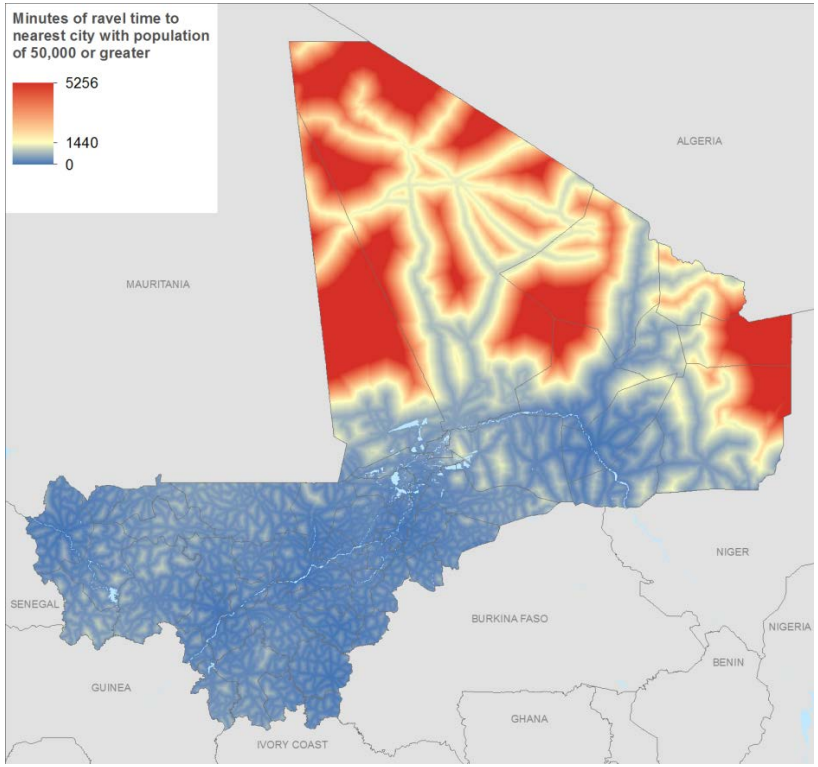

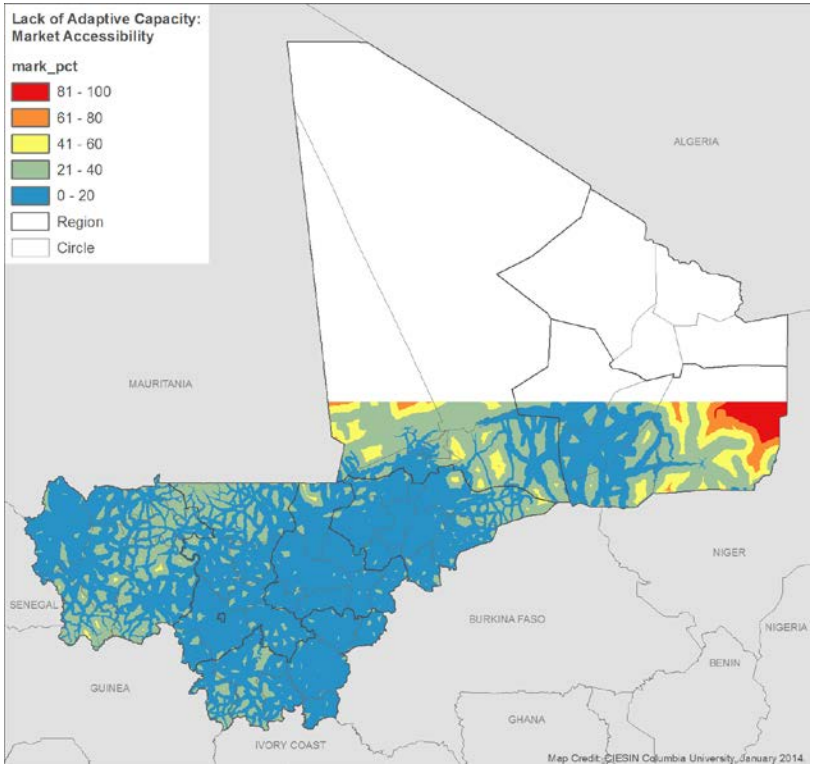

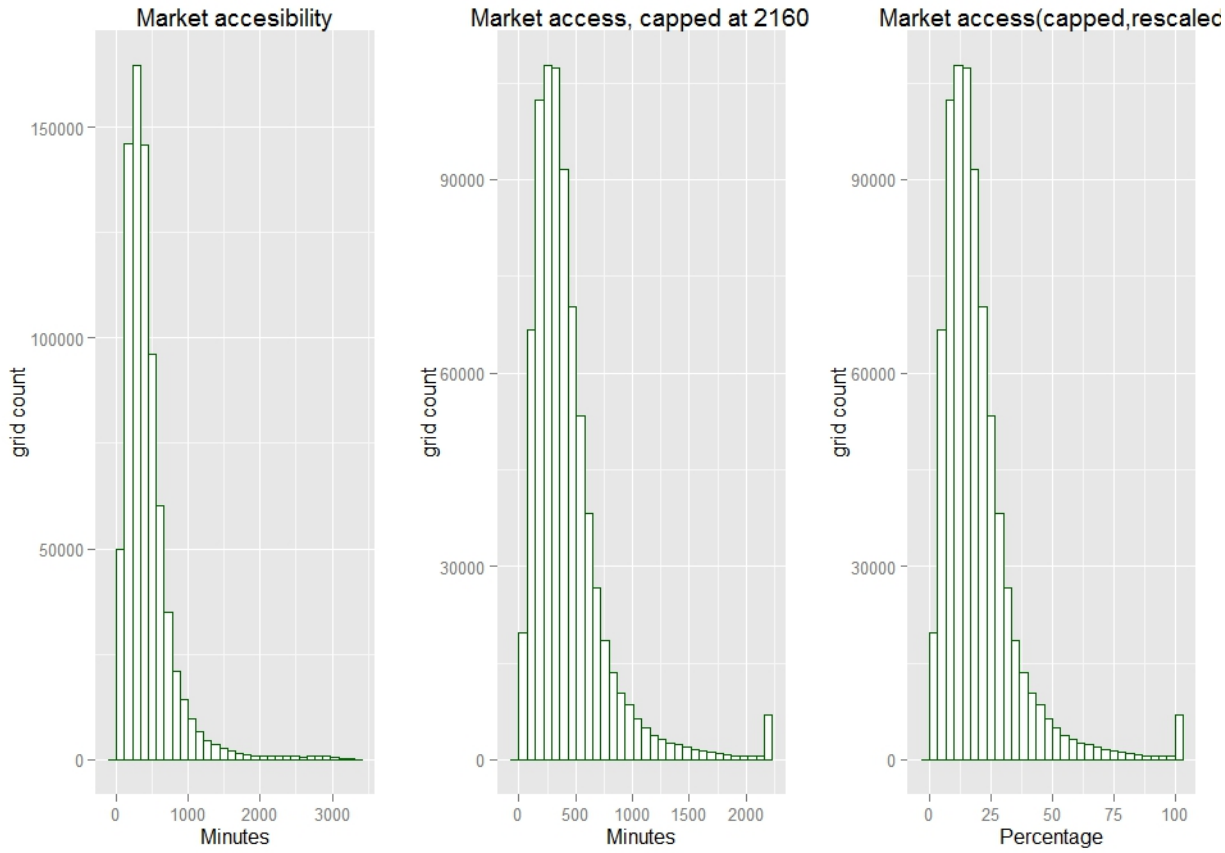

Title:	Market Accessibility
Indicator Code:	MARK
Component:	Adaptive Capacity
Rationale:	An extensive literature shows that road networks and market accessibility play an important role in development and access to health care and other social services. Greater spatial isolation is assumed to produce higher sensitivity to climate stressors.

Source Data Set:	Travel Time to Major Cities: A Global Map of Accessibility Accessibility is defined as "the travel time to a location of interest using land (road/off road) or water (navigable river, lake and ocean) based travel." It is computed using a cost-distance algorithm that computes the "cost" (in units of time) of travelling between two locations on a regular raster grid. The raster grid cells contain values that represent the cost required to travel across them; hence, this raster grid is often termed a friction-surface. The friction-surface contains information on the transport network as well as environmental and political factors that affect travel times between locations. Transport networks can include road and rail networks, navigable rivers, and shipping lanes. The locations of interest are termed targets. In the case of this dataset, the targets are cities with a population of 50,000 or greater in the year 2000. Citation: Nelson, A. (2008). Travel time to major cities: A global map of Accessibility. Global Environment Monitoring Unit - Joint Research Centre of the European Commission, Ispra Italy. Available at: http://bioval.jrc.ec.europa.eu/products/gam/index.htm. Accessed 9/3/2013.
Units:	Pixel values represent minutes of travel time to nearest city with a population of 50,000 or greater in the year 2000.
Computation:	The data were subset to the Mali national boundary extent using ArcGIS Extract by Mask tool and a 30 arc-second raster mask generated from a 30 arc-second fishnet. Raster values were extracted using ArcGIS Extract Values to Points tool and the 30 arc-second fishnet centroids. The output was exported to a .csv table for re-coding and statistical analysis.
Statistics for raw data:	Min=0, Max=3309, Median=348, Mean=429.8, Standard Deviation=356.14 [computed for all of Mali below 17.2 degrees N latitude]
Scoring system:	Data values were winsorized at 2160 minutes. The data were then then re-scaled to 0-100, so that high travel time represents high adaptive capacity.
Statistics for transformed data:	Min=0, Max=100, Median=16.11, Mean=19.70, Standard Deviation=15.30 [computed for all of Mali below 17.2 degrees N latitude]
Limitations:	Dates of input data sources range from 1987 (e.g., navigable rivers) to 2008 (e.g., shipping layers). The road network is based on available public domain data. The data are not to be used for characterizing the general accessibility of an area. It is a measure of access to markets. The website indicates that "The assumptions made in the generation of this accessibility map can be found in the description and data sources links on the left," but no description of assumptions were found.
Spatial Extent:	Global
Spatial Resolution:	The data are in geographic projection with a resolution of 30 arc-seconds (~1km).
Year of Publication:	2008
Time Period:	Dates of input data sources range from 1987 (e.g., navigable rivers) to 2008 (e.g., shipping layers).
Additional Notes:	The roads data for Mali are derived from the Vector Map Level 0 (VMap0). VMap0, released by the National Imagery and

	Mapping Agency (NIMA) in 1997. Populated places are from: CIESIN, Columbia University; International Food Policy Research Institute (IFPRI); The World Bank; and Centro Internacional de Agricultura Tropical (CIAT). 2004. Global Rural-Urban Mapping Project (GRUMP), Alpha Version: Settlement Points. Palisades, NY: Socioeconomic Data and Applications Center (SEDAC), Columbia University. Navigable rivers were extracted from the Central Intelligence Agency World DataBank II, which is a collection of world map data consisting of vector descriptions of land outlines, rivers, and political boundaries.
Date:	Downloaded from: http://bioval.jrc.ec.europa.eu/products/gam/index.htm on 9/3/2013
Format:	Esri Grid (integer)
File Name:	access_50k.gdb
Contact person:	N/A

Health Infrastructure

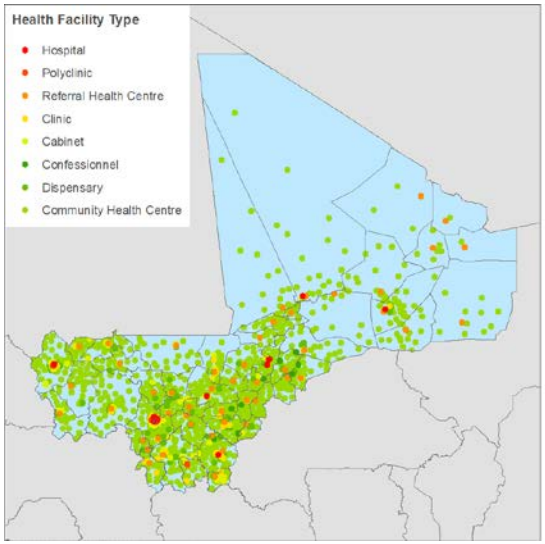

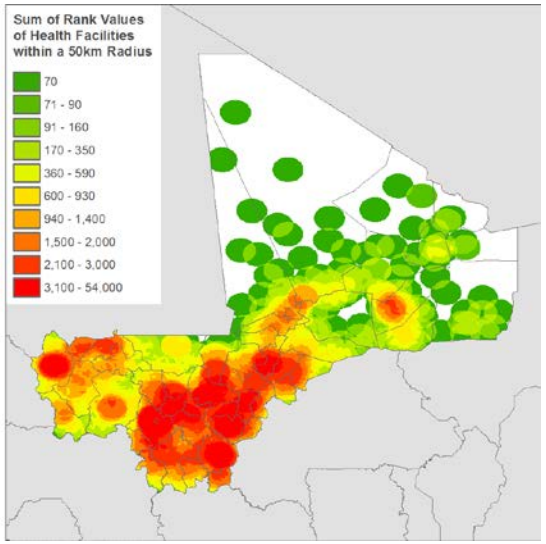

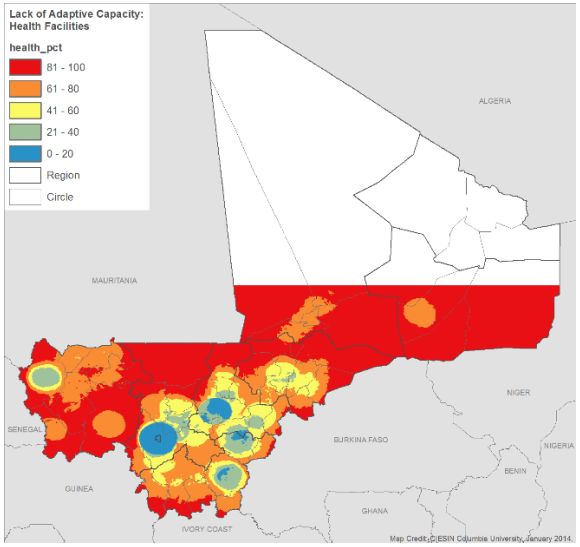

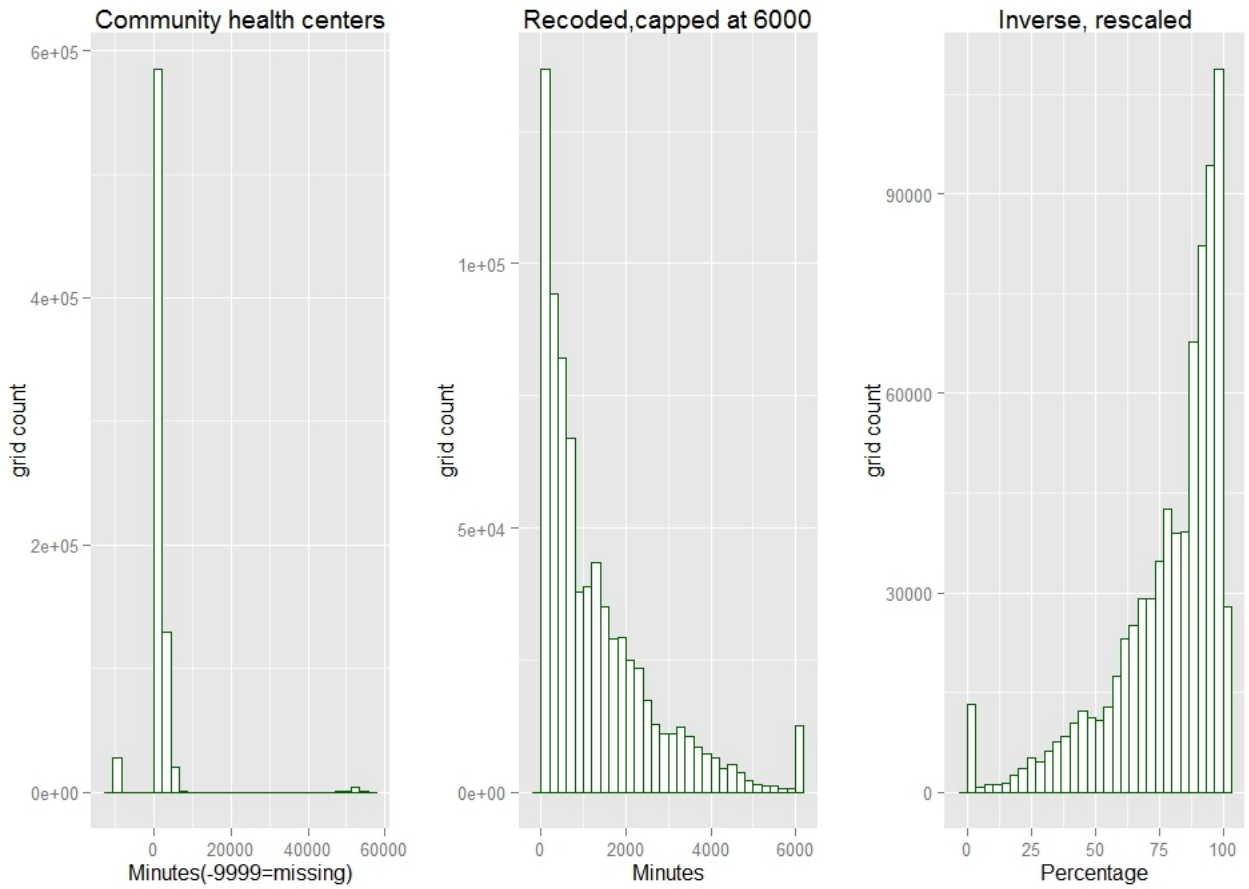

Title:	Health Infrastructure
Indicator Code:	HEALTH
Component:	Adaptive Capacity
Rationale:	Access to health care services is important for both sensitivity and adaptive capacity. Here we take access to health infrastructure both as a measure of adaptive capacity in and of itself, and as a proxy for access to other social service

	infrastructure. It is assumed that regions with greater access to infrastructure will be able to better cope with adverse climate impacts.
Source Data Set:	Mali Health Facilities Global Positioning System (GPS) coordinates and facility attributes. Provided by Amadou Diakite (adiakite@usaid.gov), who reported that the data set was created in 2012 by the UN Office for the Coordination of Humanitarian Affairs (OCHA) in Mali. Mali has a network of public and private health posts represented by the eight types of facilities in the "Facility Type" field of the data set: Hospital, Polyclinic, Referral Health Centre, Clinic, Cabinet, Confessionel, Dispensary, and Community Health Center. Residents of a given commune may attend any type of facility in any commune. They are not restricted to facilities in their home commune. The Government of Mali health service delivery structure is a pyramid: 1) At the Community level: • 20,000 community health volunteers (CHVs) form the largest cadre at the bottom of the pyramid, • immediately above are the Community Health Centers (CSCOMs), which are managed by Community Health Associations (ASACOs) 2) At the District/Cercle level: • Reference (i.e., Referral) Health Centers (CSREFs) supported by the Ministry of Health 3) At the Regional level: • Regional Hospitals 4) At National level: • National Hospitals In addition, there are private sector entities (clinics, drugstores, and laboratories). Although people seek care in their location through the health pyramid, they are free to choose where to go and to choose between public or private facilities, CSCOM, CSREF, or hospitals.
Units:	N/A
Computation:	Each type of health facility in the Facilitiy_Type field in the data set (see left-hand map above) was assigned a rank value from 70 to 100 according to the scoring system below. ArcGIS Point Statistics tool was used to generate a raster based on the sum of point values within a 50-km circular moving window (see right-hand map above). Grid cells with no points in their 50-km neighborhood were assigned a value of zero. The data were then subset to the Mali national boundary extent using ArcGIS Extract by Mask tool and a 30 arc-second raster mask generated from a 30 arc-second fishnet.

	Raster values were extracted using ArcGIS Extract Values to Points tool and the 30 arc-second fishnet centroids. The output was exported to a .csv table for recoding and statistical analysis.
Statistics for raw data:	With missing values: Min=-9999, Max=54180, Median=840, Mean=1486, Standard Deviation=5871.94 [computed for all of Mali below 17.2 degrees N latitude] Without missing values: Min=0, Max=54180, Median=840, Mean=1848, Standard Deviation=5446.01 [computed for all of Mali below 17.2 degrees N latitude]
Scoring system:	*Each health facility type was assigned a rank value as follows:* Hospitals = 100 Polyclinic = 90 Referral Health Centre = 90 Clinics = 80 Cabinet = 80 Confessionel = 80 Dispensary = 75 Community Health Center = 70 The missing values were recoded to zero, representing high vulnerability. For the sum of ranked values of health facilities, values above 6,000 were considered to represent 0 vulnerability.
Statistics for transformed data:	Min=0, Max=100, Median=86, Mean=78.34, Standard Deviation=21.98 [computed for all of Mali below 17.2 degrees N latitude]
Limitations:	The transformed indicator suffers from two deficiencies. First, the scoring and aggregation system (the 50-km circular moving window) is potentially arbitrary, as is the winsorization at 6,000. Ideally this measure would be normalized by population, since what matters is the relative accessibility of health facilities in relation to population distribution. We attempted a division of the raw HEALTH score by population distribution, but the results contained spatial artefacts that were problematic. Furthermore, it could be argued that — whether an area is densely or sparsely settled — that those people in remote areas without access to health facilities are objectively more vulnerable. In the future, it may be worth experimenting with tools that identify spatial gaps in health facility coverage.
Spatial Extent:	Mali
Spatial Resolution:	N/A
Year of Publication:	2012
Time Period:	2012
Additional Notes:	Three health posts did not have XY coordinates. Amadou was able to provide coordinates for only one of these, Aljanabandja public health post. The other two were removed.

Date:	Received from Amadou Diakité on 9/9/2013.
Format:	Tabular data set of health facilities with GPS coordinates in decimal degrees. (A shapefile of health districts was also provided.)
File Name:	Mali Health Facility (160513) Benard.xlsx
Contact person:	Amadou Diakité, Program Information Management Specialist (PIMS), USAID Mali / PRM

Anthropogenic Biomes

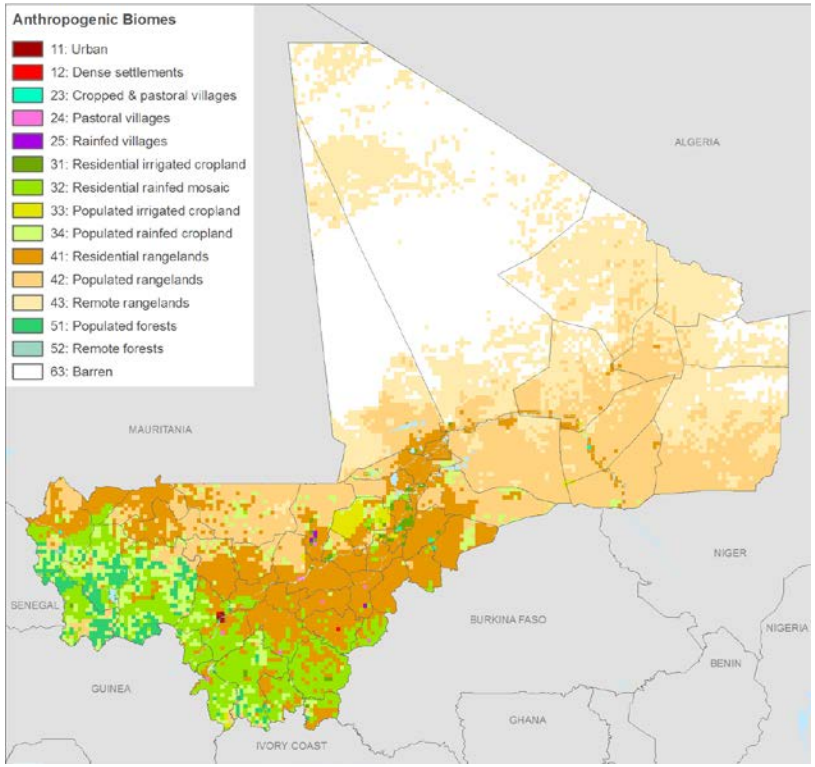

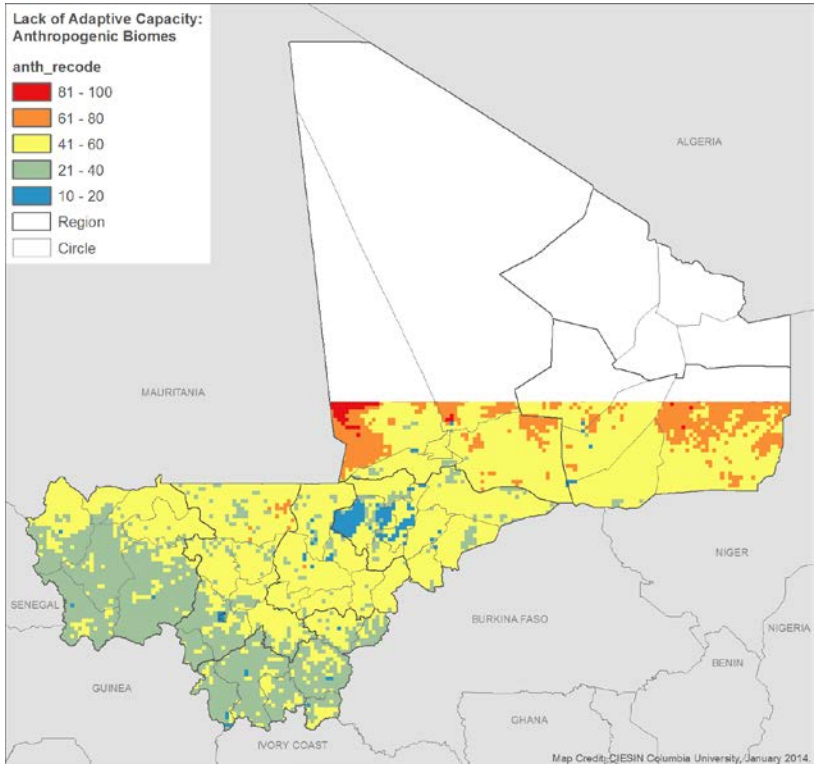

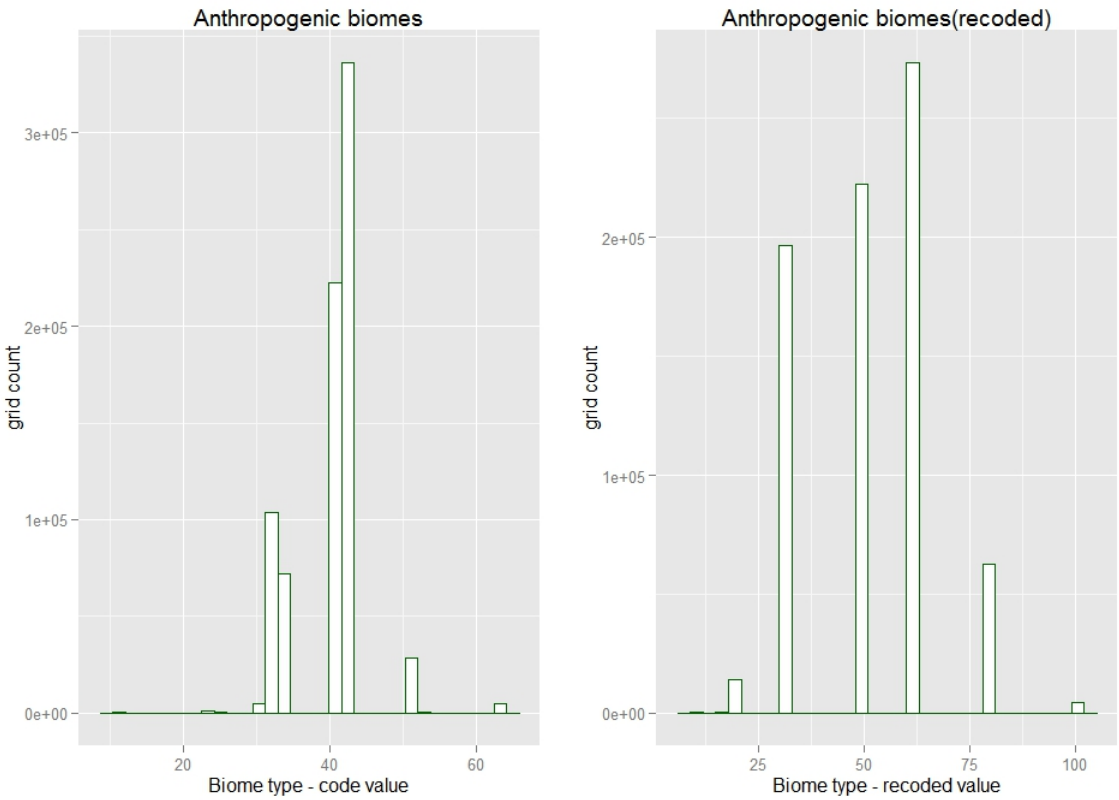

Title:	Anthropogenic Biomes of the World, v1 (2001-2006)
Indicator Code:	ANTH
Component:	*Adaptive Capacity*
Rationale:	Anthropogenic biomes (anthromes) describe what are in essence livelihood zones using a combination of land cover, land use, and population data. They does so at a spatial resolution that is superior to the livelihood zones available from the Institut de l'Economie Rurale (IER). Although it is challenging to map these to vulnerability levels, the basic approach we followed was to assign lower vulnerability to anthromes that offer multiple livelihood options.

Source Data Set:	Anthropogenic Biomes of the World, v1 (2001-2006) The Anthropogenic Biomes of the World, Version 1 data set describes globally-significant ecological patterns within the terrestrial biosphere caused by sustained direct human interaction with ecosystems, including agriculture, urbanization, forestry, and other land uses. Anthropogenic biomes were identified and mapped using a multi-stage procedure based on population (urban, non-urban); land use (percent area of pasture, crops, irrigation, rice, and urban land); and land cover (percent area of trees and bare earth). Input datasets include population data (Landscan 2005); land use data (percent area under cropland, pasture, irrigation, and rice); and land cover (vegetation, continuous fields, tree cover, and bare earth proportion layers). Citation: Ellis, E.C., and N. Ramankutty. (2008). Anthropogenic Biomes of the World, Version 1. Palisades, NY: NASA Socioeconomic Data and Applications Center (SEDAC). Available at: http://sedac.ciesin.columbia.edu/data/set/anthromes-anthropogenic-biomes-world-v1. Accessed 6 September 2013.
Units:	Biome analysis was conducted at 5 arc-minute resolution (5' grid cells cover ~ 86 km^2 at the equator), a spatial resolution selected as the finest allowing direct use of high-quality land-use area estimates.
Computation:	The data were subset to the Mali national boundary extent using ArcGIS Extract by Mask tool and a 30 arc-second raster mask generated from a 30 arc-second fishnet. Raster values were extracted using ArcGIS Extract Values to Points tool and the 30 arc-second fishnet centroids. The output was exported to a .csv table for recoding and statistical analysis.
Statistics for raw data:	Min = 11, Max=63, Median=41, Mean=40.03, Standard Deviation=4.88 [computed for all of Mali below 17.2 degrees N latitude]
Scoring system:	*Raster values were recoded as follows:* 11 (urban) = 10 12 (dense settlements) = 15 22 (irrigated villages) = 15 [not present in Mali] 23 (cropped pastoral villages) = 20 24 (pastoral villages) = 30 25 (rain-fed villages) = 30 26 (rain-fed mosaic villages) = 30 [not present in Mali] 31 (residential irrigated cropland) = 20 32 (residential rain-fed mosaic) = 30 33 (populated irrigated cropland) = 20 34 (populated rain-fed cropland) = 30 35 (remote croplands) = 50 [not present in Mali] 41 (residential rangelands) = 50 42 (populated rangelands) = 60

	43 (remote rangelands) = 80 51 (populated forests) = 30 52 (remote forests) = 50 61 (wild forests) = 20 [not present in Mali] 62 (sparse trees) = 30 [not present in Mali] 63 (barren) = 100
Statistics for transformed data:	After recode: Min=10, Max=100, Median=50, Mean=50.61, Standard Deviation=15.54 [computed for all of Mali below 17.2 degrees N latitude]
Limitations:	According to the authors, the data set is a conceptual model and not intended to replace existing biome systems based on climate, terrain, and geology. Rather in is intended that wide availability of an anthropogenic biome system will encourage a richer view of human-ecosystem interactions across the terrestrial biosphere; and that this will, in turn, guide our investigation, understanding, and management of ecosystem processes and their changes at global and regional scales. The data set has the inherent limitations and uncertainties associated with global data sets that are not optimized to any given region.
Spatial Extent:	Global
Spatial Resolution:	Raster cell sizes are 5 arc-minute or 0.08333 degree decimal (about 10 kilometers at the equator)
Year of Publication:	2009
Time Period:	2001–2006
Additional Notes:	
Date:	Obtained: 9/6/2013
Format:	Raster data available in GeoTiff and Esri Grid formats. The Africa Esri Grid was downloaded for this analysis.
File Name:	af_anthrome
Contact person:	Socioeconomic Data and Applications Center (SEDAC), CIESIN, Columbia University.

Irrigated Areas

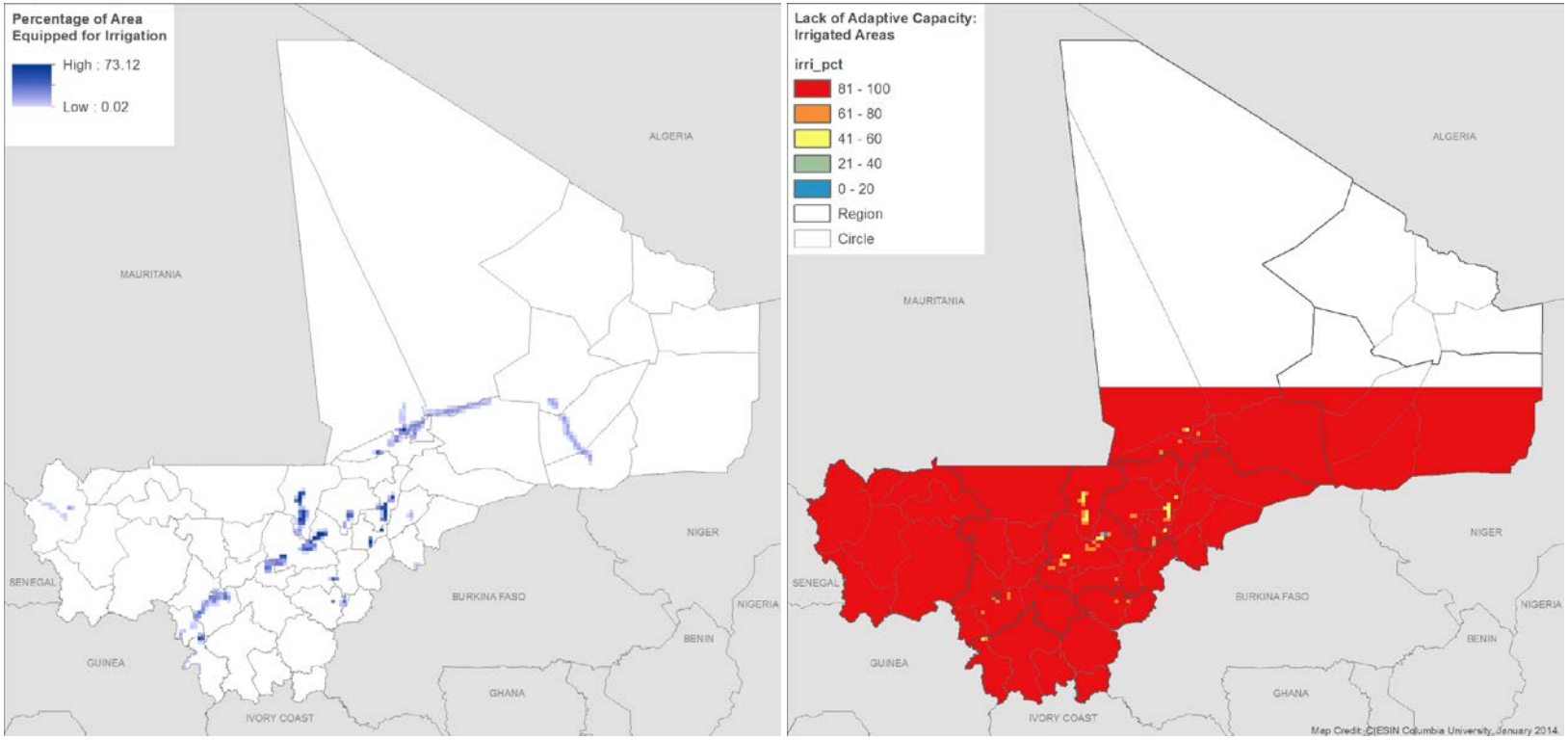

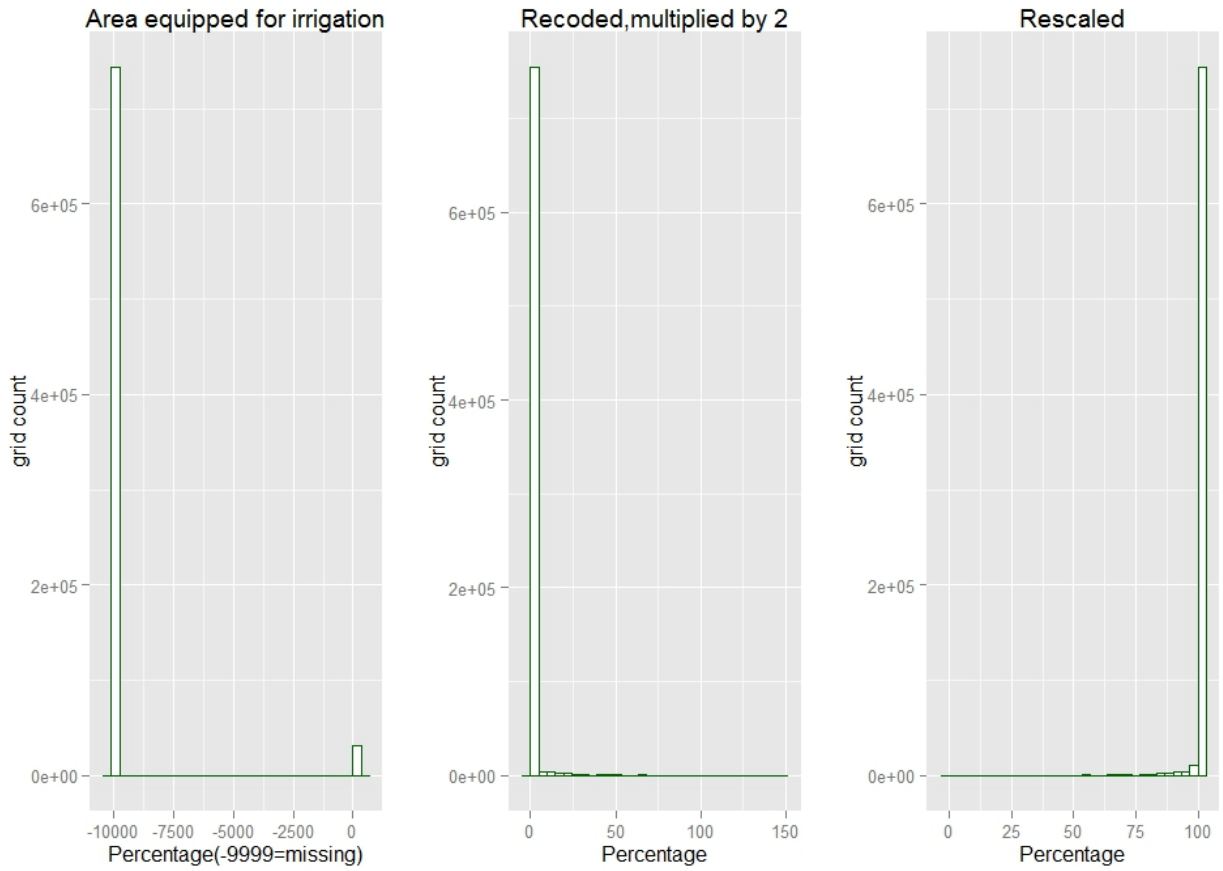

Title:	Global Map of Irrigation Areas version 4.0.1
Indicator Code:	IRRI
Component:	Adaptive capacity
Rationale:	Access to irrigation helps make farming systems more resilient to climate variability and especially to drought.
Source Data Set:	Grid with percentage of area equipped for irrigation with a spatial resolution of 5 arc-minutes or 0.0833 decimal degrees. This dataset is developed in the framework of the AQUASTAT program of the Land and Water Development Division of

	the Food and Agriculture Organization of the United Nations and the Johann Wolfgang Goethe Universität, Frankfurt am Main, Germany. The map shows the amount of area equipped for irrigation at the end of the 20th century as a percentage of the total area on a raster with a resolution of 5 minutes. The area actually irrigated was smaller, but is unknown for most countries. Citation: Siebert, S.; Döll, P.; Feick, S.; Hoogeveen, J.; and Frenken, K. (2007). *Global Map of Irrigation Areas version 4.0.1*. Johann Wolfgang Goethe University, Frankfurt am Main, Germany/Food and Agriculture Organization of the United Nations, Rome, Italy.
Units:	The percentage of the area of a 5-minute grid cell equipped for irrigation at the end of the 20th century.
Computation:	The data were subset to the Mali national boundary extent using ArcGIS Extract by Mask tool and a 30 arc-second raster mask generated from a 30 arc-second fishnet. Raster values were extracted using ArcGIS Extract Values to Points tool and the 30 arc-second fishnet centroids. The output was exported to a .csv table for recoding and statistical analysis. Cells without irrigation were characterized by "no data" (-999), and these were recoded to 0.
Statistics for raw data:	With missing values: Min=-9999, Max=73.12, Median=-9999, Mean=-0.9596, Standard Deviation=1966.973 [computed for all of Mali below 17.2 degrees N latitude] Without missing values: Min=0, Max=73.12, Median=0, Mean-0.37, Standard Deviation=2.79 [computed for all of Mali below 17.2 degrees N latitude]
Scoring system:	Missing data values, where no irrigation is present, were converted to 0-percent irrigated. Given the generally low percentage of irrigation within grid cells, the percentage of the grid cell under irrigation was multiplied by 2 and subtracted from 100. In other words, a pixel with 7 percent of its area under irrigation would result in a score of 86 (100-14).
Statistics for transformed data:	Min=0, Max=100, Median=100, Mean=99.5, Standard Deviation=3.82 [computed by Vali for all of Mali below 17.2 degrees N latitude]
Limitations:	Due to the map generation method, the quality of the map can never be uniform. The overall quality of the map heavily depends on the quality of the national-level data for each country. The quality of the Mali inputs is unknown.
Spatial Extent:	Global
Spatial Resolution:	5-minute grid cell; 0.0833 decimal degrees (~10 kilometers)
Year of Publication:	2007
Time Period:	1990–2000

Additional Notes:	Additional information on the dataset is available at: http://www.fao.org/geonetwork/srv/en/metadata.show?id=5020 Methodology (brief version) is available at: http://www.fao.org/nr/water/aquastat/irrigationmap/index30.stm Paper describing methodology in depth is in the Literature folder, available at: Siebert_etal_2005_IrrigationAreas.pdf Assessment of Map Quality is available at: http://www.fao.org/nr/water/aquastat/irrigationmap/index40.stm
Date:	Downloaded on 4 September 2013 from http://www.fao.org/nr/water/aquastat/irrigationmap/index.stm
Format:	Ascii grid
File Name:	gmia_v4_0_1_pct
Contact person:	

U.S. Agency for International Development
1300 Pennsylvania Avenue, NW
Washington, DC 20523
Tel: (202) 712-0000
Fax: (202) 216-3524
www.usaid.gov